Net sediment transport under sheet flow conditions

Measurements in the Large Wave Flume, Hannover

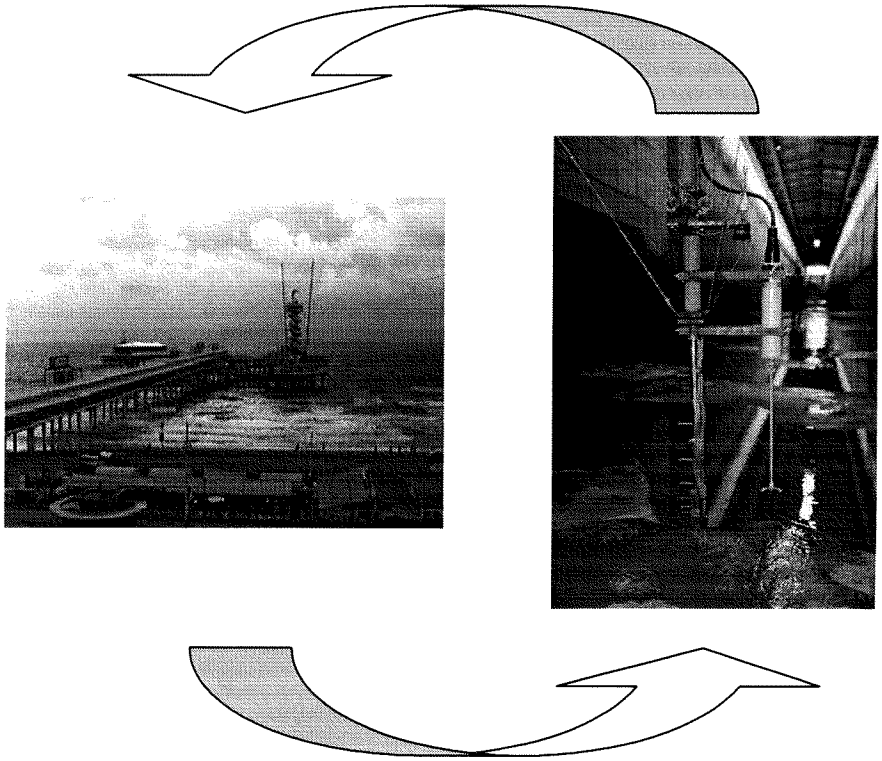

TU Delft
Delft University of Technology

Faculty of Civil Engineering and Geosciences
Section of Hydraulic Engineering

Net sediment transport under sheet flow conditions

Measurements in the Large Wave Flume, Hannover

September-2000

T.W.Westgeest

Committee: Prof. ir. K. d'Angremond
Dr.ir. J.van de Graaff
Dr.ir. M. Dohmen-Janssen
ir. P. Sistermans

Acknowledgements

This study is part of an experiment co-ordinated by the University of Twente and carried out in the large wave flume of the ForschungsZentrum Küste (FZK) in Hannover, Germany. Different students and researchers participated in the experiments and I really enjoyed working with all the different people there. My stay in Hannover for about 3 months and working in the flume (almost 10 hours a day) was a great learning experience in different ways. I would like to thank the Universities of Santa Barbara and Florida for 'sharing' the data of their instruments, which I used for my study. I would also like to thank my co-ordinator at Delft University, J.vd Graaff for his guidance and having the initial idea to participate in this experiment. Last but not least, I would like to thank the University of Twente for making it all possible, especially my main supervisor M. Dohmen-Janssen who put a lot of effort in guiding me through my MSc project.

Summary

This study focuses on time-averaged sediment transport in oscillatory flow in the sheet flow regime. The tests, used in this study, are part of the experiments, carried out under the name **SISTEX99** (Small-scale **I**nternational **S**ediment **T**ransport **Ex**periments 19**99**).

SISTEX99 focuses on near-bed sediment transport processes under influence of regular and irregular non-breaking waves in different wave conditions. The main goal is to increase insight in these processes by obtaining quantitative data of bedform characteristics, near-bed flow velocities, near-bed sediment concentrations and net transport rates. This information can be used for the verification, improvement and development of mathematical models.

The main objectives of this study were:

- To obtain a detailed data set on time-averaged sediment transport rates, measured under progressive waves in sheet flow conditions.
- To compare the measured time-averaged sediment transport rate with different sediment transport models and other experimental data sets in order to verify if there are differences between net transport rates, measured in a purely horizontal oscillatory water motion (water tunnel) or measured under progressive waves.

Experimental research

The experiments for this study were carried out in the Large Wave Flume (Großer WellenKanal, GWK) of the ForschungsZentrum Küste (FZK) in Hannover, Germany.
Four different test conditions in the sheet flow regime with monochromatic asymmetrical waves with varying wave heights and periods, above a horizontal sand bed, were carried out. The sand bed consisted of uniform sand with a median grain diameter of 0.24 mm. The net sediment transport rates were calculated from the measured bed profiles, using a mass conservation technique. Near-bed oscillatory flow velocities were measured, just outside the wave boundary layer. Also spatial measurements of the wave heights and periods were carried out during the tests.

Sediment transport models

The net transport rate data are used for the verification of four sediment transport models: three quasi-steady models (Bailard, 1981; Ribberink & Al-Salem, 1993; Ribberink, 1998) and one semi-unsteady model (Dibajnia & Watanabe, 1992).
All transport models underpredict the measured net transport rates. The quasi-steady model of Bailard (1981) underpredicts the measured net transport rates with about a factor 2. The quasi-steady model of Al-Salem (1993) underpredicts the measured transport rates. When coefficient A=5 (1993) is applied, the measured transport rate is underpredicted with about a factor 3 and applying coefficient A=4 (1994) leads to an underprediction with about a factor 3-4. The quasi-steady model of Ribberink (1998) underpredicts the measured net transport rate with about a factor 4. The semi-unsteady model of Dibajnia & Watanabe performs best. The transport rates are underpredicted with about factor 1-2.

Other experimental data-sets

In addition, a comparison is made with three other experimental data sets, obtained from the Large Oscillating Water Tunnel (LOWT) of WL|Delft Hydraulics: series B, conducted by Al-Salem (1993), series E, conducted by Katopodi et al. (1994) and series J, conducted by Janssen & V.d. Hout (1997). The experimental conditions of Al-Salem consisted of regular and irregular asymmetric oscillatory water motions. The conditions of Katopodi et al. (1994) and Janssen & V.d. Hout (1997) consisted of a symmetrical oscillatory water motion, superimposed on a net current. In series B, E and J sand with a median grain diameter of 0.21 mm was applied, opposed to 0.24 mm of the present experimental sand.
A comparison with the experimental data-set of Al-Salem (1993) shows that the present results are about a factor 2-3 larger than results under comparable conditions. The present results are larger than series E, conducted by Katopodi (1994) and series J, conducted by Janssen & V.d. Hout (1997), larger than about a factor 7-8.

Contents

List of Figures

List of Tables

Chapter 1 Introduction

1.1 General

A coastline consisting of sand and mud is continuously changing as a result of changing natural conditions and human activities. To manage a coastal zone properly it is important to be able to predict the sediment transport rates along a coast. Along the Dutch coastline a distinction is made between long-shore and cross-shore sediment transport. Long-shore sediment transport is caused by processes like tidal motion and wave-induced currents. Changes in the sea-bed topography caused by these processes develop very gradual, with a time scale of years. Cross-shore sediment transport is mainly dominated by the orbital motion of the waves, which work on much shorter time scales. For example, during storm conditions the cross-shore profile can change within a few hours.

Most of the time, sediment will be transported cross-shore during light and moderate conditions. In these cases near-bed velocities are small and sand ripples might appear. In more severe conditions these ripples will disappear due to higher near-bed velocities and higher bed shear stresses and as a result the bed will be flattened. In this situation a large part of the total sand transport (bed-load and suspended-load) is transported in a thin moving layer of sand on top of the sea-bed. This moving layer of sand with high concentrations is called a sheet flow layer. The largest changes in the cross-shore profile occur during these storm conditions, therefore it is important to investigate sheet flow.

In the past few years laboratory experiments have been carried out in order to improve the understanding of sand transport processes in sheet flow conditions. These experiments were mainly performed in full-scale laboratory facilities like water tunnels, where sediment behaviour can be investigated in horizontal oscillating flow conditions. However, experimental data on sediment processes in sheet flow conditions at prototype scale under real progressive waves are still scarce.

In order to increase insight in the near-bed sediment transport processes, experimental research was carried out in the Large Wave Flume (Großer WellenKanal, GWK) of the ForschungsZentrum Küste (FZK) in Hannover, Germany.

1.2 Framework and Scope of the experiments

The experiments on near-bed sand transport processes were carried out in the period 10 May-17 September 1999 under the name **SISTEX99** (**S**mall-scale **I**nternational **S**ediment **T**ransport **Ex**periments 19**99**) in the following frame work:

- Human Capital and Mobility Program of the European Union (EU).
- Research program Kust*2000 (Coast*2000) of Rijkswaterstaat, the Netherlands, funded by the Dutch ministry of Transport, Public Works and Watermanagement (Directorate General Rijkswaterstaat, National Institute for Coastal and Marine Management /RIKZ).
- Naval International Collaborative Opportunity Program (NICOP), funded by the U.S. Office of Naval Research (ONR). Project "International Collaboration on Local sand Transport Processes and Morphological Evolution".

Different participants were involved in the experiments: University of Twente (UT; co-ordinator), University of Florida (UF), University of California, Santa Barbara (UCSB), University of East Anglia (UEA), Delft University of Technology (DUT) and Albatros Flow

Research. The experimental facility plus some extra instruments were supplied by the ForschungsZentrum Küste (FZK).

SISTEX99 was focussed on near-bed sediment transport processes under influence of regular and irregular non-breaking waves in different wave conditions. The main goal is to increase insight in these processes by obtaining quantitative data of bedform characteristics, near-bed flow velocities, near-bed sediment concentrations and net transport rates. This information can be used for the verification, improvement and development of mathematical models.

During the first phase (first seven weeks) of the experiments sediment transport processes in rippled-bed conditions were researched. This part of the experiments was focussed on the development of and equilibrium in bedforms as well as the suspension processes that were involved.
In the second phase (last two weeks), the experiments were focussed on sediment transport in sheet flow conditions. These experiments were focussed on measurements of sediment concentrations in the sheet flow layer together with measurements of the near-bed velocities, suspension processes and net transport rates.

The test conditions during SISTEX99 consisted of monochromatic waves, random waves, bi-modal random waves and wave groups, both in the sheet flow and in the rippled bed regime. All measurements were performed above a horizontal sand bed, which consisted of uniform sand with a median grain diameter of 0.24 mm.

1.3 Scope of the present study

The present study focuses on the experiments, carried out in the second phase of SISTEX99. The main objectives of this study are:

- To obtain a detailed data set on time-averaged sediment transport rates, measured under progressive waves in sheet flow conditions. This information can be used for verification and further development of transport models.
- To compare the measured time-averaged sediment transport rates with different sediment transport models and other experimental data sets in order to verify if there are differences between net transport rates, in a purely horizontal oscillatory water motion and under progressive waves.

In order to accomplish the first objective; the recorded raw data needs to be processed in order to obtain time-averaged sediment transport rates. For this purpose software has to be developed which also can be used for the processing of the remaining data of SISTEX99.

Four different test conditions in the sheet flow regime with monochromatic asymmetrical waves were carried out with varying wave heights and periods. The following parameters, necessary for calculating and verifying the net transport rates, were measured: near-bed oscillatory velocities (just outside the wave boundary layer), bed level heights, wave heights and periods.

The net transport rate data are used for the verification of four sediment transport models: three quasi-steady models (Bailard, 1981; Al-Salem, 1993; Ribberink, 1998) and one semi-unsteady model (Dibajnia & Watanabe, 1992).
In addition, a comparison is made with three other experimental data sets, obtained from the Large Oscillating Water Tunnel (LOWT) of WL|Delft Hydraulics: series B, conducted by Al-Salem (1993), series E, conducted by Katopodi et al (1994) and series J, conducted by Janssen & V.d. Hout (1997). The experimental conditions of Al-Salem consisted of regular and irregular asymmetric oscillatory water motion. The conditions of Katopodi et al (1994)

and Janssen & V.d. Hout (1997) consisted of a symmetrical oscillatory water motion, superimposed on a net current.

Many quasi-steady formulas are based on the assumption of a direct relation between instantaneous sediment transport and the instantaneous horizontal free-stream velocity during the wave-cycle. Therefore, emphasis is placed on the sediment transport rate in relation to the free-stream velocity.

1.4 Outline of the study

In Chapter 2, backgrounds and theories on sheet flow are discussed. The experimental data sets obtained from the LOWT are discussed and attention is paid to the differences between water tunnels and wave flumes. At last, three different quasi-steady models and one semi-unsteady sand transport model are presented.

Chapter 3 presents the experimental set-up, including: a brief description of the wave flume, the measuring techniques and the instruments. Also the applied test conditions and the experimental procedures are discussed.

The experimental results are presented in Chapter 4. Near-bed velocities, measured just outside the wave boundary layer together with the bed level measurements and the applied calculation method are presented. The net transport distribution is calculated from the bed level measurements and a representative net transport rate is determined. The representative net transport rate is analysed and finally the accuracy of the results is determined quantitatively.

In Chapter 5 the measured net transport rates are compared with the predicted net transport rates of four sand transport models. The experimental data sets are compared with present results in order to determine if the results obtained from water tunnels and wave flumes are different.

Conclusions and recommendations can be found in Chapter 6.

Chapter 2 Background and theories on sediment transport

2.1 Introduction

In Sections 2.2, 2.3 and 2.4 the background of sediment transport and specific sheet flow processes will be discussed. In the past, net transport rates in sheet flow conditions were studied in different types of laboratory facilities like the Large Oscillating Water Tunnel (LOWT). Results of different experiments conducted in the LOWT are discussed in Section 2.5. In Section 2.6 attention is paid to the difference between a water tunnel and a wave flume. Cross-shore sand transport models are treated in Section 2.7 and three quasi-steady models and one semi-unsteady model are treated in Section 2.8.

2.2 Orbital motion

The orbital water motion is caused by propagating non-breaking waves. In the case of a small water depth/wave length ratio (h/L) waves will be asymmetrically shaped. An example of an asymmetric propagating wave is shown in Figure 2.1.
The asymmetry of the waves results in asymmetric orbital motions with larger horizontal velocities in the direction of wave propagation and smaller velocities in the opposite direction. In this case water particles describe more or less elliptical orbits. These orbits will be smaller and more elliptical with decreasing height above the bed. Near the bottom the velocities are basically horizontal, because no vertical mass flux can exist at the seabed.

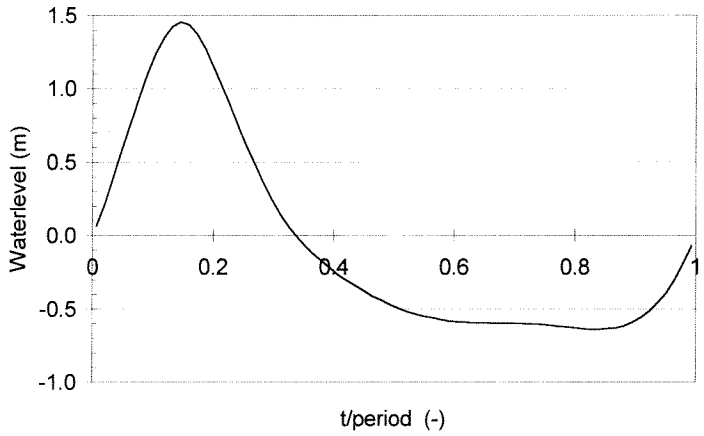

Figure 2.1: Example of an asymmetric progressive wave.

In case of an oscillatory water motion above a bed, a boundary layer will be present. This is the transition region between the free stream where no influence of the bed can be detected and the point where the velocity is zero (at the bed). The thickness of the boundary layer depends on the period of the oscillatory motion, the free stream velocity and the roughness height. In case of a tidal wave with a very long period, the boundary layer can develop over the complete water depth. If the period is small, the velocity will reverse long before the boundary layer can fully develop. This is shown in Figure 2.2, where the difference in velocity distribution due to boundary layer effects can be seen. Increased roughness of the bed will lead to an increased thickness of the boundary layer. The thickness of a boundary layer can be calculated with different expressions. For example, Sleath (1987) defined an expression for the thickness of the boundary layer over a bed of 3-dimensional roughness

elements. The boundary layer thickness $\delta_{0.05}$ (m) is defined as the level where the actual velocity differs 5% from the free-stream velocity. The expression reads:

$$\frac{\delta_{0.05}}{k_s} = 0.26\left(\frac{a}{k_s}\right)^{0.7} \tag{2.1}$$

Here, k_s (m) is the roughness height of the bed and a (m) is the semi-excursion length of a water particle. In Figure 2.2 can be seen that the thickness of the wave boundary layer is small compared to the current boundary layer. Therefore the velocity gradient within the wave boundary layer is much larger. Because turbulent shear stress depends on the velocity gradient, this results in larger shear stresses near the bed. This explains why short waves are so important for the near-bed sediment transport, which is mainly caused by bed shear stress.

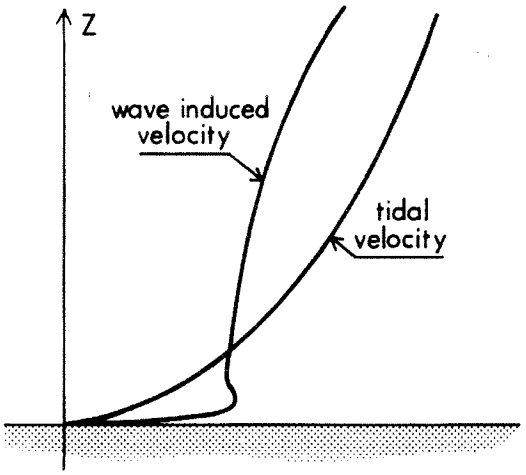

Figure 2.2: Wave and current induced boundary layers.

2.3 General background of sediment transport

Under influence of flowing water sediment can be transported. This occurs when the mobilising forces F_R (N) are larger than the stabilising forces F_g (N). Mobilising forces on the sediment grains consist of lift and drag forces, caused by the flow of water over the sediment. The weight of a grain forms the stabilising force.
The stability of a sediment grain in flowing water can be expressed by the ratio of shear stress to normal stress. The normal stress can be written as the submerged weight of the grain. The shear stress, acting on the bed τ_b (N/m^2) can be written as:

$$\tau_b = C_D \rho u^2 \tag{2.2}$$

Here, C_D (-) is the drag coefficient, ρ (kg/m^3)is the density of water and u (m/s) is the horizontal flow velocity.
In oscillatory flow the drag coefficient C_D can be replaced by the wave friction factor of Jonsson (1966): $C_D = \frac{1}{2} f_w$. The ratio of shear stress to normal stress is called Shields parameter θ:

$$\theta(t) = \frac{\tau_b(t)}{(\rho_s - \rho)gD} = \frac{\frac{1}{2} f_w \rho u^2(t)}{(\rho_s - \rho)gD} \approx \frac{F_R}{F_g} \tag{2.3}$$

In which:

$\theta(t)$	=	Shields parameter	(-)	
$\tau_b(t)$	=	bed shear stress	(N/m^2)	
ρ_s	=	density of sediment	(kg/m^3)	
ρ	=	density of water	(kg/m^3)	
g	=	gravity acceleration	(m/s^2)	
D	=	grain diameter of the sediment	(m)	
f_w	=	wave friction factor	(-)	
u(t)	=	instantaneous flow velocity near the bottom		(m/s)

With the value of the Shields parameter different transport regimes can be characterised: bed-load, rippled bed and sheet flow regime. For values of the Shields parameter smaller than about 0.03-0.06, no motion of sediment will occur. For increasing Shields parameter, the particles start to roll, slide and jump over each other, but the bed remains flat. The particles stay in contact with the bed, the bed load layer is usually assumed to be only a few grain diameters thick.
Bedforms develop when the Shields parameter further increases, ranging from small vortex ripples to large mega-ripples and dunes. Suspended sediment transport can now play a role, resulting in very different transport mechanisms compared to the mechanisms in the bed-load regime.
For values of the Shields parameter larger than 0.8-1.0 small ripples are washed out and the bed becomes plain again. A thin layer with high sand concentrations is moving in a sheet along the bed. The thickness of this sheet flow layer is relatively large, 10-100 grain diameters.
The high values of the Shields parameter in sheet flow conditions, correspond to high bed shear stresses due to large oscillating near-bed velocities. The high concentrations in the sheet flow layer in combination with large velocities results in high sediment fluxes.

The wave-induced oscillatory flow interacts with the bed mainly through the bed-shear stress. The bed-shear stress can be divided into two contributions namely, the form drag and the skin friction. The form drag is generated by bedforms but has no effect on the stability of

individual surface sediment particles. For generation of sediment transport, the skin friction is considered to be the most important part of the bed shear stress. A well known (skin) friction factor for oscillatory flow, defined by Jonsson (1966) and re-written by Swart (1974) is;

$$f_w = \begin{cases} \exp\left[5.213\left(\frac{k_s}{a}\right)^{0.194} - 5.997\right] & for \quad \frac{k_s}{a} \le 0.63 \\ 0.3 & for \quad \frac{k_s}{a} > 0.63 \end{cases} \qquad (2.4)$$

The ratio k_s/a is known as the relative roughness height. With a the semi-excursion length of the water particles due to the horizontal oscillatory flow and k_s the roughness height of the bed. For the fully developed rough turbulent regime, the wave friction factor only depends on the relative roughness height k_s/a.

Over a plane bed without sheet flow the roughness height is often expected 1 or 2 times the median grain diameter. In plane mobile beds with sheet flow the roughness height may be much larger than 1 or 2 times the median grain diameter. There are many expressions for the roughness height in the sheet flow layer but it is often assumed that the roughness height in sheet flow conditions is of the order of the sheet flow layer thickness.

Whether a flow is laminar or turbulent is determined by the Reynolds number, which in case of oscillatory flow is defined as $Re=u_a a/\nu$ (-), in which ν is the kinematic viscosity of water, a is the semi-excursion length of the water particles and u_a is the amplitude of the horizontal oscillatory velocity . For values of the Reynolds number smaller than about 10^4 the flow is laminar. Turbulent flow corresponds to values of the Reynolds number larger than about $5*10^5$.

2.4 Effects of unsteady flow

Many existing models for sand transport in oscillatory sheet flow are based on the assumption that the sand transport reacts instantaneously to changes in velocity, because the majority of the sand is transported very close to the bed. The reaction can be considered instantaneous if the phase lag between the sediment concentration or sediment transport and the velocity, is small compared to the time scale on which the velocity varies. In oscillatory flow this is the period T (see Figure 2.3). In this case the sand transport behaves quasi-steady and is proportional to a power of the instantaneous velocity, larger than one. If the transport behaves quasi-steady under asymmetric oscillatory flow, the net transport will be in the direction of the largest velocity, due to the non-linear relation with the velocity, with exponent larger than one.

If the response time of the sediment is not small compared to the oscillation period, the concentration may lag significantly behind the velocity (see Figure 2.3). Sediment particles are entrained into the flow during the positive half wave cycle but have not enough time to settle back to the bed. Because the particles remain entrained, the particles will be transported in the negative direction during the succeeding negative half wave cycle. Due to the asymmetric oscillatory flow with larger velocities in the positive half of the wave cycle, the entraiment of the sediment particles into the flow during the positive half wave cycle will be higher and may need more time to settle back to the bed. This results in a larger phase lag between concentration and velocity than in the negative half wave cycle. This means that phase lag effects reduces the net transport rate in asymmetric flow.

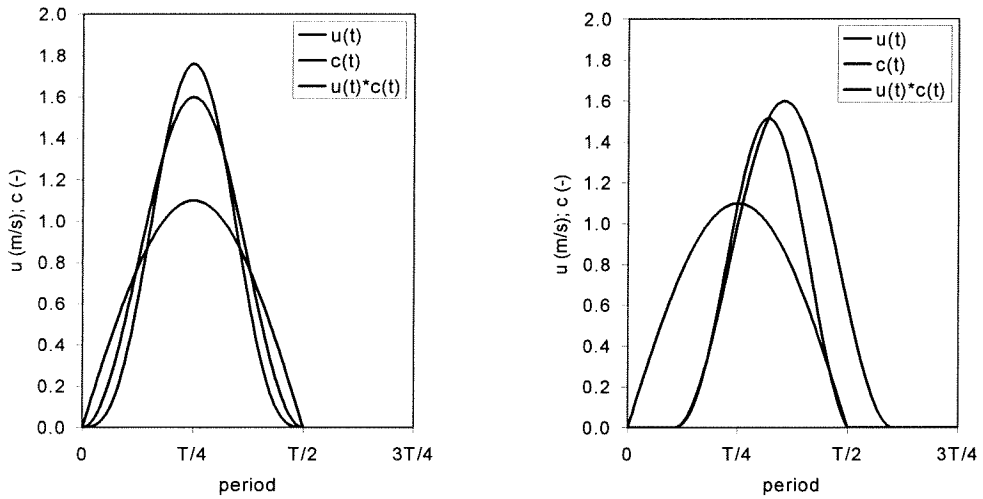

Figure 2.3: Flow velocity u(t), concentration c(t), sediment flux u(t)*c(t),in case of instantaneous sediment response to the flow velocity (left-hand side panel) and in case of delayed sediment response due to a fixed time-lag between the concentration and the velocity (right-hand side panel).

Phase lag effects can be characterised by the settling time of the grains δ_c/W_s, a characteristic thickness of the moving sediment layer divided by the fall velocity of the sediment and the wave period. This means that phase lag effects can be characterised with the following parameter:

$$p = \frac{\delta_c / W_s}{T} = \frac{\delta_c}{W_s T} \tag{2.5}$$

In which δ_c/W_s stands for the required fall time (t_{fall}), the period T can be seen as the available fall time.
The study of Dohmen-Janssen (1999) showed that even in sheet flow conditions, where the majority of the sand is transported close to the bed, phase lags between flow velocity and sand transport rate are significant and reduce the net transport rate if the following criterion is fulfilled:

$$p = \frac{\delta_s \omega}{W_s} > 0.5 \tag{2.6}$$

Here, δ_s (m)is the thickness of the sheet flow layer, ω (s^{-1}) is the angular frequency of the wave and W_s (m/s) is the settling velocity of the sediment. For the thickness of the sheet flow layer (δ_s), the following expression is found for median grain diameters larger than 0.2 mm:

$$\frac{\delta_s}{D_{50}} = 13\theta_w \tag{2.7}$$

Here, D_{50} (m) is the median grain diameter of the sediment and θ_w is the maximum Shields parameter, based on the oscillatory velocity amplitude u_a and on a friction factor f_w, according to expression of Swart (1974) with a roughness height equal to D_{50}.
The phase lag parameter p shows that phase lag effects can be expected to be important for large flow velocities (high entrainment into the flow), fine sand (small settling velocity) and small wave periods (small available settling time).

Recent study conducted by Dohmen-Janssen (1999) showed that additional phase lag effects may reduce the net transport rate due to limited pick-up. The sediment load that could be eroded from the bed depends on the required pick-up time. If the available pick-up time, which is determined by the wave period, is shorter than the required pick-up time, the sediment load entrained into the flow will be limited, leading to a reduced sand transport rate.

Experiments (Al-Salem, 1993; Ribberink and Chen, 1993; Katapodi et al.,1994; Ribberink et al.,1994) have shown another unsteady phenomenon of oscillatory sheet flow. Time-dependent concentration measurements showed sharp peaks around flow reversal, both in the sheet flow and in the suspension layer. These peaks are called suspension ejection events. Sediment is entrained just before flow reversal and transported during the succeeding half wave cycle in opposite direction, probably affecting the net transport rate. The cause for these suspension ejection events is not clear yet. Field observations and model results (Foster et al., 1994 and Savioli & Justesen, 1997) suggest that the suspension ejection events are caused by shear instabilities in the wave boundary layer.

2.5 Laboratory experiments

In the past, experimental research on net transport rates under sheet flow conditions, is mainly carried out in laboratories. The reason that there are only a few field studies is the fact that it is very difficult to measure close to the bed during rough conditions. The spatial and temporal variability's of both waves and bed topography and the fact that rough conditions in which sheet flow occur do not take place all the time, makes it difficult to measure sand transport.

Because of this, sheet flow processes are often studied in small-scale or full-scale laboratory facilities, using oscillating plates, oscillating water tunnels and wave flumes. Full-scale facilities have the advantage that prototype material can be used, scaling of the sediment is not necessary. Also prototype conditions can be simulated, conditions which occur in nature with specific periods and velocities. In the past different experiments were conducted by various researchers, leading to different expressions for the net sand transport in sheet flow. Most expressions were based on a description of the sediment transport which depended on the near-bed velocity, raised to a certain power n ($<u|u^{n-1}|>$). Some remarks on early investigations (Manohar, 1955; Kalkanis, 1964, Abou-Seida, 1965; Sleath, 1978; Horikawa et al, 1982; Sawamoto et al, 1986; Roelvink, 1988; King, 1991) are:

- Most of the experimental data were collected using small-scale facilities like oscillating plates and oscillating water tunnels. With some of the used facilities it was not possible to simulate realistic full-scale sheet flow conditions.
- The laboratory experiments showed a large variation of the power n (range 2-6).
- In more laboratory experiments sediment transport averaged over a half-cycle of sinusoidal oscillatory motion was investigated than over a full cycle.

More recent experiments, conducted under more realistic sheet flow conditions (Al-Salem 1993), showed that the power n has a tendency to be n=3. These experiments were carried out in the Large Oscillating Water Tunnel (LOWT) of WL|Delft Hydraulics. In the LOWT it is possible to generate a steady current, combined with an oscillating water motion. An overview of previous series of experiments is given in Table 2.1:

series	Waves/ Current	Asym./ Sym.	D_{50} (mm)	T (s)	measurements	Conducted by
B	W	As	0.21	5-12	$<q_s>$	Al-Salem (1993)
C	W	As/S	0.21	6.5-9.1	u(z,t),c(z,t)	Al-Salem (1993)
D	W	As	0.13	6.5	$<q_s>$	Ribberink & Chen (1993)
C-I	W+C	As	0.21	6.5	$<q_s>$	Ramadan (1994)
C-II						Ribberink et.al. (1994)
E	W+C	S	0.21	7.25	$<q_s>$,u(z,t),c(z,t)	Katopodi et al (1994)
H	W+C	S	0.13	4-12	$<q_s>$,u(z,t),c(z,t)	Janssen et al (1996)
I	W+C	S	0.32	4-12	$<q_s>$,u(z,t),c(z,t)	Janssen & V.d. Hout (1997)
J	W+C	S	0.21	7.2	$<q_s>$	Janssen & V.d. Hout (1997)

Table 2.1: Experiments conducted in the LOWT of WL|Delft Hydraulics.

Series B and C were carried out in the LOWT were conducted by Al-Salem (1993) and can be compared with the present study. Periods, velocities and the median sediment diameter are in the same range as the present experiment. The test sand had a median diameter of 0.21 mm. Al-Salem used regular and irregular asymmetric waves, see Table 2.2.
In the following tables the following parameters can be found: number of test with the same condition N, the degree of wave asymmetry R [$=U_c/(U_c+U_t)$], the third order moment of the

time averaged flow velocity $<U^3>$, the net time averaged transport rate (without pores) $<q_s>$ and the standard deviation σ of $<q_s>$

Exp #	T (s)	r/ir asym.	N	R (-)	$<U^3>$ (m^3/s^3)	$<q_s>$ ($10^{-6}m^2/s$)	σ ($10^{-6}m^2/s$)
B1	6.5	ir	12	0.62	0.074	12.3	8.30
B2	6.5	ir	12	0.61	0.019	3.3	0.34
B3	6.5	ir	8	0.61	0.046	8.0	0.30
B4	9.1	ir	8	0.62	0.067	14.6	0.60
B5	9.1	ir	8	0.62	0.021	4.1	0.14
B6	9.1	ir	6	0.61	0.037	12.0	0.34
B7	6.5	r	6	0.66	0.102	12.4	0.94
B8	6.5	r	7	0.65	0.256	38.9	2.34
B9	6.5	r	6	0.67	0.562	69.8	4.73
B10	9.1	r	10	0.64	0.104	18.6	2.25
B11	9.1	r	5	0.64	0.220	44.8	1.88
B12	9.1	r	5	0.64	0.574	120.9	2.00
B13	6.5	r	6	0.57	0.114	21.0	2.43
B14	9.1	r	9	0.56	0.094	22.0	4.52

Table 2.2: Tests with regular/irregular asymmetric waves, conducted by Al-Salem (1993).

Series E (Katopodi et al, 1994) and series J (Janssen & V.d. Hout, 1997) were also obtained from the LOWT. These series of tests were carried out with a sinusoidal oscillatory water motion (with velocity amplitude u_a) superimposed on a net current (with velocity u_m). Both series used experimental sand with a median grain diameter D_{50} of 0.21mm. The measured net sand transport rates $<q_s>$ are corrected for the existence of a lateral velocity gradient, due to the side-walls. The results of series E can be found in Table 2.3, series J in Table 2.4.

Exp #	T (s)	u_a (m/s)	u_m (m/s)	$<U^3>$ (m^3/s^3)	$<q_{sr}>$ ($10^{-6}m^2/s$)	σ ($10^{-6}m^2/s$)
E1	7.23	1.69	0.18	0.718	107.2	7.0
E2	7.22	1.47	0.23	0.726	111.8	8.4
E3	7.23	1.14	0.31	0.586	80.8	9.5
E4	7.23	0.95	0.44	0.617	84.4	7.9

Table 2.3: Katopodi et al. (1994), series E.

Exp #	T (s)	u_a (m/s)	u_m (m/s)	$<U^3>$ (m^3/s^3)	$<q_{sr}>$ ($10^{-6}m^2/s$)	σ ($10^{-6}m^2/s$)
J1	7.20	1.06	0.24	0.425	46.3	3.3
J2	7.20	1.28	0.25	0.625	74.4	2.4
J3	7.20	0.46	0.41	0.205	9.0	0.3
J4	7.20	0.65	0.41	0.328	25.3	0.5

Table 2.4: Janssen & V.d. Hout (1997), series J.

2.6 Differences between Water Tunnel and Wave Flume

Water tunnels can be used to study sediment behaviour under influence of a full-scale simulation of the horizontal orbital motion near the bed. A water tunnel is a U-shaped tube, with a piston in one of the cylindrical risers, which generates an oscillatory flow. In the middle of the horizontal part of the tube, a test section is created. Due to the tunnel configuration the water flow in the test section oscillates only in horizontal direction, without a free surface. As a result the water motion in a tunnel is uniform without any vertical orbital velocities. Also no phase differences exist in horizontal direction.

In case of a water tunnel, the flow can be described by a 1DV-approximation (flow uniform in flow direction and no vertical orbital velocities). The 1DV-approach is an acceptable approximation for the near-bed flow under surface waves if certain criteria are fulfilled (Dohmen-Janssen, 1999). These criteria are: horizontal flow velocity small compared to the wave celerity and the water depth small compared to the wave length.

The water motion under propagating surface waves is not restricted to a horizontal oscillatory flow only, the water particles describe elliptical orbits. The oscillatory water motion, generated in a wave flume contains all properties of propagating surface waves, including the elliptical orbits.

Away from the bed, the vertical orbital velocity is 90° out of phase compared to the horizontal orbital velocity. However, due to the viscous boundary layer they are not exactly 90° out of phase. This results in a small net current, close to the bed, in the direction of wave propagation. This boundary layer drift is called Longuet-Higgins streaming (Longuet-Higgins, 1956). Because the flow is purely horizontal flow in a water tunnel, the Longuet-Higgins streaming is absent.
It is not clear if the Longuet-Higgins streaming influences the net transport rate in asymmetric oscillatory flow conditions.
Propagating waves over a horizontal bottom cause pressure differences along their direction of propagation which influences the pressures in the bed. In a water tunnel no pressure differences are present. Pressure differences in the bed can influence the sand transport.

No gradients exist perpendicular to the direction of wave propagation. In laboratory facilities velocity gradients may be present due to the presence of side-walls. The width of a full-scale wave flume is often several meters. Therefore the influence of the lateral velocity gradients is expected very small near the bed.
Because water tunnels are often narrower than full-scale wave flumes, the distance from the bed where the influence of the lateral velocity gradients can be noticed, is much smaller than in wave flumes. It is expected (see Dohmen-Janssen, 1999) that the influence of the side-walls can be neglected if the distance from the bed is small, compared to half the width of the tunnel.

It is concluded that there are differences between water tunnels and wave flumes. It is expected that lateral velocity gradients do not make a difference if the distance from the bed is small enough so that the velocity gradients do not influence the near-bed velocities. Pressure differences in the bed, vertical orbital velocities and the Longuet-Higgins streaming might influence the sand transport in wave flumes. It is not very clear how much these effects influence the sediment transport rate. An important research question will be the difference (quantitatively) between net transport rates, measured in water tunnels and wave flumes.

2.7 Cross-shore sand transport models

In order to predict sand transport in oscillatory sheet flow, different kind of models have been developed. Sediment transport is defined as the product of instantaneous flow velocity and sediment concentration, integrated over the water depth. The formula is given by:

$$q_s(t) = \int_0^{h(t)} u(z,t) \cdot c(z,t) dz \tag{2.8}$$

q_s (t)	=	instantaneous transport rate per unit width	(m^2/s)
u	=	horizontal velocity	(m/s)
c	=	sediment concentration	(m^3/m^3)
h	=	water depth	(m)
z	=	level above the bed	(m)
t	=	time	(s)

The transport is expressed in volume of solids (without pores), per unit width and unit time (m^2/s). Both velocity and concentration can be split up into a steady and an oscillatory component.

$$\begin{aligned} u &= \langle u \rangle + \tilde{u} \\ c &= \langle c \rangle + \tilde{c} \end{aligned} \tag{2.9}$$

In which: $\langle\ \rangle$ = notation time averaged components
$\sim$ = notation oscillatory components

These expressions can be substituted in Eq. (2.8)

$$q_s(t) = \int_0^{h(t)} \left(\langle u(z) \rangle \cdot \langle c(z) \rangle + \tilde{u}(z,t) \cdot \langle c(z) \rangle + \langle u(z) \rangle \cdot \tilde{c}(z,t) + \tilde{u}(z,t) \cdot \tilde{c}(z,t) \right) dz \tag{2.10}$$

The net transport rate is given by averaging this equation over the wave period and neglecting the sediment transport between wave trough and wave crest (i.e. integration to the level of the wave trough, h_t):

$$\langle q_s \rangle = \int_0^{h(t)} \left[\langle u(z) \rangle \cdot \langle c(z) \rangle + \langle \tilde{u}(z,t) \cdot \tilde{c}(z,t) \rangle \right] dz \tag{2.11}$$

The first term on the right-hand side of Eq. (2.11) is called the current related sand transport rate, the second term is called the wave-related sand transport rate.

Models that predict the sand transport rates can be divided in 3 different main types: time-averaged, quasi-steady and unsteady models.
Time-averaged models are developed to derive the current related sand transport rate. The important wave related sediment flux is neglected in these models and they are therefore not included in this study.
Quasi-steady models are based on the assumption that the instantaneous transport rate is directly related to the instantaneous near-bed oscillatory velocity or bed-shear stress. The wave related component is implicitly taken into account. Processes in the boundary layer are only determined by the free stream velocity above it.

Unsteady models are based on a more fundamental approach; the distributions of velocity and concentration over the water depth at each instant are determined. Still, most of the unsteady models do not take the different transport mechanisms within the sheet flow layer into account.

2.7.1 Quasi-steady models

In case of sheet flow conditions, bed-load is the dominating transport mode. This implies that the largest part of the total sand transport can be expected to occur very close to the bed. This would mean that the settling time of the grains δ_c/W_s (i.e. a characteristic thickness of the moving sediment layer divided by the fall velocity of the sediment) would be much shorter than the wave period. In this case it is likely that the sand transport will immediately react to changes in flow condition and a quasi-steady approach can be used. In quasi-steady models the instantaneous transport rate is directly related to some power of the free stream velocity. Due to a non-linear relation between instantaneous transport rate and flow velocity with exponent larger than one, quasi-steady models will always predict a net (wave averaged) transport rate in the direction of the largest velocity.
Quasi-steady models do not include the distribution of the velocity and the concentration over the water depth, only the near-bed horizontal velocity is taken into account. In the most simple form these models can be written as:

$$\langle q_s \rangle = A\langle |U^{n-1}|U \rangle \qquad (2.12)$$

In which:	<...>	=	notation for wave-cycle averaging
	q_s	=	transport rate per unit width
	A	=	factor depending on several parameters (e.g. grain size and friction factor)
	U	=	horizontal free-stream velocity near the bed
	n	=	power

The power n of the free stream velocity needed in Eq. 2.12 is considered important. Different investigators (Al Salem,1993; Sawamoto & Yamashita, 1986) proposed a power 3 or power 3-4 (Bailard,1981) relationship.

2.7.2 Unsteady models

If the response time of the sediment is not small compared to the oscillation period, the sediment concentration (and therefore the sand transport rate) may lag behind the instantaneous velocity, this phase lag will affect the net sand transport rate. The assumption of quasi-steadiness is not valid anymore. Therefore unsteady models have been developed that include the effects of unsteadiness.

In these models a more fundamental way is used to predict the sand transport rate: the distribution of both velocity and concentration over the water depth at each instant are taken into account (see Eq. 2.8). Unsteady models require solutions of the unsteady continuity and momentum equations to find the unsteady velocity. The unsteady concentration can be derived from the mass-balance of the sediment and is given by an advection-diffusion equation. A distinction can be made here between models that take sediment-flow interaction into account and those that do not. In the latter, the flow velocity is used to derive the sediment concentration. However, this concentration does not affect the flow velocity. If sediment-flow interaction is included, the equations for both flow velocity and sediment

concentration are solved iterartively, because the sediment concentration that depends on the flow velocity affects in turn the flow velocity.

2.7.3 Intermediate model

Models that take phase lag into account without describing the vertical distribution of the time-dependent horizontal velocity and sediment concentration are called semi-unsteady models (e.g. Dibajnia and Watanabe 1992).

2.8 Applied models

The quasi-steady approach is suitable for a simple comparison between different experiments. By applying quasi-steady (or semi-unsteady) transport models, a detailed description of the instantaneous velocity profiles and sediment concentration profiles is avoided. The quasi-steady approach is also chosen because phase lag effects are not expected to play a significant role during the present experiment. However, a semi–unsteady model (Dibajnia and Wantanabe, 1992) is included in case phase lag effects do occur. The phenomenon of limited pick-up is not included in the quasi-steady models, which assume an instantaneous sediment response. The semi-unsteady model of Dibajnia & Watanabe (1992) only takes the delayed settling of the sediment into account.
The following models are based on various data sets, and are therefore a valuable source of information which can be used for a comparison with the results of this study. In this section four different models will be treated: Bailard (1981), Dibajnia and Watanabe (1992), Al-Salem (1993) and Ribberink (1998).
Except for the theoretical model of Bailard, the discussed models are mostly derived from own experimental data and data from other experiments. An overview will be given in Table 2.5.

Model	Bailard (1981)	Dibajnia and Watanabe (1992)	Al-Salem (1993)	Ribberink (1998)
Based on	Theory	Own data	Own data and data from: King (1991) Roelvink (1988) Sawamoto et al. (1986) Horikawa et al. (1982)	Data from: Katopodi et al. (1994) Ramadan (1994) Ribberink & Al Salem (1994) Nnadi et al. (1992) King (1991) Van den Berg (1986) Sawamoto et al. (1986) Guy et al. (1986) Horikawa et al (1982)
Experimental conditions		Small scale lab experiments Purely oscillatory flow Sand: D_{50}=0.20 mm (all sheet flow)	Small and full scale laboratory exp. Purely oscillatory flow Sand: D_{50}=0.2-1.10 mm θ_{max}=0.1-1.8	Small and full scale laboratory and field exp. Steady, oscillatory and combined wave-current flow Sand: D_{50}=0.13-3.8 mm θ_{max}=0.03-8

Table 2.5: Experimental conditions and data used to derive transport models.

2.8.1 Quasi-steady models

Bailard (1981)

Bailard's model is based on an adaptation of the theoretical energy consideration derived by Bagnold (1963). Bagnold assumed that the sediment transport rate is proportional to the available fluid power, i.e. the product of the absolute value of the fluid shear stress and the velocity. The available fluid power is equal to the whole fluid energy dissipated into heat. The power expended in transporting the bed and suspended load is only a portion of the total available fluid power, therefore Bagnold used efficiency factors, resp. ε_b and ε_s. Bailard used this concept to derive a total load transport model in case of oscillatory flow. The model predicts the net transport rate (in volume of solids per unit time per unit width [m^2/s]) in case of a time–varying flow over an arbitrary sloping bottom, resulting in:

$$q_t(t) = q_b(t) + q_s(t) \tag{2.13}$$

In which:				
	q_t	=	total transport rate	(m^2/s)
	q_b	=	bed-load transport rate	(m^2/s)
	q_s	=	suspended transport rate	(m^2/s)

$$q_b(t) = \frac{\rho c_f \varepsilon_b}{(\rho_s - \rho) g \tan\varphi}\left[|u(t)|^2 u(t) - \frac{\tan\beta}{\tan\varphi}|u(t)|^3\right] \tag{2.14}$$

$$q_s(t) = \frac{\rho c_f \varepsilon_s}{(\rho_s - \rho) g W_s}\left[|u(t)|^3 u(t) - \frac{\varepsilon_s}{W_s}\tan\beta|u(t)|^5\right] \tag{2.15}$$

In which:				
	ρ	=	density of water	(kg/m^3)
	ρ_s	=	density of sediment	(kg/m^3)
	c_f	=	friction factor	(-)
	W_s	=	fall velocity of sediment	(m/s)
	g	=	gravity acceleration	(m/s^2)
	ε_b , ε_s	=	efficiency factors for resp. bed- and suspended load	(-)
	φ	=	angle of internal friction of sediment	(-)
	tanβ	=	bed slope	(-)
	u(t)	=	instantaneous near-bed velocity	(m/s)

In case of a horizontal bed tanβ will be zero and the second terms on the right-hand side of Eq. (2.14) and Eq. (2.15) are zero. For on-offshore sediment transport, Bailard found values for the efficiency factors of ε_b=0.1 and ε_s=0.02. Bailard does not specify an expression for the friction factor c_f. In case of an oscillatory flow, caused by waves only, the wave friction factor of Jonsson (1966) can be used (c_f=½f_w). To calculate the wave friction factor a roughness height equal to D_{50} is applied.

Al-Salem (1993)

Al-Salem (1993) derived an empirical sediment transport model, based on a relation between the dimensionless transport parameter q_s/W_sD_{50} and the dimensionless flow parameter $u^*(0.5f_w)^{1/2}/W_s$. Based on his own data, Al-Salem chose a third order velocity moment in his description for the net transport rate, which can be written as follows;

$$\frac{\langle q_s \rangle}{W_s D_{50}} = A\left(\frac{\sqrt{\frac{1}{2}f_w}}{W_s}\right)^3 \langle u^3(t) \rangle \tag{2.16}$$

In which	$<q_s>$	=	wave averaged transport rate	(m^2/s)
	W_s	=	fall velocity of the sediment particles	(m/s)
	D_{50}	=	median grain diameter	(m)
	f_w	=	wave friction factor	(-)
	u(t)	=	free-stream velocity	(m/s)
	A	=	constant	(-)

Al-Salem carried out his experiments in a Large Oscillating Wave Tunnel and used a median sand diameter of 0.21 mm. The transport model was calibrated with different data sets in order to obtain a value for constant A. Most data were obtained from oscillating water tunnel experiments (see Table 2.5), except for the experiment conducted by Roelvink. This experiment was carried out in a wave flume. After calibration, Al-Salem found a value of A=5. After more experiments in the LOWT, Ribberink and Al-Salem (1994) suggested a different value for constant A. After curve fitting they found a value of A=4.

Ribberink (1998)

Ribberink derived a bed-load model assuming that transport of sediment will occur when the actual time-dependent bed shear stress is larger than the critical bed shear stress. Ribberink considers all transport in the sheet flow layer as bed-load transport. The bed shear stress and the critical bed shear stress are expressed in terms of the Shields parameter (see Eq. 2.3) in the following expression for the transport rate:

$$q_s(t) = m\sqrt{(s-1)gD_{50}^3}\left(|\theta(t)| - \theta_{cr}\right)^n \frac{\theta(t)}{|\theta(t)|} \qquad (2.17)$$

In which:	θ_{cr}	=	critical Shields parameter	(-)
	$\theta(t)$	=	time-dependent Shields parameter	(-)
	s	=	relative density (ρ_s/ρ)	(-)
	m,n	=	empirical coefficients	(-)

The values of the coefficients m and n are based on data of laboratory and field experiments in steady and oscillatory flow, with the Shields parameter varying between 0.1 and 2 for oscillatory flow. After curve fitting the following values for m and n were found: m=11, n=1.65. The value of the critical Shields parameter is a function of the non-dimensional grain-size, expressed as:

$$\theta_{cr} = f(D_*) \quad with \quad D_* = D_{50}\left[\frac{g(s-1)}{\nu^2}\right]^{1/3} \qquad (2.18)$$

In which:	D_*	=	non-dimensional grain size	(-)
	ν	=	kinematic viscosity of water	(m^2/s)

The value of the Shields parameter is calculated using the friction factor of Swart (see Eq. 2.4) for oscillatory flow. For calculating the friction factor the roughness height k_s is needed. Ribberink included the value of the Shields parameter in an expression for k_s to account for the larger roughness heights in sheet flow conditions. The expression for the roughness height in oscillatory flow reads:

$$k_{s,w} = \max\left\{D_{50}; D_{50}\left[1 + 6\left(\langle|\theta|\rangle - 1\right)\right]\right\} \qquad (2.19)$$

In which: $<|\theta|>$ = time-averaged absolute value of the Shields parameter (-)

This means that if the second right hand term between brackets of Eq. 2.19 is used, k_s has to be calculated iteratively.

2.8.2 Semi-unsteady model

Dibajnia and Watanabe (1992)

The model of Dibajnia and Watanabe can be seen as an intermediate model between quasi-steady and unsteady models. The model derives the net transport sediment rate in a direct relation to the velocity above the wave boundary layer (a quasi-steady approach). However, a time lag effect to account for the effects of unsteadiness is included. Based on data from sheet flow experiments with 0.2 mm sand in a small oscillating water tunnel, Dibajnia and Watanabe found the following equation for the dimensionless total transport rate (Φ);

$$\Phi = \frac{\langle q_s \rangle}{W_s D_{50}} = 0.001|\Gamma|^{0.55}\frac{\Gamma}{|\Gamma|} \qquad (2.20)$$

In which:				
	$<q_s>$	=	net sand transport rate	(m^2/s)
	W_s	=	fall velocity of sediment	(m/s)
	D_{50}	=	median grain diameter	(m)
	Γ	=	dimensionless transport parameter	(-)

Dibajnia and Watanabe described the net transport rate (bed load and suspended load) as the difference between the amount of sand transported in positive and negative direction. Transport in positive direction consists of the amount of sand that is entrained and transported during the positive half wave cycle (Ω_c) and the amount of sand (entrained during the negative half wave cycle), that has not settled back to the bed during the preceding negative half wave cycle and is transported in positive direction (Ω'_t). A similar transport mechanism occurs during the negative half wave cycle, represented by the parameters Ω_t and Ω'_c These phenomena are expressed by the non-dimensional transport parameter Γ;

$$\Gamma = \frac{u_c T_c\left(\Omega_c^3 + \Omega_t'^3\right) - u_t T_t\left(\Omega_t^3 + \Omega_c'^3\right)}{\left(u_c + u_t\right)T} \qquad (2.21)$$

In which:			
	T	=	wave period (s)
	u_c, u_t	=	equivalent sinusoidal velocity amplitude for resp. the positive part and the negative part of the wave cycle (m/s)
	T_c, T_t	=	duration of resp. the positive and the negative part of the wavecycle ($T=T_c+T_t$) (s)

The parameters u_c and u_t are defined by (i=c,t):

$$u_i^2 = \frac{2}{T_i}\int_0^{T_i} u^2(t)dt \tag{2.22}$$

When the fall time of a particle is larger than T_c, part of the sand, entrained in the positive half wave cycle, will still be suspended in the flow and transported in negative direction during the succeeding negative half of the wave cycle. This unsteady effect can be indicated with ω_c, which is the ratio of the fall time of a particle and the positive part of the wave period;

$$\omega_c = \frac{t_{fall}}{T_c} \tag{2.23}$$

The fall time of a sand particle during the positive part of the wave cycle depends on the ratio of the level to which the particles are stirred up (z_s) and the fall velocity of the particles (W_s) . The fall time is given by:

$$t_{fall,c} = \frac{z_s}{W_s} = \frac{\frac{1}{2}u_c^2}{(s-1)gW_s} \tag{2.24}$$

Here, s is the relative density ($s=\rho_s/\rho$). Parameter ω_c determines if unsteady effects might occur and therefore determines the values of Ω_c and Ω'_c;

$$\omega_c \le 1 \quad \begin{cases} \Omega_c = 2\omega_c \dfrac{W_s T_c}{D_{50}} \\ \Omega'_c = 0 \end{cases} \tag{2.25}$$

$$\omega_c > 1 \quad \begin{cases} \Omega_c = 2\dfrac{W_s T_c}{D_{50}} \\ \Omega'_c = 2(\omega_c - 1)\dfrac{W_s T_c}{D_{50}} \end{cases} \tag{2.26}$$

The same is valid for the negative part of the wave cycle.

Chapter 3 Experimental set-up

3.1 Introduction

This chapter describes the experimental set-up that is relevant for this study. Section 3.2 and 3.3 describes the laboratory facility and the layout of the test section. The measuring techniques and the instruments are presented in Section 3.4. The experimental test conditions and the experimental procedures are described in the Sections 3.5 and 3.6.

3.2 Wave flume

The large wave flume (Großer Wellen Kanal) of the ForschungsZentrum Küste in Hannover has a length of 300 m, a width of 5 m and a depth of 7 m. This facility can generate different kinds of regular and irregular waves with wave heights up to 2 m and periods ranging from 2 s to 15 s. It is possible to generate random waves with different spectra.
The wave paddle is equipped with reflection compensation. By measuring the reflected waves on the wave paddle a compensation for the incoming reflected waves can be made by adapting the steering signal of the wave paddle. As a result most of the short reflected waves can be filtered out of the flume. This reflection compensation does not work for long standing waves.
At the end of the flume the bottom raises gradually with a slope of 1:6. Dissipation of the wave energy was achieved by constructing a beach profile on this sloping bottom, consisting of sand or loose stones.

A movable carriage was used along the flume to make local and spatial measurements. The carriage is equipped with a bed-profiling frame and instruments can be placed on a vertical pole that can be moved in vertical direction. Data acquisition computers connected to the different instruments can be placed on the carriage. The wave flume is equipped with wave height meters, which are placed in various positions along one side of the flume. The water that was used during the experiment was taken from a nearby waterway. Normally the water would be filtered roughly and pumped in a reservoir where the fine particles could settle. In this experiment the reservoir could not be used and therefore the water contained a lot of fine silt.

The following main axes are used throughout the report:

- x-axis, starting from the wave paddle, positive towards the beach, along the length direction of the flume
- y-axis in the cross direction of the flume, starting from the right wall (when facing the beach), positive towards the left-hand side-wall
- z-axis, positive upward, starting from the concrete bottom of the flume

3.3 Test section

A test section was created over the complete width of the concrete flume bottom. The test section consisted of a 45 m long sand bed with a thickness of 0.75 m and was situated between x=85 m and x=130 m (x = 0 at wave paddle). The general layout of the flume with the test section is schematically shown in Figure 3.1.

Raised asphalt bottoms with a length of 17.8 m were placed on both sides of the sand bed. This raised bottom was made of sand, covered with geo-textile and an asphalt layer. At 9

positions filter stones were placed within the asphalt in order to avoid high pressures underneath the asphalt layer. In both raised bottoms sand traps were constructed with a length of 1.5 m over the complete width of the flume. The sides of the traps were formed by concrete angle-elements.

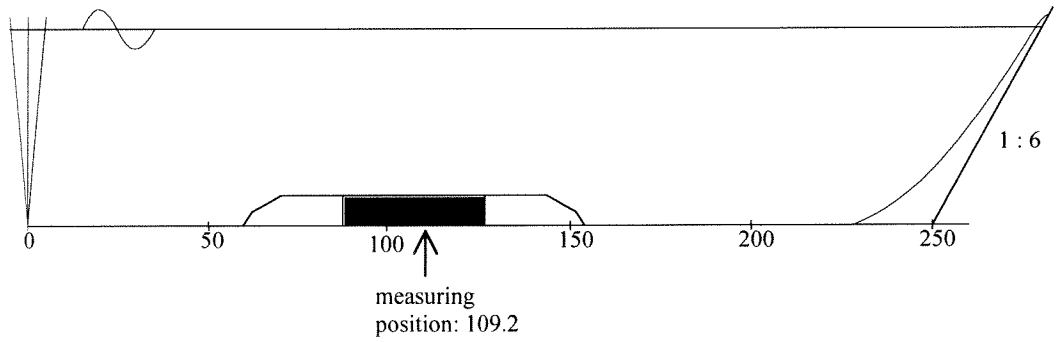

Figure 3.1: Layout wave flume.

On both sides of the raised bottoms concrete blocks were placed over a length of 7 m for the upstream section and 4.5 m for the downstream section, with a slope of 1:20. The transition with the flume bottom was made of lose, natural stones over a length of 2.5 m and a slope of 1:7. On the sloping flume bottom a beach profile was created with a slope of 1:10 to dissipate the wave energy. The beach profile begins at x = 200 m and consists of sand with a D_{50} of 0.3 mm. Figure 3.2 shows the layout of the test section, with the dimensions in m.

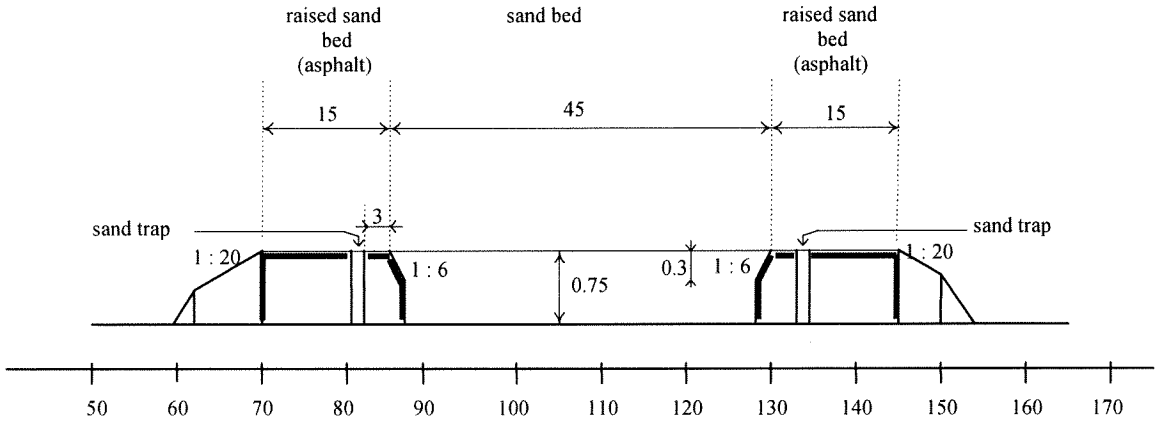

Figure 3.2: Layout test section.

The test section was made of sand with a D_{50} of 0.247 mm, narrow graded and a small content of fine material (e.g. silt<1%). In Figure 3.3 the grain size distribution of the sediment is shown. The sand had the following characteristics:

D_{10} (mm)	D_{50} (mm)	D_{90} (mm)	σ_g (-)	W_s (mm/s)
0.182	0.247	0.305	1.14	34.6

Table 3.1: Characteristics of experimental sand.

In which: D_{10} = diameter, 10% by weight is finer
D_{50} = diameter, 50% by weight is finer
D_{90} = diameter, 90% by weight is finer
σ_g = geometric standard deviation = $\frac{1}{2}*(D_{50}/D_{16} + D_{84}/D_{50})$
W_s = settling velocity of a grain with a diameter equal to D_{50}

The settling velocity is determined according to Van Rijn (1993), which derived the following formula for the settling velocity of natural grains:

$$w_s = \frac{10\nu}{D}\left(\sqrt{1+\frac{0.01(s-1)gD^3}{\nu^2}}-1\right) \qquad \text{for} \quad 0.1\text{mm} < D < 1.0\text{mm} \qquad (3.1)$$

In which:				
	W_s	=	settling velocity of a single grain in still water	(m/s)
	s	=	relative density ($s=\rho_s/\rho$)	(-)
	ρ_s	=	density of sediment	(kg/m^3)
	ρ	=	density of water	(kg/m^3)
	g	=	gravity acceleration	(m/s^2)
	D	=	grain diameter of a particle	(m)
	ν	=	kinematic viscosity of water	(m^2/s)

The sand is comparable with sand used in some wave tunnel experiments (Al-Salem, 1993; Ramadan, 1994; Katopodi et al., 1994; Janssen en Van der Hout, 1997) which had a D_{50} of 0.21 mm and a geometric standard deviation of 1.3.

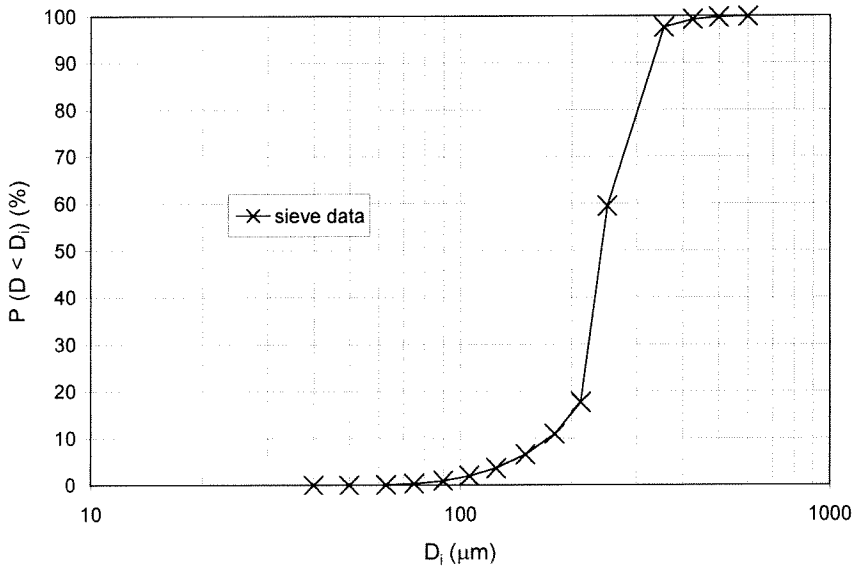

Figure 3.3: Grain size distribution.

3.4 Measuring techniques and instruments

3.4.1 Measured parameters

Various parameters were measured during these experiments. This report focuses on the following parameters:

- near-bed horizontal velocities U(z,t), just outside the boundary layer
- bed level height $z_t(x)$ of the test section
- underwater weight (G) of the trapped sediment
- time-dependent wave heights H(z,t) and periods T(t) at various positions along the flume

From the measured bed level along the test section the following parameters can be derived:
- dimensions of the bedforms and steepness of the bed
- net time-averaged sand transport rates $<q_s>$
- sand loss from the test section

3.4.2 Overview instruments

Four universities participated in the experiment, each of them using different instruments. To give some insight in the kind of data that was collected, a list of used instruments is given in Appendix A.. An overall set-up of the instruments is given in Figure 3.4.
The University of Florida (UF) and the University of East Anglia (UEA) used instruments mounted on frames along both sides of the flume wall. The University of Florida also had a profiler mounted on the profiling frame of the carriage. The University of Twente (UT) and the University of California Santa Barbara (UCSB) used instruments mounted on the pole of the carriage and one was buried in the sand bed. A third frame was supplied by the Grosser Wellen Kanal (GWK). An overview of the instruments is given below:

1) The UF-frame, attached to the right-hand side-wall, was equipped with optical and acoustic instruments to measure suspended sediment concentrations, flow velocities and bedform characteristics.
2) The UEA-frame, attached to the left-hand sidewall, was equipped with an acoustic instrument to measure suspended concentrations profiles and profiles of horizontal and vertical flow velocity and was equipped with an electromagnetic flow meter (EMF) to measure flow velocities in a single point.
3) A Transverse Suction System (TSS) and Acoustic Doppler Velocimeter (ADV) were mounted on the vertical pole of the measuring carriage. The TSS is used to measure vertical time-averaged suspended sediment concentration profiles. The ADV is used to measure near-bed velocities and records the level underneath the ADV, close to the CCM.
4) A Conductivity Concentration Meter system (CCM), installed in a waterproof tank and buried under the sand bed, is used to measure concentrations and grain velocities in the sheet flow layer.
5) A Rotating Scanner Sonar (RSS) attached to the sidewall is used to measure bedform characteristics over a circular area (∅ 5 or 10 m) of the sand bed.
6) A vertical array of 4 Electro Magnetic Flow meters (EMF) and 3 Acoustic Doppler Velocimeters (ADV), attached to the sidewall is used to measure velocities in different positions above the bed.
7) A Multiple Transducer Array (MTA), mounted on a bed profiling frame hanging under the carriage, is used to profile the bed along the test section.

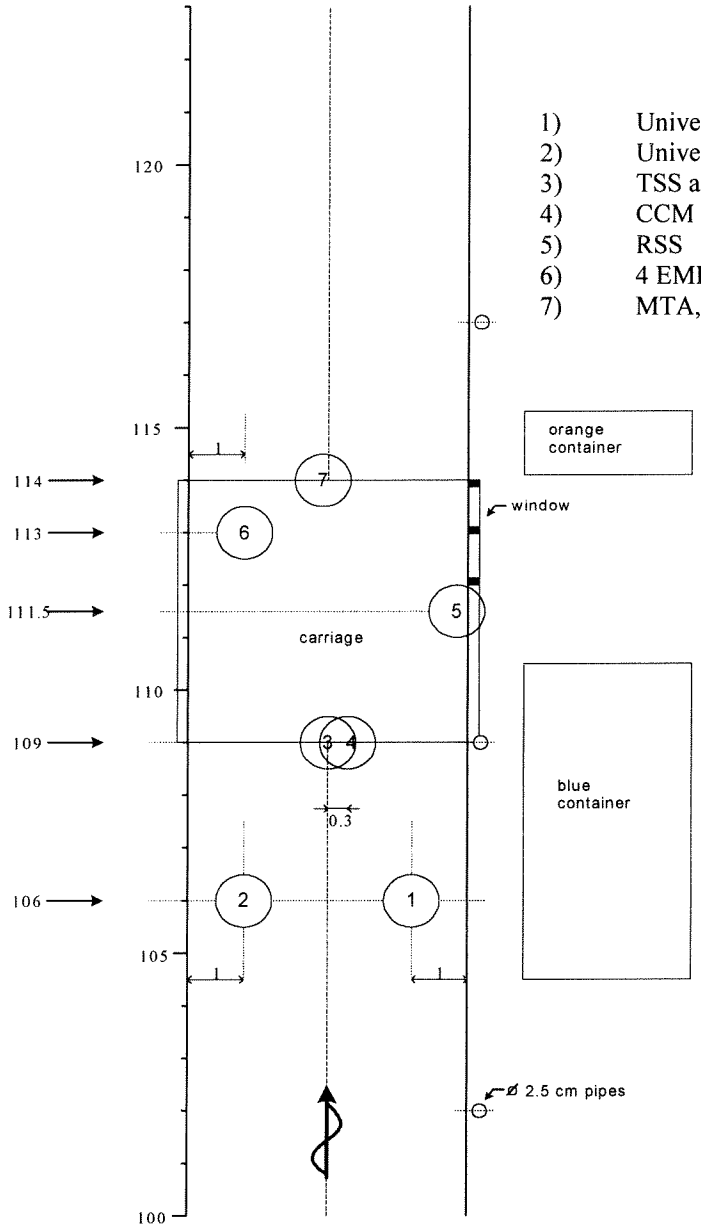

Figure 3.4: Instrument set-up in the wave flume.

For this study not all available instruments were used. To measure bed level heights along the test section a Multiple Transducer Array (MTA), mounted on the bed-profiling frame of the carriage is used. The bottom transport is trapped with the sand traps. To measure the horizontal velocities just outside the wave boundary layer, an acoustic Doppler velocity meter (ADV) on the pole is used. To check the wave heights and periods along the test section, the wave height meters were used.

The parameters that are discussed in Section 3.4.1 were measured by different instruments, an overview of the measuring instruments and techniques is given in Table 3.2. The used instruments and techniques will be discussed in more detail in the following sections.

calculating/measuring	technique/instrument
net transport rates along the test section	mass conservation technique
height of the bed level $z_t(x)$ along the test section, measured after each test	Multiple Transducer Array
underwater weight of the trapped sediment, measured after each test	sand trap
time-series (for each run about 7 intervals with a duration of 1-3 minutes each) of horizontal flow velocities U(z,t) at a single point (usually somewhere between 3 cm and 12 cm above the bed, in the middle of the flume) and bed level z_b underneath the ADV , before and after the test (without wave motion) and about 6 times during each half-hour run (with wave motion)	Acoustic Doppler Velocity meter
time-series of wave heights H(z,t) and periods T(t), at 22 positions along one side of the test section	Wave Height Meters

Table 3.2: Overview measuring instruments and techniques.

3.4.3 Mass-conservation technique

Large Oscillating Wave Tunnels (LOWT) have the possibility to apply a mass-conservation technique to estimate the time or wave-averaged sediment transport rates in the test section. This means that the volume of sand collected in the sand traps must be equal to the change of volume in the test section during the tunnel run. By solving a continuity equation (see Eq. 3.2), starting from the left or the right sandtrap of the wave tunnel the net transport rate distribution can be calculated.

During the present experiment it was tried to apply the mass-conservation technique in the wave flume, using the sandtraps. It was found that the mass-conservation technique could not be applied the same way it was applied for the wave tunnel. The reason for this was that the sand traps did not function well, only a small portion of the sand transported out of the test section was caught by the trap. Therefore, the results of the weight measurements were too inaccurate.
Because it was observed that no sand passed the upstream boundary of the test section (no sand was found in or upstream of the sand trap), it was possible to apply the mass-conservation technique for the upstream sandtrap. As a result the continuity equation can only be solved, starting from a location, upstream of the test section. The net sediment transport rate q_s (without pores) can be described using the continuity equation (see Eq.3.2). In Figure 3.5 the net transport calculation parameters are schematically shown.

$$q_s(x+\Delta x)\cdot W = \left(q_s(x) - \frac{\Delta x \cdot \Delta z}{\Delta t}(1-\varepsilon_0) \right) W \qquad (3.2)$$

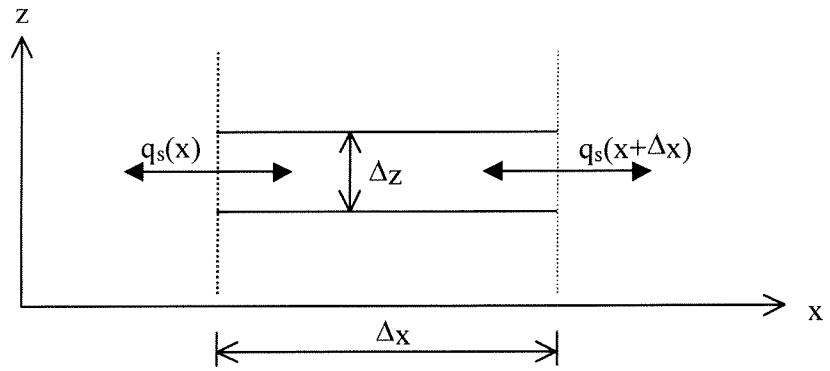

Figure 3.5: Net transport calculation parameters.

In which:				
	q_s	=	total net sand transport per unit width	(m^2/s)
	Δx	=	step size	(m)
	Δz	=	difference in bed level height between two tests	(m)
	Δt	=	duration of a test	(s)
	x	=	length co-ordinate, with axis beginning upstream of the test section, positive towards the beach	(m)
	ε_0	=	porosity of the bed	(-)
	W	=	width of the flume	(m)

To solve the continuity equation an upstream boundary condition for the transport rate q_s is needed.
Because it was found that no sand was trapped in the upstream sand trap and no sand was detected upstream of this trap, the boundary condition of the continuity equation can be described as:

at x = 0: $q_s(0) = 0$

In case of a working sand trap, this transport rate could be known from the quantity of sand, trapped in the upstream sand trap. The trapped volume of sand (ΔV per unit width [m^3/m]) can be determined from the difference in weight measured with the sand trap before and after the test. For the start value of the continuity equation this means:

at x = 0: $q_s(0) = -\Delta V(1-\varepsilon_0)/\Delta t$

When $q_s(x)$ is known, $q_s(x+\Delta x)$ can be calculated using the continuity equation. For this purpose the change in bed level height along the test section ($\Delta z(x)$) must be known. In this way the whole test section can be evaluated and as a result the distribution of the net transport rate along the test section is known. The parameters Δx and $\Delta z(x)$ are both determined from the bed level height data, recorded with the MTA. The MTA and the sand traps will be discussed here.

MTA

A Multiple Transducer Array was used to profile the bed. The transport rates were calculated from the difference in bed level between two bed profiles, measured before and after a test. The MTA was mounted on a frame, hanging under the movable carriage. The frame, which could be lowered by hand, was lowered to a predetermined level such that the distance between the MTA and the flume bottom was about 1.15 m, this means a distance of 0.40 m between the top of the sand bed and the MTA. The level of the MTA was fixed by 2 steel cables, which connected the bed-profiling frame to the carriage.
The measurement range of the MTA is from about 1 m below the MTA to about 0.1 m below the MTA. Therefore the MTA was not able to measure the sand bed that lay at a level below 0.1-0.2 m above the flume bottom.

The MTA consists of a plate with dimensions l*w*h=64*10*1.5 cm, that holds 32 transducers. The spacing between the transducers is 2 cm. Every 0.6 s an acoustic pulse is sent out. The return signals are picked up by the transducers and sent to a laptop standing on the carriage. A schematic picture of the MTA is shown in Figure 3.6.

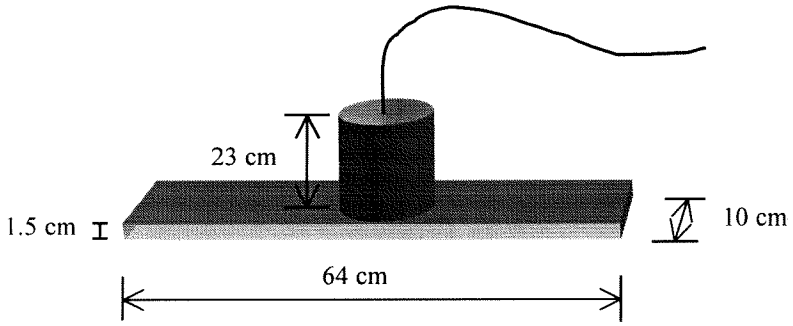

Figure 3.6: Dimensions of the MTA.

It was decided to rotate the MTA with an angle of 45 degrees, oriented in a horizontal plane with the x-direction of the flume (according to the main axis definition, see Section 3.2). This was done to survey the sand bed around the CCM (which was located in the sand bed at y=2.15m and x=109.2m) and underneath the TSS (y=2.50m) and the ADV (y=2.25m), both mounted on the movable pole.
As a result the transducers are shifted in x and y-direction and the MTA measures the bed in a 43.8 cm wide strip, with a transducer spacing of 1.41cm in lateral and longitudinal direction of the flume (see Figure 3.7). The MTA was positioned 0.18 m off centre from the middle of the flume. As a result the first transducer is located at y=254.24 cm, the last transducer is located at y=210.40 cm. The total width of the wave flume is 5 m, it is clear that only a part of the test section in cross direction is measured.

To measure the bed profile the carriage was moved along the flume with a speed of 6.5 m per minute or 0.108 m/s. This means that each transducer measures the sand bed with 0.065m intervals.

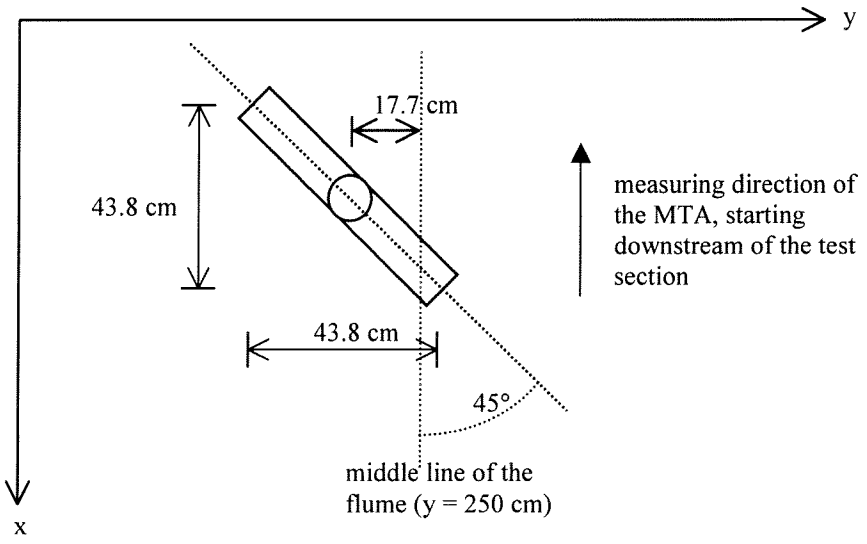

Figure 3.7: Placement of the MTA.

Sand trap

The bed-load transport was supposed to be measured using the bed profiles and the downstream sand trap. In the sand trap downstream of the test section a container was installed (l*w*h=0.8*0.6*0.6 m^3), about 0.1 m outside the centreline of the flume. Figure 3.8 shows the dimensions of the downstream sand trap and the installed container.
The trapped sediment is weighed after each test. With the measured difference of the underwater weight of the trapped sediment between measured before and after a test, the volume of the sediment and thus the bed-load transport can be calculated.
In the raised asphalt bottoms on both sides of the test section sand traps were constructed, downstream of the test section between x=80.5 m and x=82 m and upstream of the test section between x=133 m and x=134.5 m. Both sand traps cover the total width of the flume and have a length of 1.5 m.

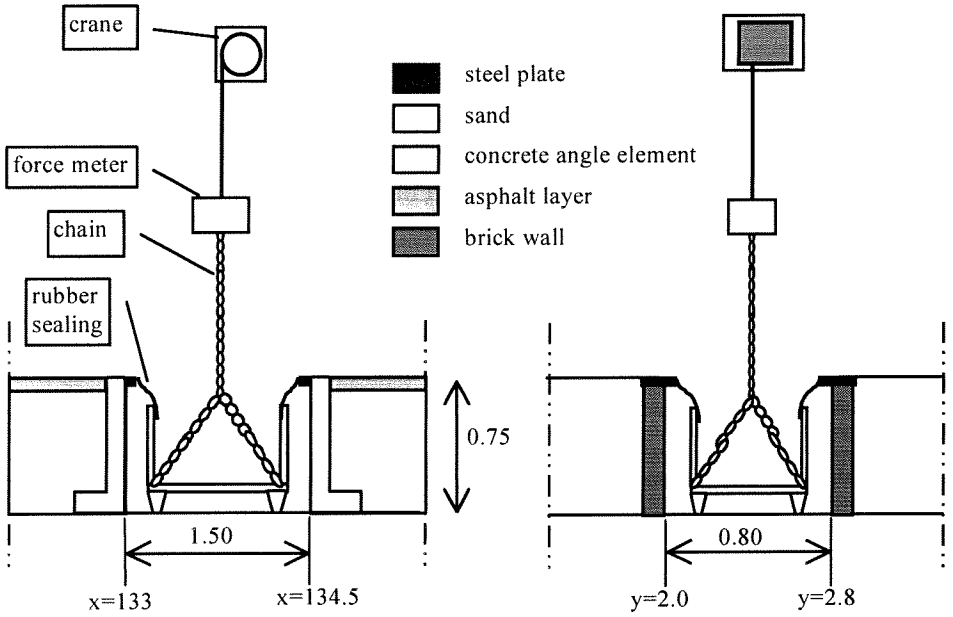

Figure 3.8: Dimensions of the downstream sand trap.

The container was standing loose on the flume bottom and could be lifted about 15-20 cm with a chain attached to a movable crane. To prevent sand coming underneath the container from the sides, two brick-walls are constructed across the trap, at each side of the container. The sealing between the container and the sidewalls of the traps and the two brick walls is made by some flexible rubber. The brick walls are equipped with filter stones to let water flow in, when the container is raised. A force meter measured the underwater weight of container and sediment.

It was found that the results of the sand trap weighing were very inconsistent and difficult to interpret. This was probably caused by the construction of the chain to the container. One long chain was connected to four short chains, which in turn were connected to the four corners of the container. During a test, sand entered the container from the upstream side and accumulated in the container. The accumulated sand was not spread out evenly over the container bottom and as a result the container may have been out of balance. In that case part of the container may have maintained in contact with the flume bottom when it was lifted, making a correct weighing of the container impossible.

Later it was found that a lot of sand that was supposed to be trapped with the container, passed the sandtrap. As a result it was not possible to measure a realistic bed-load transport rate using the sand trap. Therefore the sand trap results are not included in this study. As a consequence, the net transport rates can only be determined starting from the upstream end of the test section.

3.4.4 Near-bed velocity measurements with ADV

An acoustic Doppler velocity meter was used to measure the near-bed velocity outside the wave boundary layer. The ADV measures 3D velocities in a small sampling volume, which is located about 0.06 m below the probe tip. With the probe tip about 0.1 m above the bed it is possible to measure velocities in relatively high sediment concentrations.

The ADV probe consists of three receive transducers that record the returned scattered signal sent by a transmit transducer (see Figure 3.9). It samples the velocities with 25 Hz by measuring the frequency shift between the sent and the received signal, caused by the moving sand particles.
The ADV is mounted on the vertical pole of the carriage, together with the transverse suction system. The ADV was positioned 0.25 m off the centreline of the flume at y=2.25 m (according to the main axis definition, see Section 3.2). The carriage was positioned in such a way that the ADV was located at x=109.2 m. The vertical position of the pole can be adjusted by hand. To reduce the movement of the pole due to wave action during the tests, the pole was fixated with 4 steel wires, attached to the fence of the wave flume and the lower end of the pole.

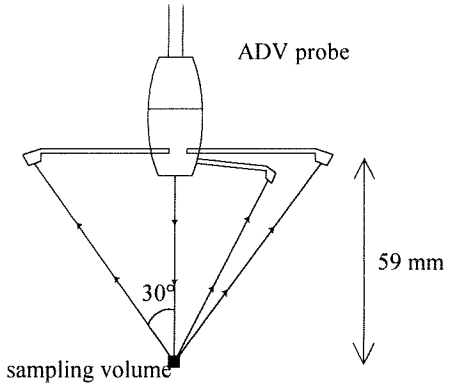

Figure 3.9: Probe tip and sampling volume of the ADV

The height of the sampling volume above the bed is checked with the ADV itself. The ADV is able to detect the boundary (the bed), outside the sampling volume by sending pulses and recording the return signal. The distance between the probe tip and the top of the sand bed underneath the ADV (δ_{ADV}) can be read from a laptop that was standing on the carriage.

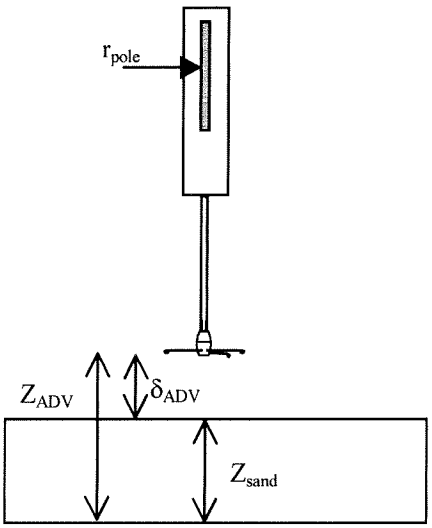

Figure 3.10: Definition of parameters in order to determine the bed level height underneath the ADV.

Also the height of the ADV probe tip above the concrete flume bottom (Z_{ADV}) was determined by reading out a mm-scale on one side of the pole (r_{pole}), in this way the height of

the level of the sand bed can be determined. This was measured to determine the level of the CCM relative to the sand bed, during a run. Also before and after a run the height of the bed level is determined. These measurements can be used to check the height of the profiles taken with the MTA. Figure 3.10 shows the definition of the parameters in order to determine the bed level height underneath the ADV.

The bed level height can be determined from the measured parameters in the following way:

$$\begin{cases} Z_{ADV} = 222.0 - r_{pole} \\ Z_{sand} = Z_{ADV} - \delta_{ADV} \end{cases} \tag{3.3}$$

All parameters are in cm. The determined bed level height can be compared with the bed level height, measured with the MTA.

3.4.5 Wave height measurements with WHM

The Wave Height Meters measure the water surface elevation and the wave periods in different positions along the wave flume in order to check the uniformity of the wave conditions along the test section and to determine the wave reflection from the beach. The wave height meters were placed in groups of four or five along one side of the flume, 22 in total.
The wave height, measured with the wave height meters, is sampled with 100 Hz, using the GWK data acquisition computer.

3.5 Test conditions

During the experiment different wave conditions were studied. The first 7 weeks of the experiment were focussed on development and equilibrium in bedforms as well as the suspension processes that were involved. The following conditions were studied:

- Regular waves: asymmetrical
- Irregular waves: groups, random and bimodal

During the last 2 weeks the experiment was focussed on sheet flow processes under non-breaking waves. The following conditions were studied:

- Regular waves: asymmetrical, with periods of 6.5 and 9.1 s and wave heights in the range 1.1-1.7 m
- Irregular waves: natural groups, with peak periods of 6.5 and 9.1 s and significant wave heights of 0.9 and 1.0 m

The natural wave groups are formed by a very narrow-distributed Jonswap spectrum (γ=10), with groups that consisted of 10-15 waves. Also a few tests were carried out under random (also with Jonswap spectrum) and "natural" wave conditions. The natural wave conditions consisted of a reproduction of a time series of surface elevations, measured in the field.

For the present study four different conditions with monochromatic waves are used. The water level was 4.25 m above the flume bottom during all conditions. This means a water level of 3.50 m above the sand bed. The duration of all tests was set at 30 minutes.

Condition	T (s)	H (m)	U_{rms} (m/s)	N	h (m)
me	9.1	1.5	0.75	6	3.50
mf	9.1	1.3	0.65	6	3.50
mh	6.5	1.6	0.75	4	3.50
mi	6.5	1.35	0.63	4	3.50

Table 3.3: Test conditions for present experiment.

In which:

T	=	wave period
H	=	wave height at the wave paddle
U_{rms}	=	root-mean square velocity near the bottom according to linear wave theory
N	=	number of tests
h	=	water depth above the sand bed

These asymmetric waves are "Corrected Shallow Water Trochoidal (CSWT) waves. The conditions were chosen in such a way, that they could be compared with the conditions used by Al-Salem (1993).

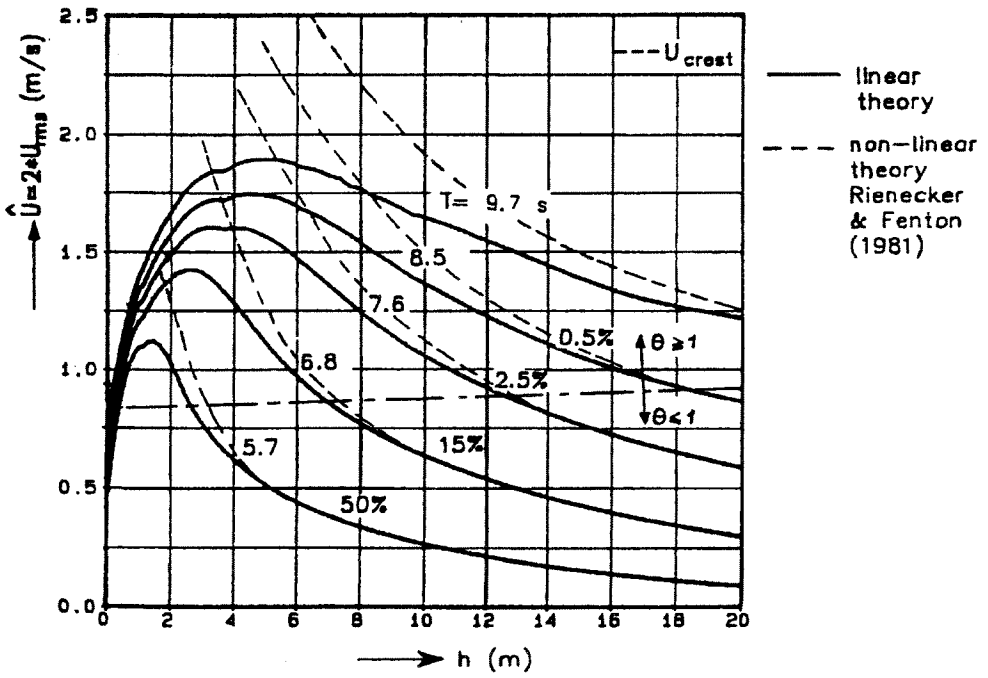

Figure 3.11: Significant wave height and near-bed orbital velocity amplitude as a function of water depth (Al-Salem, 1993; Janssen, 1995).

Al-Salem estimated relevant wave conditions and near-bed orbital velocity conditions for the Dutch coastal zone. Computations were carried out with a one-dimensional wave energy decay model (ENDEC, Battjes and Stive, 1985). Linear wave theory is applied for the computation of the near-bed orbital velocity amplitudes. To estimate the wave asymmetry the non-linear streamfunction theory of Rienecker and Fenton (1981) is applied.
A measured (North Sea) wave climate with (spectral peak) wave periods ranging between 5 and 10 s is used as an offshore boundary condition for the ENDEC computations.

Figure 3.11 shows the computed behaviour of the significant wave height with their waveheight exceedance percentages and the near-bed orbital velocity amplitude as a function of the local water depth. It can be observed that outside the surfzone the near bed orbital velocity increases because the waterdepth decreases. Inside the surfzone the waveheight will strongly decrease due to wave breaking. Here the near-bed velocity reaches a maximum, which is followed by a decrease until the shoreline.

The deformation of the near-bed orbital velocity amplitude as caused by wave asymmetry is also visualised in Figure 3.11. The onshore directed crest velocity U_{cr} (based on the non-linear theory of Rienecker and Fenton, 1981) deviates from the linear result for decreasing water depth. For example, the asymmetry of waves with a period of 6.8 s starts to become important for a waterdepth h < 9-10m. The computed degree of asymmetry r ($U_{cr}/(U_{cr}+U_{tr})$) varies in the range 0.5–0.7.

In this figure also a line is added representing the value of the Shields parameter of $\theta \approx 1$, to indicate roughly in which conditions sheet flow will occur (see Janssen, 1995). The Shields parameter (see Eq. 2.3) is calculated for a median grain diameter D_{50} of 0.2 mm. The wave friction factor for oscillatory flow was derived with the expression of Swart (see Eq. 2.4), in which the roughness height k_s has a value of $2.5*D_{50}$. This points out once more the relevance of sheet flow conditions. Although the probability of occurrence for larger waves that cause sheet flow conditions is rather low, they are still relatively important for the sand transport. This is explained by the fact that that the sand transport is proportional to a power larger than

one. As a result the larger velocities contribute relatively more to the total occurring sand transport.

Relevant wave conditions for the North sea can be generated in the wave flume (GWK) with following maximum velocity limits (with wave reflection compensation):

Irregular waves:	$\hat{U} < 1.0$ m/s
Regular waves:	$\hat{U} < 1.7$ m/s

Al-Salem (1993) carried out a number of experiments in the Large Oscillating Wave Tunnel (LOWT), applying monochromatic asymmetric oscillatory velocities. Most of the tests consisted of wave conditions with near-bed root-mean square velocities in the range 0.5-0.9 m/s and periods of 6.5 s or 9.1 s. In order to compare these results, the present experiment consists of asymmetric monochromatic waves with the same periods, similar near-bed velocities and a similar degree of wave asymmetry. Most LOWT measurements under sheet flow conditions were performed with a flat bed in order to minimise the effect of flow separation and vortex shedding. In a wave tunnel it is possible to flatten the bed after each test. This is not really possible in a wave flume without emptying the flume, it would take 9-11 hours to drain, flatten and refill the flume. From the LOWT experiments it is known that large asymmetric near-bed velocities help to keep the bed flat. This can be achieved by applying large wave heights with low water depths.

The duration of a run was based on the following considerations:

- For the net transport rate measurements sufficient sand must have been transported in order to be able to measure it. This would plea for as long a duration as possible. However, in order to get more than one estimate of the net transport rate, the bed should be measured several times for one condition. This can be achieved by relative short runs, in between which the bed profile can be measured.
- The minimum duration of a run is determined by the measurements with the CCM (Dohmen-Janssen, 2000). It was found that about 100 waves were needed. This corresponds to 11-15 minutes.
- The duration of a run is further limited by the requirement to check the instruments, their elevation above the sand bed and the level of the sand bed around the instruments. This can only be done between two runs. Some instruments recorded data with very large resolutions. These data files, recorded during one run could become too large for the data acquisition computers.

Based on these considerations a run duration of half an hour was selected. The number of runs per condition were determined by the CCM measurements and the net transport measurements. To achieve a certain statistical accuracy for a condition, the conditions have to be repeated 3-5 times. For the CCM-measurements about 1200 waves are needed for one condition. This corresponds to 4 runs for condition mh and mi, both with a period of 6.5 s or 6 runs for condition me and mf, both with a period of 9.1 s.

3.6 Experimental procedures

The experimental procedure for each condition was the same. The procedures for the measurements were as follows:

Bed profiling procedure
- The carriage is moved to the starting position of the bed level measurement, downstream of the test section. The bed-profiling frame with the MTA is lowered. The data acquisition software on the laptop on the carriage, connected with the MTA, is started.
- The carriage moves along the flume with a velocity of 6.5 m/min., the MTA profiles the bed with a stepsize of 6.5 cm.
- When the end position is reached, the data acquisition and the carriage are stopped and the bed-profiling frame is being raised.
- The carriage is moved back to the measuring position at x = 109.2 m.

Profiling procedure scour hole
- After the carriage returned to the measuring position at x = 109.2 m, the MTA is lowered again to measure the scour hole and the bed level near the CCM in more detail. After raising the MTA, the pole with the ADV is lowered and the steel wires are being attached again.

Weighing procedure container
- The crane is moved to the downstream sand trap at x = 133.8 m. The chain of the container, hanging at the side of the flume wall is hooked to the crane. The crane is placed directly over the sandtrap. The middle of the sandtrap is determined with a marked line, suspended across the flume.
- The container is lifted 10-15 cm in order to measure the weight.

Test procedure
- The movable pole with the ADV is lowered, using the ADV to measure the height above the bed, until the desired height above the bed is reached.
- The steel wires attached to the pole, are fastened to the side fences of the flume, fixing the pole at the desired level.
- The data cable from the carriage is connected with the data acquisition computer in the container
- Data acquisition is started in the container next to the test section and the GWK operators, in an office near the wave paddle, are being signalled by telephone to start the wave paddle.
- After 30 minutes the test ends and the data acquisition computers are stopped.
- The four steel wires, connecting the pole to the fences of the flume, are being detached and the pole is raised
- The data cable from the carriage to the container is disconnected

Procedures in following order

Before starting the first test of the experiment the test section was flattened by hand and filled with water in approximately 6 hours. First, the water level was raised carefully until it reached a level of 10-15 cm above the bed in order to prevent the water flowing too fast over the test section. After this the water level was raised till it reached a level of 3.5 m above the testsection.

- The bed is profiled (see bed profiling procedure)
- The container in the sand trap is weighed (see weighing procedure container)
- The first test is carried out (see test procedure)
- The bed is profiled (see bed profiling procedure)
- The scourhole underneath the ADV, transverse suction system and the bottom level near the CCM are measured with the MTA (see profiling procedure scour hole)
- The container in the sand trap is weighed (see weighing procedure container)
- The second test is carried out (see test procedure)
- The bed is profiled (see bed profiling procedure)
- The scourhole beneath the ADV, transverse suction system and the bottom level near the CCM are measured with the MTA (see profiling procedure scour hole)
- The container in the sand trap is weighed (see weighing procedure container)
- The third test is carried out, etc. After the last test, the bed is profiled (see bed profiling procedure), the scourhole is measured with the MTA (see profiling procedure scour hole) and the container in the sand trap is weighed (see weighing procedure container).

Water level is lowered and the test section and the rest of the flume is inspected.

Chapter 4 Experimental results

4.1 Introduction

The experimental data used in this study consisted of four different conditions. For each condition several tests were carried out. In this chapter the following results for each condition will be presented:

- near-bed velocities, outside the wave boundary layer (Section 4.2)
- measured bed level height of the test section (Section 4.3)
- time-averaged sand transport rate distribution of the test section (Section 4.4)

The time-averaged sand transport rate is calculated from the measured bed level height. The measured bed-level height is also used to obtain information about the bed steepness, the sand loss from the test section and the dimensions of the bedforms. In Section 4.5 a representative value for the net sand transport rate is determined. An analysis of the representative transport rate is carried out in Section 4.6. The accuracy of the results will be discussed in Section 4.7. A summary of the main results is given in Section 4.8.

4.2 Near-bed velocities

The near-bed velocities are ensemble-averaged for each test and averaged for each condition. The results for each test are given in Appendix B. As said before, the ADV measures the velocities not continuously but it also records the bed level during a test. This means that the ensemble averages are determined over a part of all the waves in a test. From the ensemble-averaged velocities, measured at approximately 0.1 m above the bed, the following parameters were determined:

T	=	average wave period over a run, determined from the wave height meters
U_{rms}	=	root-mean square value of the velocity, which includes <U>
<U>	=	time-averaged value of the velocity
U_c	=	maximum velocity under the crest of the wave
U_t	=	minimum velocity under the trough of the wave
R	=	degree of wave asymmetry

Definitions:

Root mean square velocity:
$$U_{rms} = \sqrt{\frac{1}{N}\sum_{i=1}^{N} U_i^{\,2}} \qquad (4.1)$$

In which

N	=	total number of time steps
U_i	=	discretized measured horizontal free stream velocity

U_{rms} is determined from the measured velocity time-series and also includes the time-averaged value of the velocity <U>.

Degree of wave asymmetry:
$$R = \frac{U_c}{(U_c + |U_t|)} \qquad (4.2)$$

condition	test	T (s)	U_{rms} (m/s)	<U> (m/s)	U_c (m/s)	U_t (m/s)	R (-)
me	b,c,d,e,f,g	9.10	0.68	-0.052	1.45	-0.64	0.69
mf	b,c,d,e,f,g	9.10	0.66	-0.035	1.30	-0.70	0.65
mh	b,c,d,e	6.50	0.62	-0.036	1.09	-0.72	0.60
mi	b,c,d,e	6.50	0.59	-0.045	0.98	-0.79	0.55

Table 4.1: Velocity parameters, averaged for each condition.

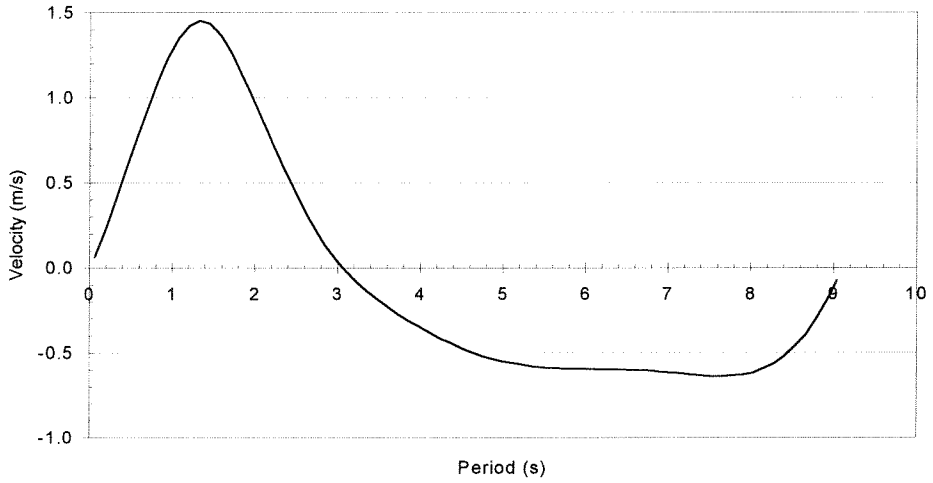

Figure 4.1: Ensemble-averaged horizontal near-bed velocity, averaged for all runs with condition me.

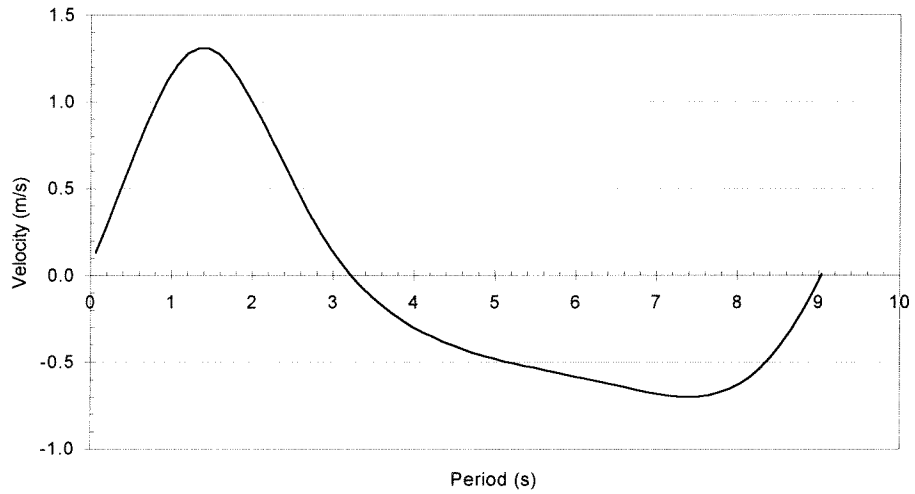

Figure 4.2: Ensemble-averaged horizontal near-bed velocity, averaged for all runs with condition mf.

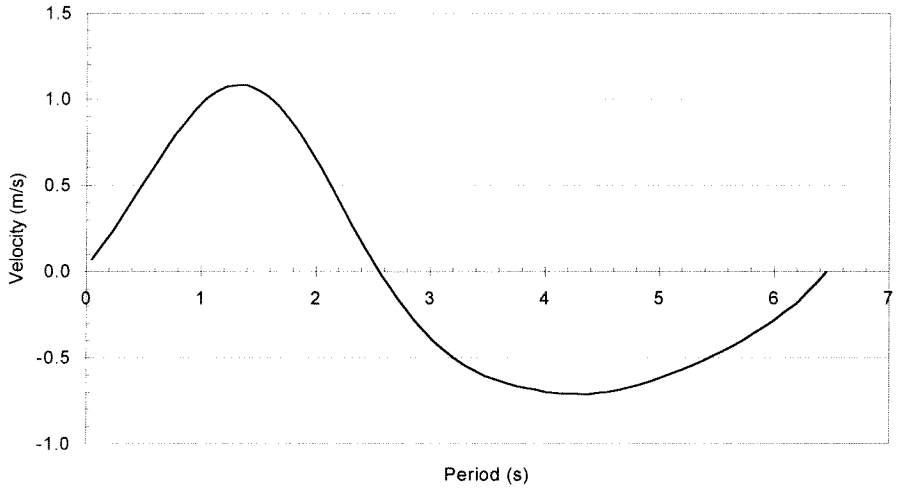

Figure 4.3: Ensemble-averaged horizontal near-bed velocity, averaged for all runs with condition mh.

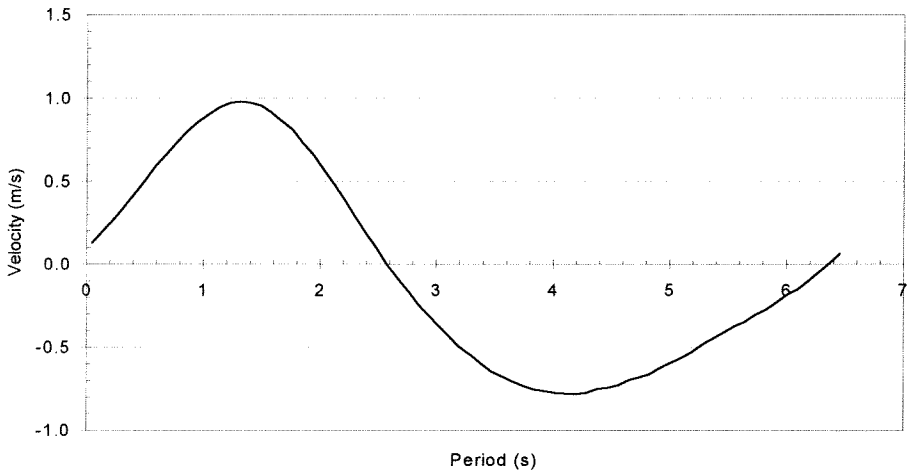

Figure 4.4: Ensemble-averaged horizontal near-bed velocity, averaged for all runs with condition mi.

The ensemble-averaged instantaneous near-bed velocities, averaged for all runs with the same condition, are shown in Figure (4.1-4.4).
Table 4.2 contains the time-averaged values of n^{th} power (n=3,4,5,6) of the velocity moments $<U^n>$, averaged for each condition. The following definition for the velocity moments is used:

n-power velocity moment:
$$< U^n >= \frac{1}{N} \sum_{i=1}^{i=N} \left(|U_i|^{n-1} U_i \right) \qquad (4.3)$$

In which:

<...>	=	time-averaged notation
n	=	power
N	=	total number of time steps

condition	test	T (s)	$<U^3>$ (m^3/s^3)	$<U^4>$ (m^4/s^4)	$<U^5>$ (m^5/s^5)	$<U^6>$ (m^6/s^6)
me	b,c,d,e,f,g	9.10	0.25	0.38	0.53	0.73
mf	b,c,d,e,f,g	9.10	0.19	0.26	0.34	0.43
mh	b,c,d,e	6.50	0.09	0.12	0.14	0.15
mi	b,c,d,e	6.50	0.03	0.05	0.06	0.06

Table 4.2: Velocity moments, averaged for each condition.

Note the low degree of wave asymmetry for condition mi, which leads to a reduction of $<U^3>$ for almost the same U_{rms}.

The thickness of the wave boundary layer ($\delta_{0.05}$) is determined to check if the free stream velocity was measured. The thickness of the boundary layer is computed with Eq.2.1. Here, the roughness height of the bed (k_s) is assumed to be equal to D_{50} as a first choice. The semi-excursion length of a water particle [$a=(a_{cr}+a_{tr})/2$] is the average value of the semi-excursion length under the crest of a wave (a_{cr}) and the semi-excursion length under the trough of a wave (a_{tr}). The level of the sampling volume of the ADV (h_{ADV}), relative to the top of the sand bed, measured before and after the run should be larger than the boundary layer thickness. From Table 4.3 it can be seen that the boundary layer thickness is about a factor 4 smaller than the level of the sampling volume of the ADV. The velocities are measured well outside the wave boundary layer.

condition	test	T (s)	a (m)	h_{ADV} (m)	$\delta_{0.05}$ (m)
me	b,c,d,e,f,g	9.10	1.33	0.100	0.022
mf	b,c,d,e,f,g	9.10	1.30	0.099	0.021
mh	b,c,d,e	6.50	1.12	0.109	0.021
mi	b,c,d,e	6.50	1.01	0.103	0.020

Table 4.3: Measured distance of sampling volume ADV above sand bed and computed thickness of the wave boundary layer.

4.3 Bed level measurements of the test section

4.3.1 Profile adjustments

In order to calculate the net transport rates the difference between two bed profiles has to be calculated. For various reasons the bed profiles were shifted in x, y and z-direction. In order to calculate the difference between two profiles in a simple way, the bed profiles are transformed to one data grid. This was done in a number of steps, each step is given below.

An example of a bed profile is given in Figure 4.5,which shows the bed level height above the flume bottom as function of the distance from the wave paddle, recorded with the MTA. The bed level height is relative to the concrete flume bottom. In the figure some features of the test section can be clearly recognised, like the sandtraps, cement blocks, upstream asphalt layer and the erosion hole and sand deposition. Note that due to the measuring range of the MTA, it was not possible to record the bottom of the sand traps, see also 4.3.1f.

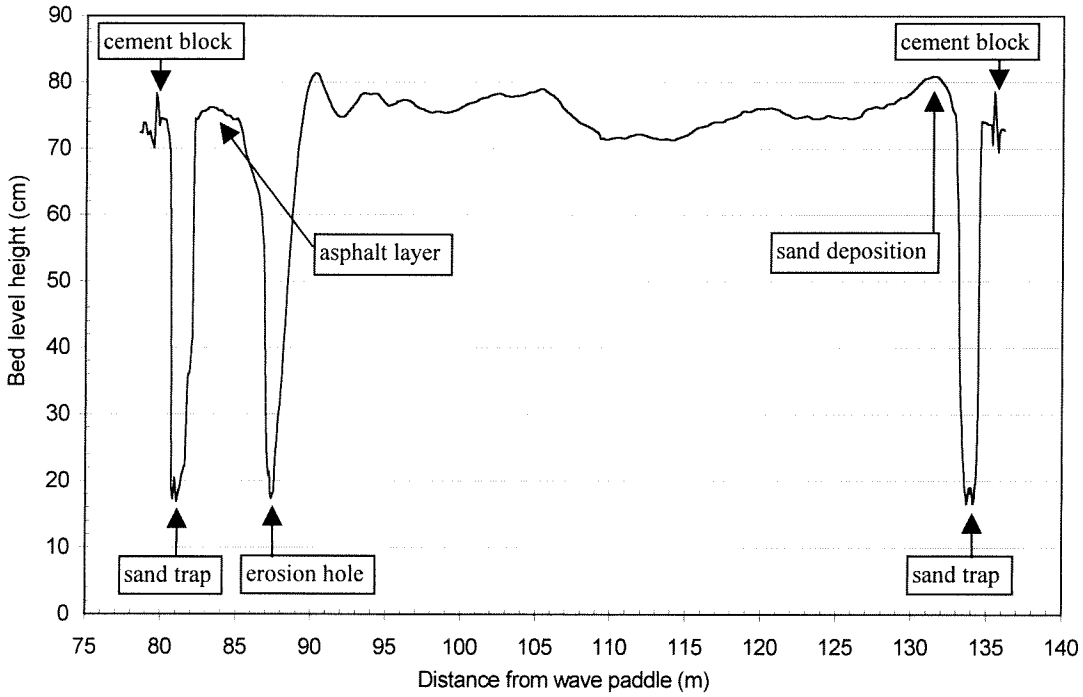

Figure 4.5: Example of a bed profile: the bed level height above the flume bottom as function of the distance from the wave paddle, recorded with the MTA.

a) spikes

The raw data recorded with the MTA contained spikes. Spikes are data points with large deviating values compared to the surrounding data points. Before the data can be analysed the data has to be despiked. This is done by leaving the spikes out and using linear interpolation to calculate the missing data points. Figure (4.6) shows a single spike in the MTA data and the linear interpolated value.

Spikes in data cause inaccuracies, the more spikes the more data is missing. The recorded MTA data consisted on average of 18% spikes. It was found that the spikes were divided over the data, no big gaps (not more than 4 successive data points) in the data were present.

The recorded data gives the distance between the MTA and the top of the sand bed. The data is converted into the bed height above the flume bottom, by subtracting the distance between the MTA and the top of the sand bed from the distance between the MTA and the flume bottom (about 1.15 m). Almost all despiking and a rough conversion to bed level height above the flume bottom is done by the UF.

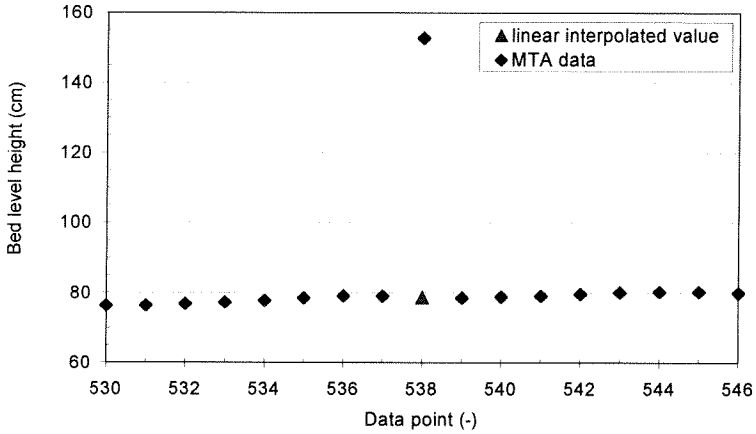

Figure 4.6: Spike in MTA data and linear interpolated data point.

b) Transducer placement

The MTA made an angle of 45 degrees, oriented in a horizontal plane with the x-direction of the flume (see Figure 3.7). Therefore all profiles taken from each transducer are shifted in x and y-direction. When all profiles are plotted in the same figure, based on the same horizontal data grid, the shift in x-direction due to the transducer placement, can be seen. Figure 4.7 shows the bed level height above the flume bottom for all transducers, as a function of distance between the wave paddle and the first transducer.

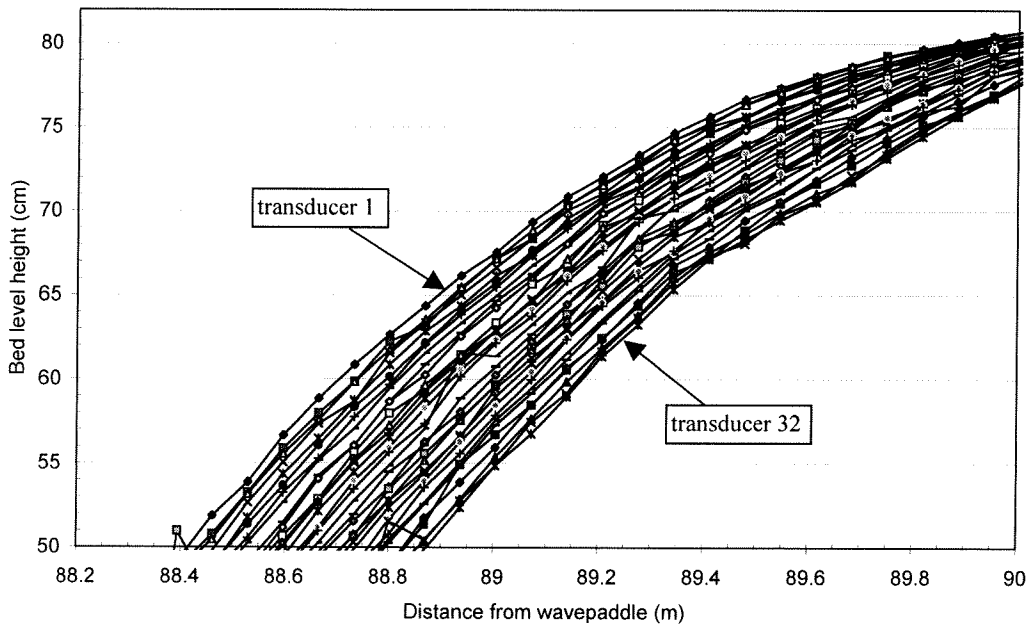

Figure 4.7: Bed level height above the flume bottom for all transducers, as a function of the distance from the wave paddle (for the first transducer).

In order to correct the shifted transducer placement, all profiles are converted to the data grid of the first transducer. A linear interpolation is used to convert the bed level heights, recorded with each transducer, to the data grid of the first transducer. The shifted transducer data grids, due to the MTA placement are shown in Figure 4.8. From this figure it can be seen that the data grids are staggered with 0.014 m (the distance between two datapoints (Δx) is 0.068m).

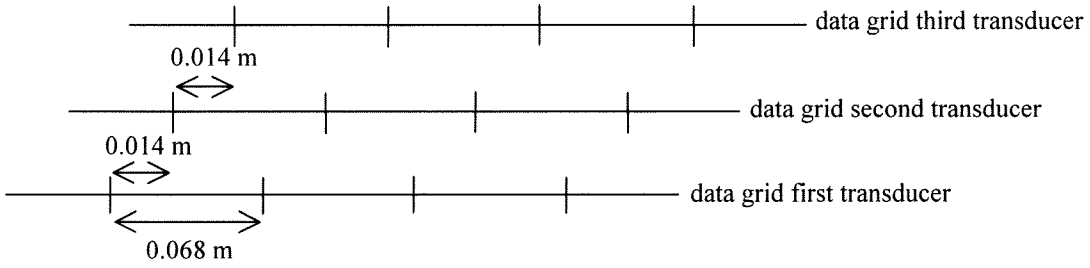

Figure 4.8: Staggered transducer data grids, due to the MTA placement.

Figure 4.9 shows the bed level heights with the adjusted transducer placement for all transducers. Here, all transducers are based on the same data grid (same distance from the wave paddle).

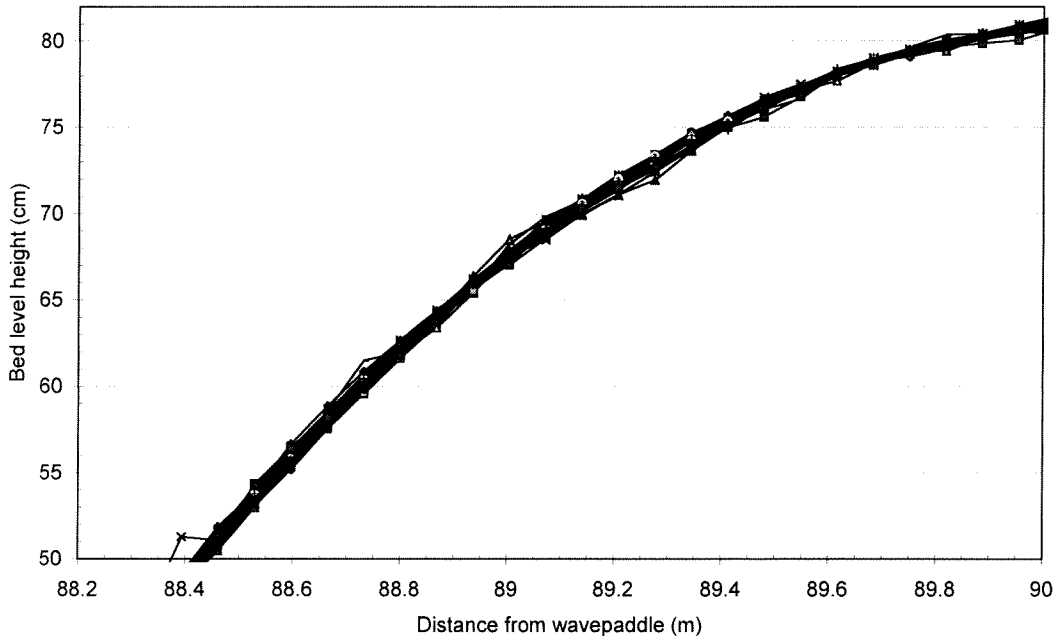

Figure 4.9: Bed level height above the flume bottom for all transducers, with adjusted transducer placement, as a function of the distance from the wave paddle (for all transducers).

c) Velocity of the carriage

The velocity of the carriage was not exactly constant while moving along the flume. As a result the length of the measured bed profiles were not exactly the same. This is corrected by using a scale factor to scale every profile to the same length as the first (reference) profile. The length of the profiles is determined by the known position of two cement blocks placed on the raised asphalt bottoms, on both sides of the test section. These blocks (see Figure 4.5) were placed in such a way that they could be recorded with the MTA. Also the sand traps and the asphalt bottoms were used to determine the length of the profile.
The reference profile is scaled to the real length by applying a value for the distance between the data points (Δx) of 0.068 m. This value is obtained from the actual length (measured by hand) between the two cement blocks, which was 55.8 m.

Figure (4.10) shows an example of a scalefactor with a value of 1.01 (-) to change the length of a profile. The scale factor is applied to a bed profile, starting downstream (start position of the measurement) of the test section. By using a scale factor smaller than one the length of a profile can be shortened.

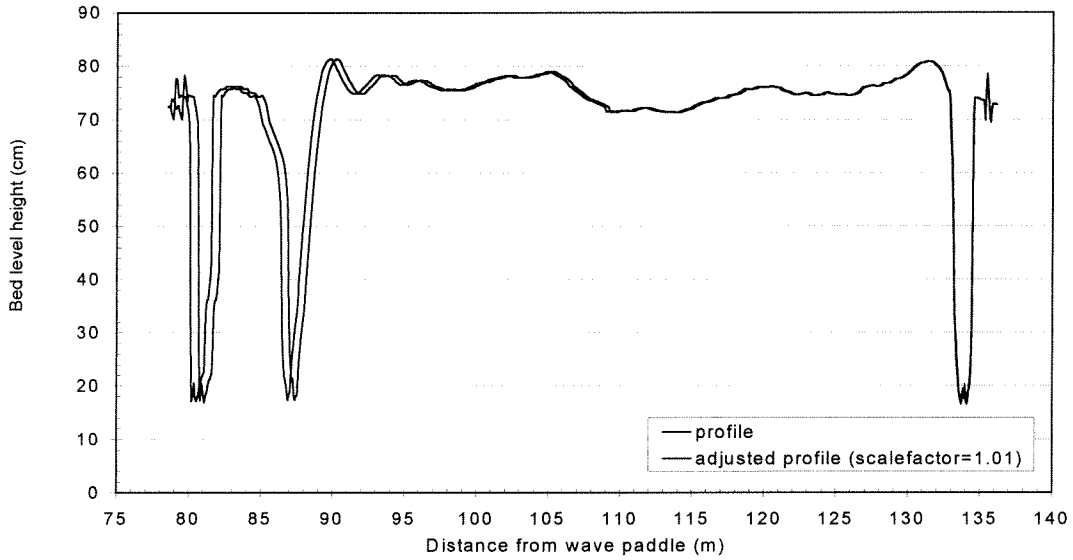

Figure 4.10: Example of a scalefactor of 1.01 (-) used to adjust the length of a bed profile.

d) Vertical shift

Some of the measured bed profiles were shifted in vertical direction. This is probably caused by a difference in the position of the MTA above the flume bottom while profiling the bed. During a few measurements of the bed it was observed that the steel wires, which holds the MTA at a fixed level above the flume bottom, were not equally loaded. This causes a difference in the level of the MTA above the flume bottom compared to the other measurements. A difference in level between two profiles causes large inaccuracies. Therefore the level of each profile above the flume bottom is determined using the raised asphalt bottom as a reference and all profiles are shifted to the first profile. Figure (4.11) shows an example of an offset in positive z-direction of 2 cm.

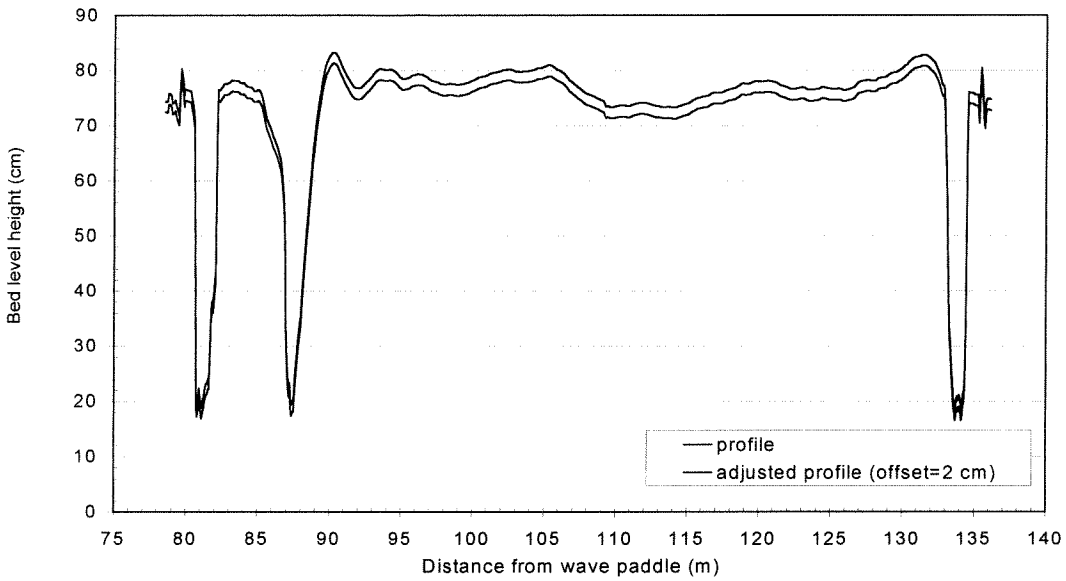

Figure 4.11: Example of a vertical shift of 2 cm in positive z-direction.

The level of the first (reference) profile is determined in two ways: the building specifications of the test section and at a later stage, a comparison between the bed level height, measured with the ADV and the MTA.
The first method is a crude approximation, because the height of the built test section was never measured accurately and it may be expected that the built test section will slightly deviate from the building specifications. Therefore a comparison between the bed level heights, recorded with the ADV and the MTA, is made. This was possible because the level of the ADV above the flume bottom was known (see Eq.3.3). This method will be discussed here in more detail.

Due to the placement of the MTA, the MTA is able to record the bed level height at the location of the ADV (x=109.2 m and y=2.25 m). The bed level height at the measuring location of the ADV is recorded with the 22nd transducer of the MTA. The bed level height underneath the ADV was computed using the calculation method, which is discussed in Section 3.4.4.

The ADV recorded the bed level height after a test had ended and before the following test would start. The difference between these two measurements gives an indication of the accuracy of the bed level measurements with the ADV. It was found that the average difference between the two measurements was 2 mm.

Figure 4.12 shows the bed level height, recorded with the MTA (z(MTA)), together with the bed level height, recorded with the ADV(z(ADV)). The bed level z(MTA) is the recorded bed level, assuming the MTA is positioned 1.15 m above the flume bottom. The bed level height z(ADV) is an average value between the measured bed level height after a test ended [z(ADV,a)] and the bed level height before the following test started (z(ADV,b)).
Appendix C includes a table with the following parameters: z(ADV,a)-z(ADV,b), z(ADV), z(MTA) and z(ADV)-z(MTA).

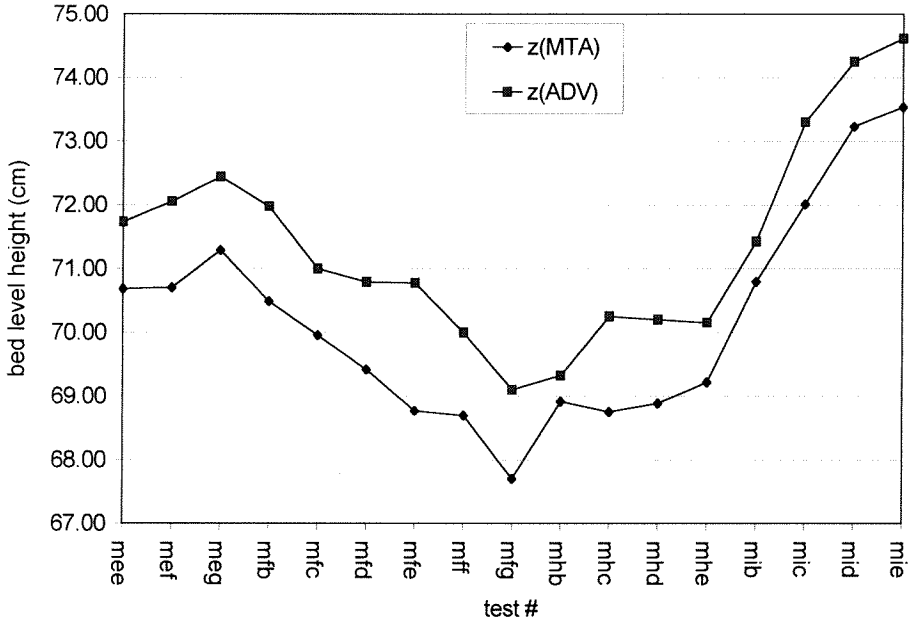

Figure 4.12: Bed level heights measured with the MTA and ADV at the measuring position of the ADV (x=109.2 m and y =2.25m), for test mee-mie.

From the figure it can be seen that the bed level height measured with the ADV is higher than the bed level height measured with the MTA. A correction is made by minimising the difference between z(ADV) and z(MTA), resulting in a constant correction value of 12 mm. This value is applied to the reference profile, to which all profiles are compared.

e) Horizontal shift

Because the start position of the carriage before profiling the bed was not exactly the same after each test, the data grid of the profiles had to be converted to the reference data grid. This is done by shifting the profiles in x-direction to the reference profile. Figure (4.13) shows an example of a horizontal shift of 102 cm in negative x-direction of a bed profile.

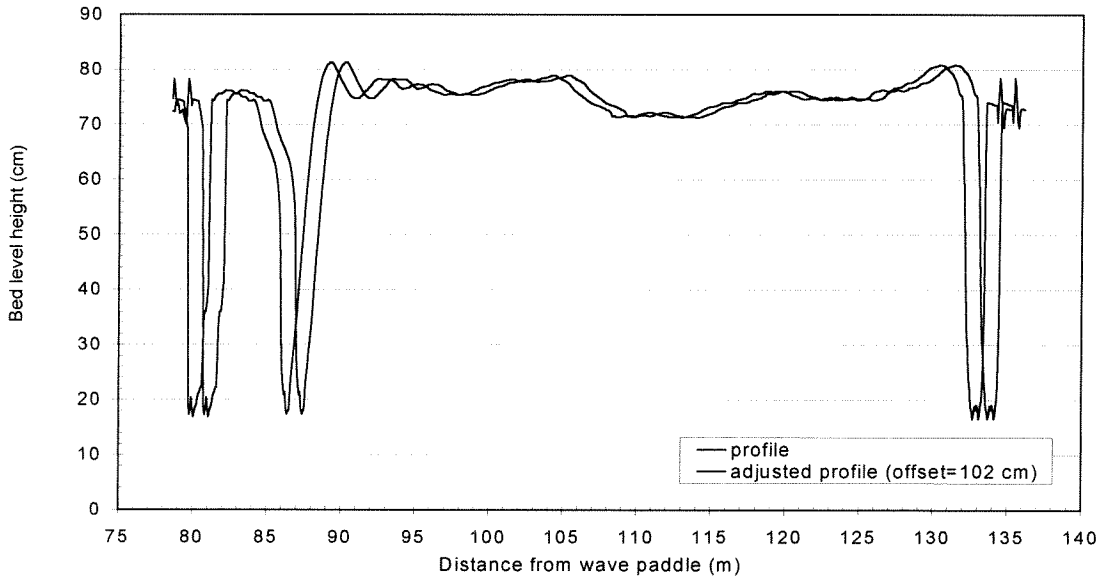

Figure 4.13: Example of a horizontal shift of 102 cm in negative y-direction of a bed profile.

f) Erosion

The erosion hole that developed at the beginning of the test section reached the bottom of the flume after about 7 runs. After the sand bed descended below a level of about 15-20 cm above the flume bottom, the MTA was not able to record the bed level height anymore (the distance between the MTA and the flume bottom was about 1.15m, the measuring range of the MTA is about 1 m). The measured bed level had to be corrected by extrapolating the measured bed level to the level of the flume bottom. This is done using an order 4-6 polynomial relation. Figure (4.14) shows the corrected bed level for the erosion hole.

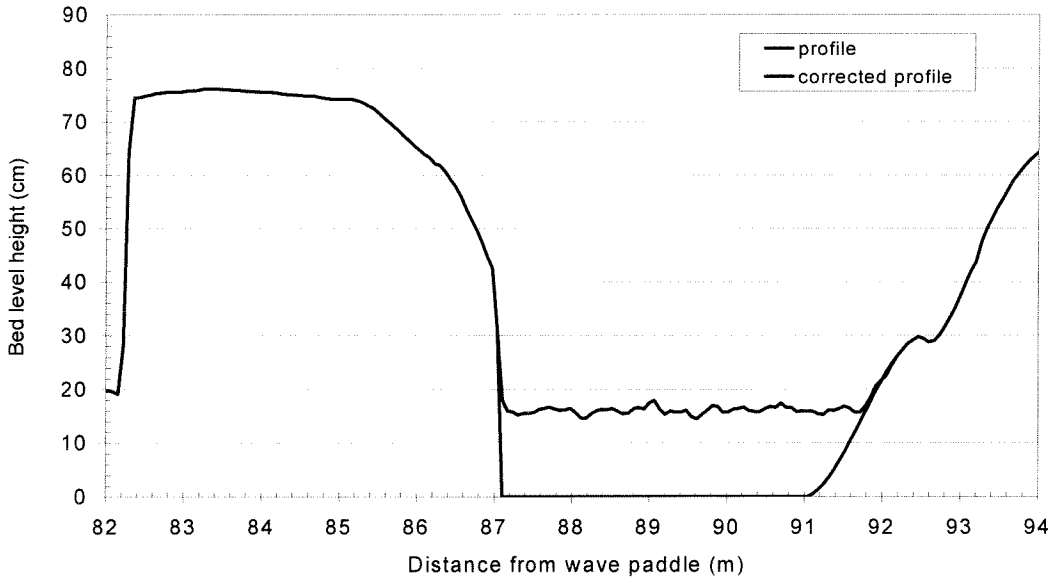

Figure 4.14: Example of a correction for the erosion hole.

The corrections are made for the averaged bed profile, this means that the bed profiles measured with the 32 transducers are averaged in cross-direction.

g) Deposition

During the experiment sand was deposited at the end of the test section. After 15 tests the deposition of sand could not be recorded properly by the MTA, because the height of the bump reached the minimal limit of the range of the MTA. This deposition of sand can be seen as a boundary effect, between the asphalt bottom with no sand and the test section. This correction does not affect the net transport rate in the middle of the test section, because the net transport is mainly in the direction of wave propagation and the transport rates are calculated starting upstream of the test section. Nevertheless the profiles are corrected by extrapolating the mean bed level, also using an order 4-6 polynomial relation. The correction is applied to be able to estimate the sand loss from the test section. Figure 4.15 shows the corrected bed level for the sand deposition.

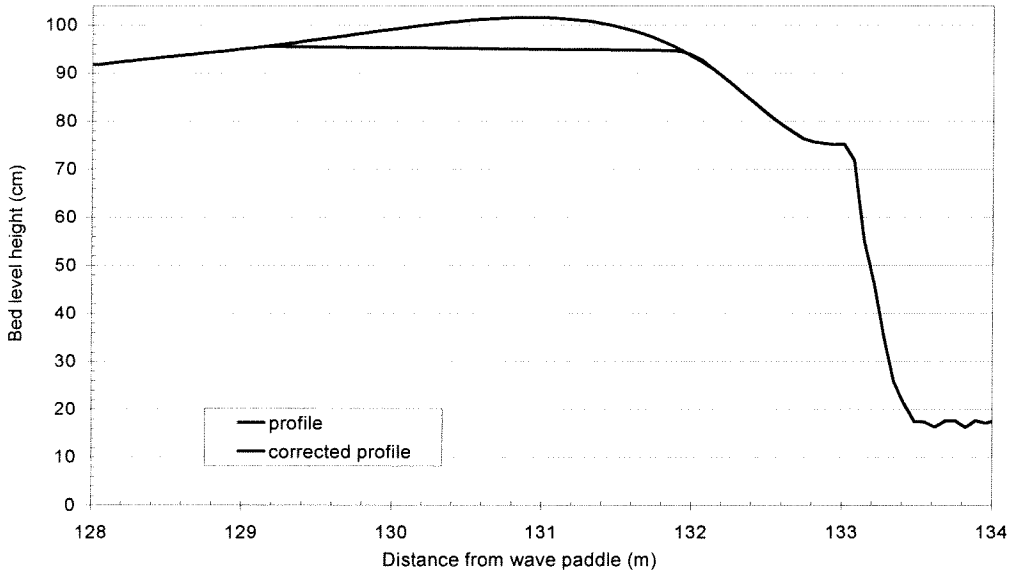

Figure 4.15: Correction for sand deposition

4.3.2 Calculation method

To handle the large quantities of data it is necessary to use a computer program that automates the different calculation steps. To make the adjustments as described in Section 4.3.1b-e a Matlab program is written. This program plots the reference profile together with another profile in the same plot and zooms in on different reference locations such as the cement blocks, the sand traps and the asphalt layer. By comparing the reference profile with the other profile, the offset in x and y direction and a scalefactor can be determined. In this way accurate adjustments are made for all profiles.

The input of the program exists of two despiked (Section 4.3.1a) profiles: the reference profile and the profile, which has to be adjusted. After plotting both profiles for all transducers, different values for the offsets and the scalefactor can be given. These values are incorporated in the adjusted profile, which is then plotted again with the reference profile. These steps are repeated until a best fit (visually determined) of the profiles is reached. After all corrections are incorporated the adjusted profile is linearly interpolated. The output of the program is an adjusted profile, averaged over all 32 transducers, based on the data grid of the reference profile.
It was seen that the bed features that developed during the tests under sheet flow conditions, varied little in cross direction. Therefore averaging in cross direction was possible without introducing extra inaccuracy. The corrections as described in Section 4.3.1f-g are applied afterwards, using different software.

A listing of an important part of the program is shown here. The parameters zoffset (see Section 4.3.1d), xoffset (see Section 4.3.1e) and scalefactor (see Section 4.3.1c) are determined in the preceding part of the program. The parameter xshift (see Section 4.3.1b) represents the shift in x-direction to compensate the different placement of the transducers. The parameter deltax (step size) represents the actual distance between two datapoints. The value $\sqrt{2}/100$ represents the difference (in m) between 2 transducers in x-direction. The parameter z represents the adjusted bed level height, based on the original data grid, desp represents the despiked profile data which have to be adjusted. The parameter zi is the adjusted bedlevel height based on the data grid of the reference profile.

```
For i = 1:32;                                   { i = transducer number}
        z = zoffset + desp(i,:);
        xi = 1:lengthprofile;                   {lengthprofile = number of data points}
        scalef = scalefactor*xi;
        xshift = (i-1)*((sqrt(2)/100)/deltax)
        x = xi + xshift + xoffset + scalef ;
        zi = interp1(x,z,xi);                   {interpolation to reference data grid}
End
```

The values for the scale factor, vertical shift (zoffset), scour hole and deposition correction, used in the program, can be found in Appendix D.

4.3.3 Results of the bed level measurements

The bed profiles recorded with the MTA are shown in Figure 4.16-4.20. Figure 4.16 shows the first 6 tests of the experiment. The initial bed profile is measured before the first test with condition mea is carried out. After the test with condition mea is carried out, the bed is profiled. Because this bed is the result of the test with condition mea, the measured bed profile will be called 'after mea'(see Figure 4.16-4.20). These 6 tests were carried out in order to check the conditions for sheet flow occurrence and to let the sand bed settle. The conditions of tests mga and mja (see Figure 4.16) are not investigated further and will therefore not be taken into account. The figures (4.16-4.20) give a rather distorted image of the bed steepness because of the large difference between the horizontal and the vertical scale.

From these figures can be seen that in all cases the upstream side of the test section eroded and sand was deposited at the downstream side of the test section. In these figures some features of the test section can be recognised. On the left-hand and right-hand side of the figure both sand traps can be seen. Between x=82.4 m and x=86.9 m the asphalt layer between the test section and the upstream sand trap can be recognised.

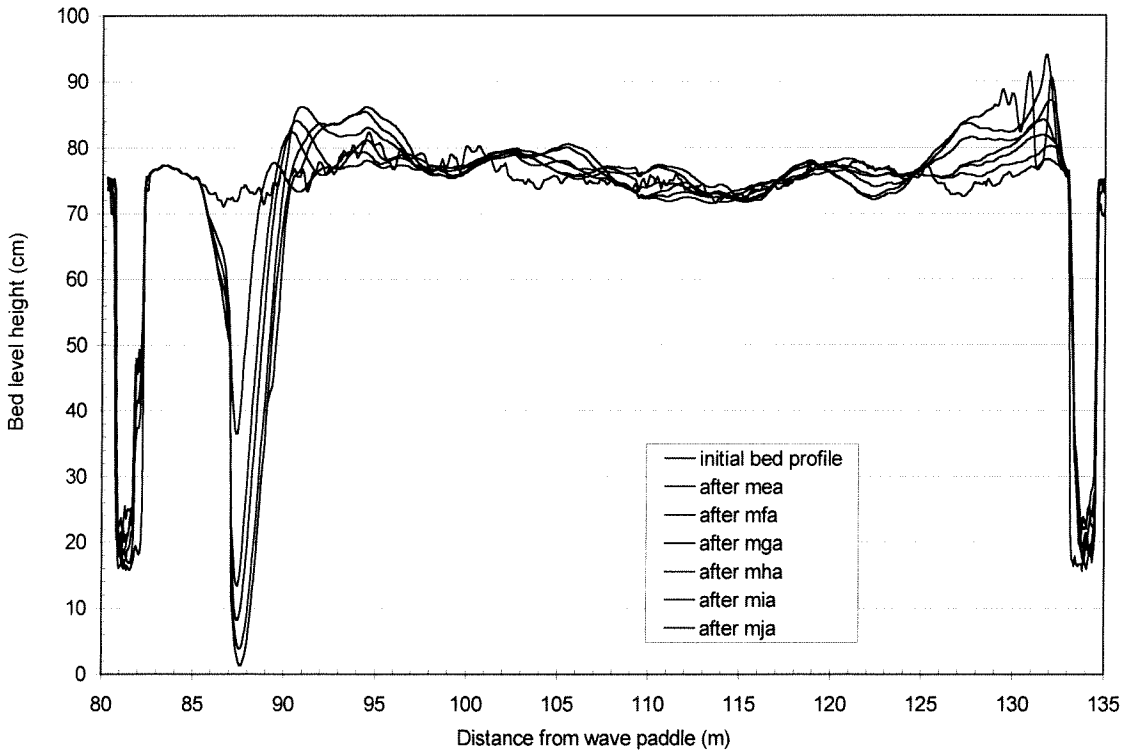

Figure 4.16: Bed profiles for the first 6 tests.

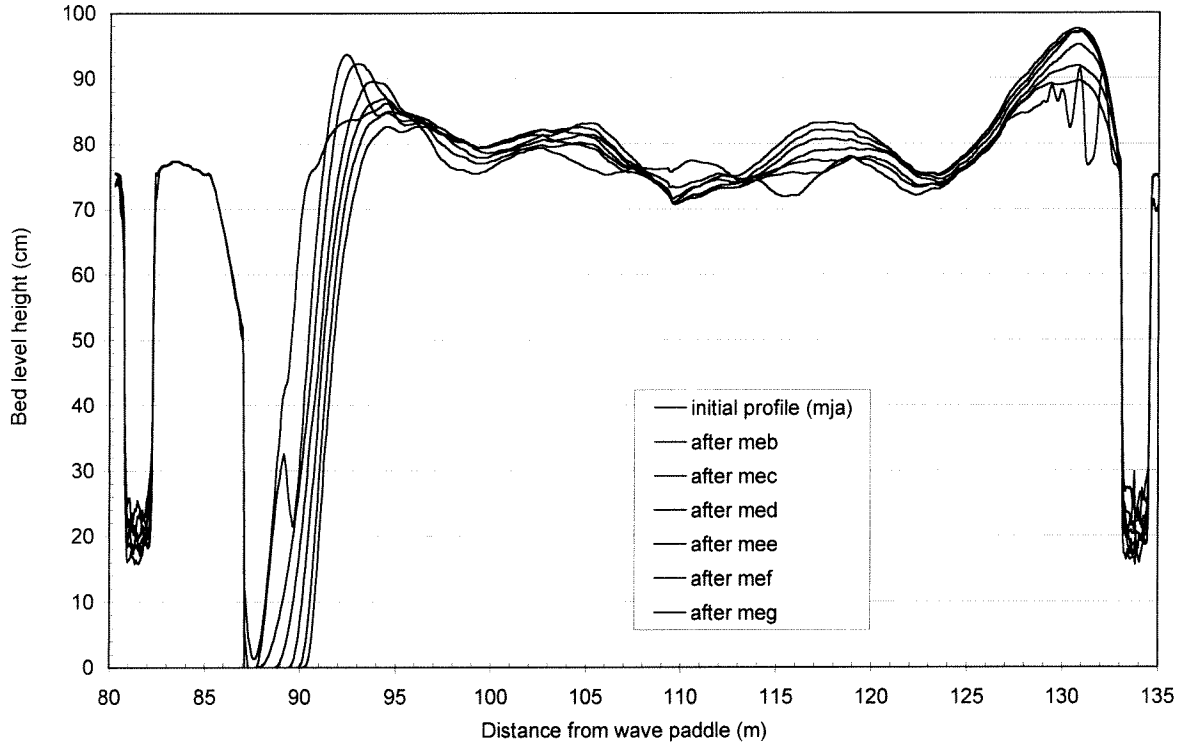

Figure 4.17: Bed profiles for condition me.

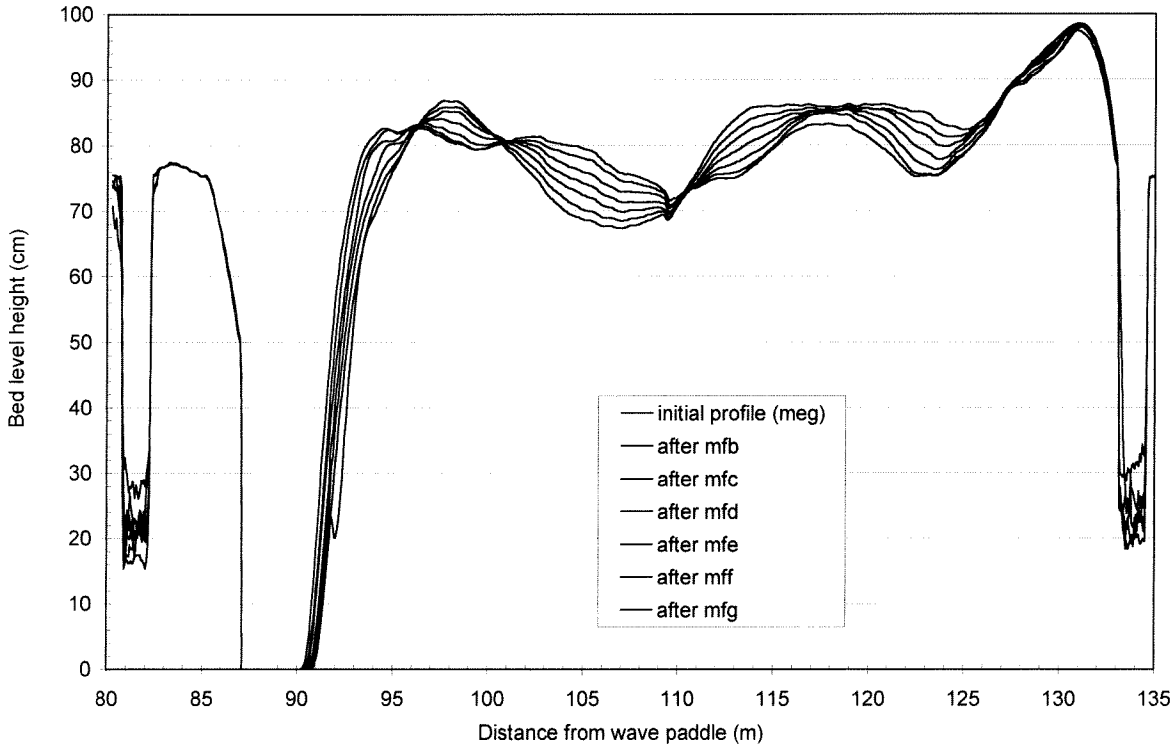

Figure 4.18: Bed profiles for condition mf.

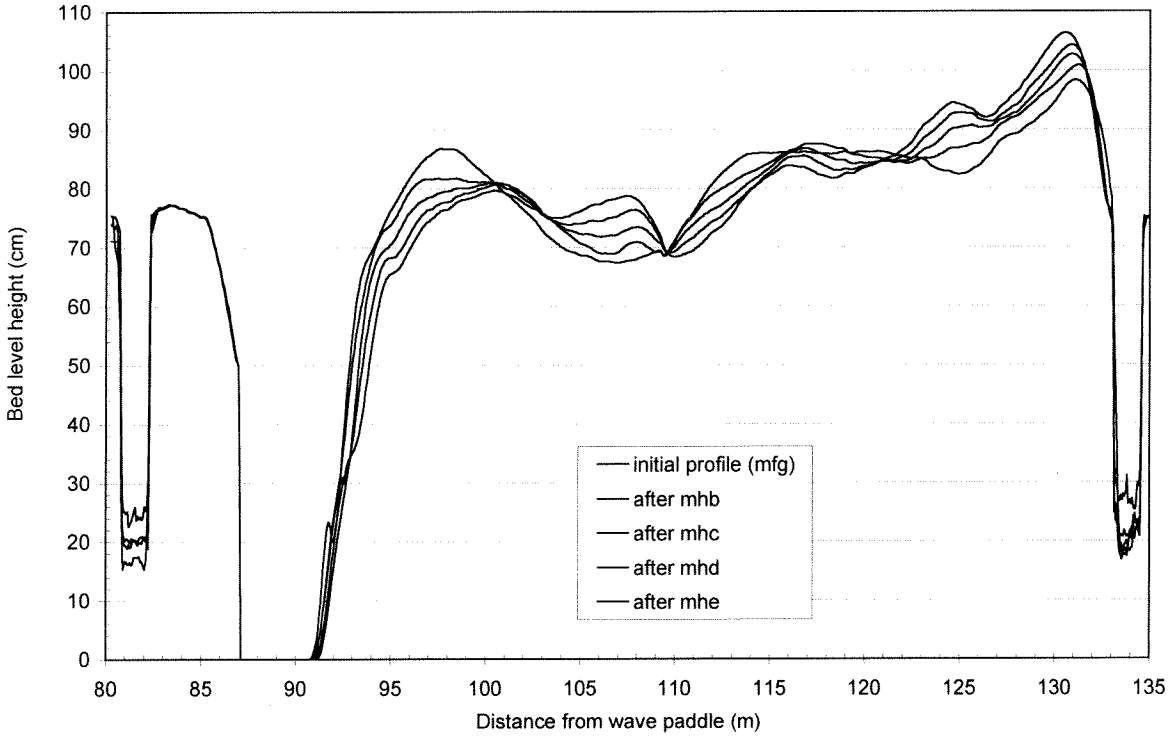

Figure 4.19: Bed profiles for condition mh.

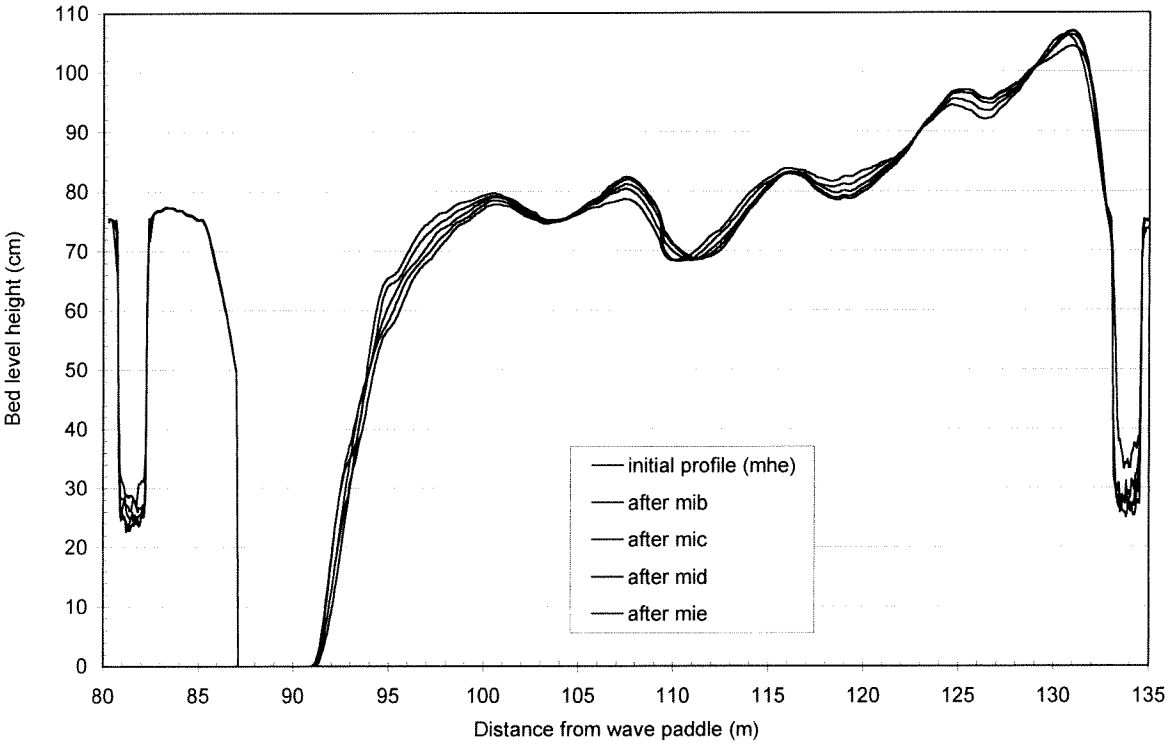

Figure 4.20: Bed profiles for condition mi.

The bed profiles show the development of the bottom topography under influence of the waves. From Figure 4.16 and 4.17 it can be seen that already after 7 tests the sand bed

reached the bottom of the flume. After the second test (mfa) was performed the sand bed in the erosion hole could not be recorded with the MTA. From this test on, the level of the sand bed here had to be corrected.

From Figure 4.17-4.20 it can be seen that large plane bedforms with a wavelength of about 12 m and a height of about 0.13 m (from crest to trough) develop for condition me and mf. The wavelength of the bedforms decreases to about 7 m and the steepness increases because the height of the bedforms stays constant with about 0.13 m, for condition mh and mi.

It must be noted that the resolution of the data is about 6.5 cm. Moreover the bed profile is averaged in cross direction of the flume. Therefore small bedforms can not be seen from these figures. When a bed profile, taken from a single transducer is considered, bedforms smaller than 6.5 cm are not recorded. From these data it can not be determined if ripples smaller than 6.5 cm are present and if the assumption of a plane bed is an acceptable one. The presence of ripples smaller than 6.5 cm, can be determined from data, recorded with another MTA, that was mounted on the instrument frame of the UF.

For all conditions some influence of the instrument set-up can be seen at x=109.2 m. It seems that the movable pole and probably the instrument frames have some influence on the bed topography. During the experiment it was decided to raise the movable pole to a higher level above the bed (about 5 cm) after 15-20 minutes to reduce the flow disturbance, induced by the pole. This is done for test med-mfd. From test mfe to the last test, the height of the pole above the sand bed was set on a higher level for the total duration of the test.

4.3.4 Steepness of the bed

An important aspect of measuring transport processes in sheet flow conditions, is that flow separation and vortex shedding do not occur. To accomplish this the bed has to be flat. Also, in order to compare the results with the results of water tunnel experiments, the bed in the present experiment should be as flat as possible.
Flattening the bed after every test is very time consuming. In a water tunnel it can be done in a reasonable amount of time, but in a wave flume it simply takes too much time to lower the water level and flatten the test section. Therefore it is useful to check whether the steepness of the bed is not exceeding the limit on which flow separation and vortex shedding have too much of an influence on the sand transport.

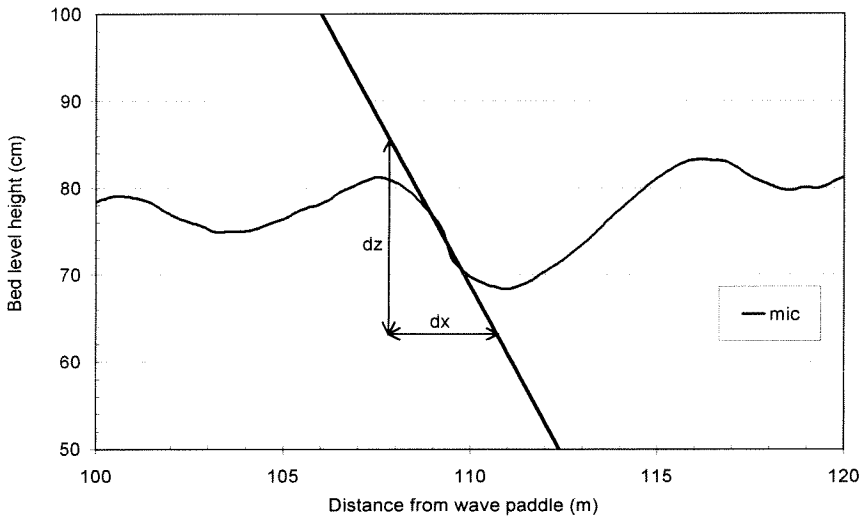

Figure 4.21: Definition of the bed steepness dz/dx for bed profile mic.

For all tests the steepness of the large bedforms is calculated from the bed profiles. The boundary effects upstream and downstream of the test section are not considered. The part of the test section that is analysed for the bed steepness lies therefore, between x=100 m and x= 125 m. The steepness is calculated by determining the slope (dz/dx) of the steepest bedform, found between x=100 m and x= 125 m (see Figure 4.21). This is even steeper than $\eta/\frac{1}{2}\lambda$, in which η is the height of the bedform and λ is the wavelength of the bedform. It must be said that the calculated steepness is different from the definition that is often used to describe the steepness of bedforms (i.e. η/λ). In Figure 4.22 the bed steepness for all tests is plotted. It can be seen that the bed steepness is increasing from test mfe towards the last test. For all tests, the steepest slopes were found in the neighbourhood of the measuring location at x = 109.2 m. The bed steepness for each test can be found in Appendix E.

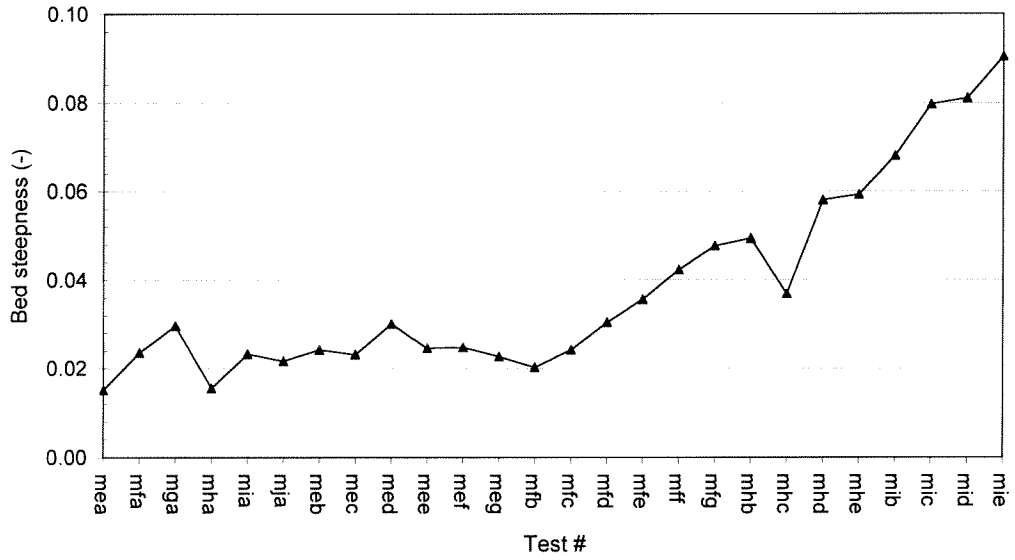

Figure 4.22: The calculated bed steepness for all tests.

The effect of a sloping bed, caused by large bedforms, on the transport rates is not clear in this case. It is expected that the slope is too small to have any influence on the net transport rate, because the occurring shear stresses are much larger than the critical shear stress for the initiation of motion. Therefore a decrease/increase of the critical value due to an upward/downward slope is relatively unimportant. Furthermore, larger shear stress, required to carry grains up the slope of bedforms is partly offset by flow acceleration over the undulations.

Vortex ripples tend to develop when there are low to moderate rates of sediment transport. Flow separation, whereby the zone of high shear leaves the bed and rejoins it at a short distance downstream, causes vortices to develop to the lee of ripples every half-wave cycle. The vortices propel grains towards ripple crests until flow reverses, when they are swept towards the crests and up into the flow. Although finer grains can be placed into suspension under more energetic conditions, most grains are deposited at the crests, making the crests relatively sharp. The wavelength of vortex ripples λ_r is typically between 1 and 2 times the orbital amplitude a. Their height is typically between 0.1 and 0.2 times their wavelength.

These vortex ripples are washed out by very large orbital velocities, to leave a flat bed with oscillatory sheet flow. However, bedforms have been found to persist in the field under high

energetic conditions with Shields parameters values larger than 1 and ripples may even develop when values are higher than 2 (Kawata et al., 1992; Osborne and Vincent, 1993). There are different ways to predict bedform occurrence. Some investigators used the mobility number Ψ (Dingler and Inman, 1976; Ribberink & Al-Salem, 1990) or the Shields parameter θ_w (Nielsen, 1979), based on the amplitude of the oscillatory velocity (see Eq. 2.3), to predict the inception of sheet flow over flat beds. Ribberink and Al-Salem (1990), for example, found Ψ>100 to 200. Nielsen (1979) found for the maximum skin-friction Shields parameter $\theta_w \geq 1.0$. The mobility number Ψ is defined by:

$$\Psi = \frac{U_a^2}{g(s-1)D_{50}} \tag{4.4}$$

Here, U_a is the oscillatory velocity amplitude and s the relative density.

Based upon detailed measurements of the flow over ripples, Sleath (1975) determined that ripples first introduce random instability, including flow separation above the lee slopes, when $a/\lambda_r \geq 0.5$. Although the flow becomes more and more chaotic as the frequency of the oscillation increases, the transition to fully developed turbulence takes place gradually. It is only completed when the ratio has become many times larger than the point at which instability or chaotic flow appears.
In Table 4.4 the values for the maximum Shields parameter θ_w (based on U_{cr} and U_{tr}), the mobility number Ψ (based on U_{cr} and U_{tr}), the wavelength of the bedforms λ and the ratio between semi-excursion length and bedform wavelength a/λ, averaged for each condition, are presented. A roughness height (k_s) of D_{50} is applied in the expression for the wave friction factor f_w (see Eq. 2.4), which is used to calculate θ_w. The values of θ_w and Ψ, based on U_{tr} and U_{cr} for each test can be found in Appendix E.

condition	test	$\theta_{w,cr}$ (-)	$\theta_{w,tr}$ (-)	Ψ_{cr} (-)	Ψ_{tr} (-)	λ (m)	a/λ (-)
me	b,c,d,e,f,g	1.77	0.34	534	104	12	0.11
mf	b,c,d,e,f,g	1.45	0.41	434	124	11	0.12
mh	b,c,d,e	1.29	0.44	377	128	8	0.14
mi	b,c,d,e	1.14	0.48	327	137	7	0.14

Table 4.4: Maximum Shields parameter, mobility number and ratio between semi-excursion length and bedform wavelength, averaged for each condition.

The values of the maximum Shields parameter θ_w and the mobility number Ψ are well in the sheet flow regime, at least for values based on U_{cr}. This indicates that a flat bed is expected, vortex ripples are not likely to occur. From the table it can be seen that $a/\lambda \leq 0.14$, this value is below the limit value on which instability and flow separation begin to appear.

No clear values for the limit of the bed steepness, on which flow separation and vortex shedding might occur, are known in literature.
The bedforms, which developed during the present tests (mea-mie), are different from typical wave-generated vortex ripples. The crests of these bed features are rounded and slightly curved and are totally different from the sharp crested vortex ripples. It is therefore expected that flow separation and vortex shedding do not appear. This is confirmed by the value of a/λ, which is well below the limit value.

4.4 Transport rate calculations

4.4.1 Calculation method

The net transport rate distributions that will be discussed in the following sections, are calculated from the difference in bed level between two bed profiles, recorded with the MTA. The used calculation method is discussed in Chapter 3.4.2.
The net sand transport rates were calculated, starting from a position upstream of the test section under the assumption that no sand had been transported upstream of this point. This was checked at the end of the experiment when the flume was emptied and indeed no sand was found in the sand traps upstream of the test section. Further upstream near the wave paddle also no sand was detected.
Downstream of the test section behind the concrete blocks (x=150 m), a sand bar had developed on top of the loose stones. This shows that a lot of sand had been transported (over the sand traps) downstream of the test section (see Appendix F). Therefore it is not possible to start a calculation from a downstream position because there is no location where the sand transport rate is known.

Corrections made for the erosion hole and the sand deposition were done by hand, using Excel. After these corrections were made, the transport rate is determined by solving Eq.3.2, this is also done with Excel. In Table 4.5 a summary is given of the used software and their specific input and output.

used software	adjustments (Section 4.3.1)	solved equation	input	output	
Matlab	b, c, d, e	-	despiked bed profiles	1	bed profiles, averaged for all transducers, lined up on same data grid of reference profile
Excel	f, g	-	output 1	2	bed profiles, corrected for the erosion hole and sand deposition
Excel	-	Eq. 3.2	output 2	3	net sand transport rate distributions for the test section

Table 4.5: Calculation methods for bed profiles and net sediment transport rates.

4.4.2 Net transport rate distributions

In Figure 4.23-4.26 net transport rate distributions as a function of distance from the wave paddle are plotted for all tests. The transport rate distribution of condition meb in Figure 4.23 is calculated from the difference between the initial bed profile (mja) and the bed profile measured after test meb, see Figure 4.17. The transport rate distributions are not shown beyond x=133 m, because the downstream sand trap, located between x=133 m and x=134.5 m, disturbs the bed level measurements in such a way that no realistic transport rates can be calculated.

The first test of the experiment (mea), after filling the flume, deviates more from the other tests than normally would be expected (see Appendix G). This is probably caused by the settling of the bed under influence of waves. This test also consisted of a cancelled run with condition md, with a period of 9.1s, a waveheight of 1.7m and a duration of 2 minutes.

Therefore the measured net transport rate is much higher than the transport rates of the other tests with the same condition.

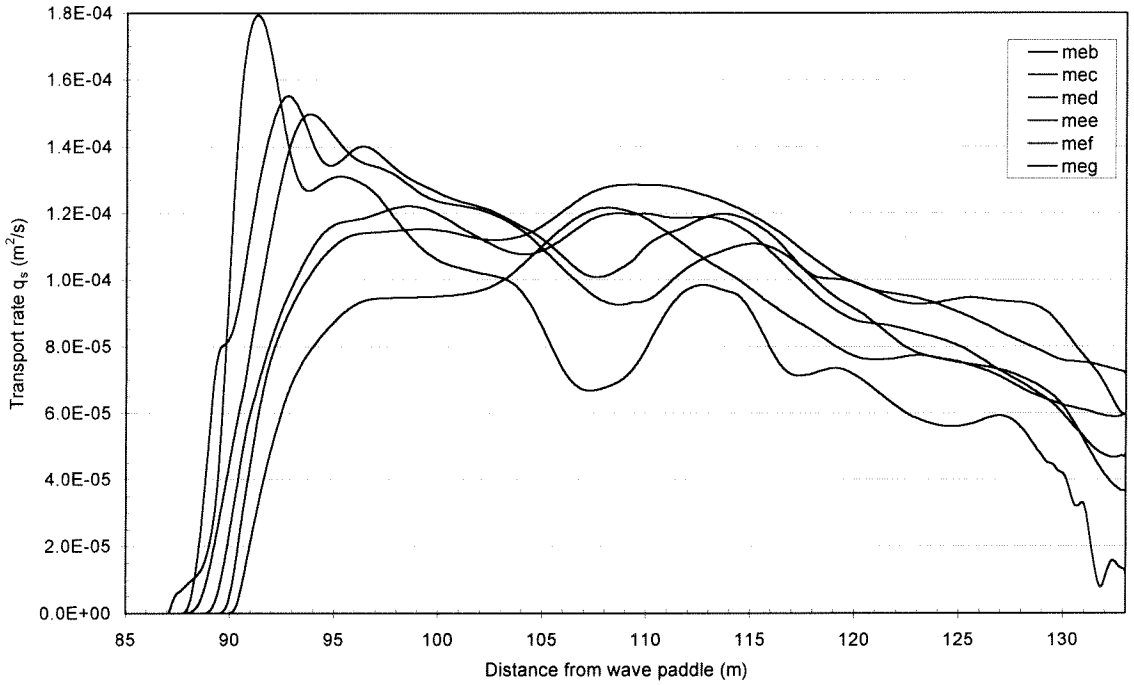

Figure 4.23: Measured net transport rates along the test section for condition me.

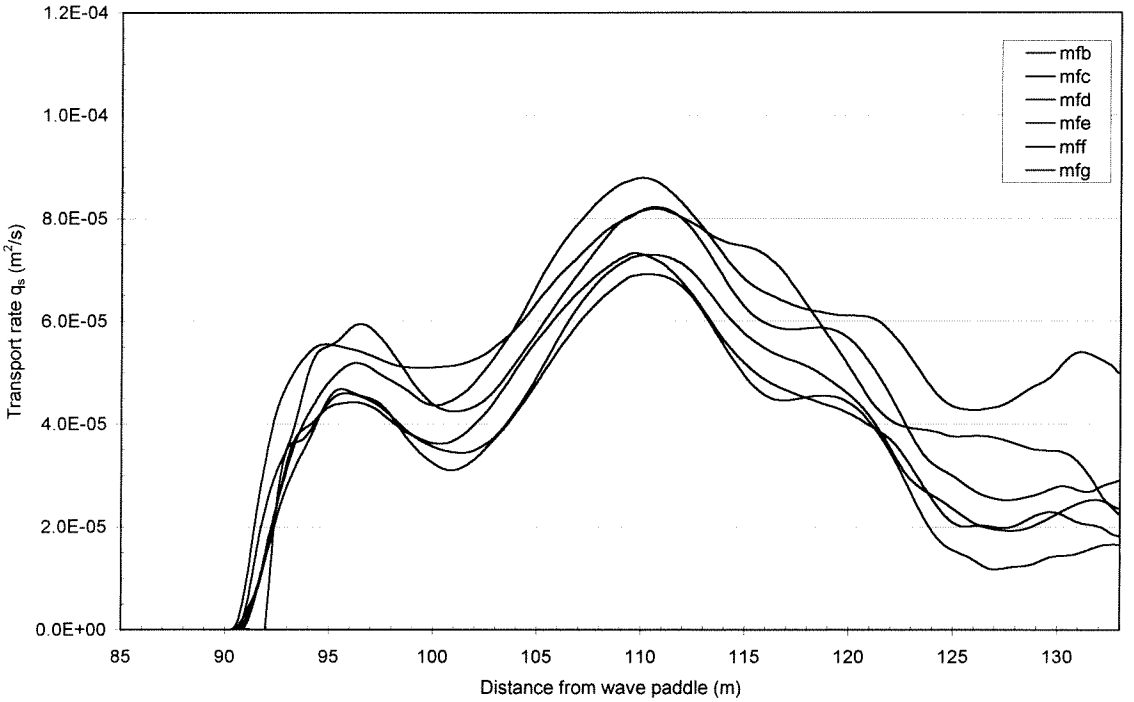

Figure 4.24: Measured net transport rates along the test section for condition mf.

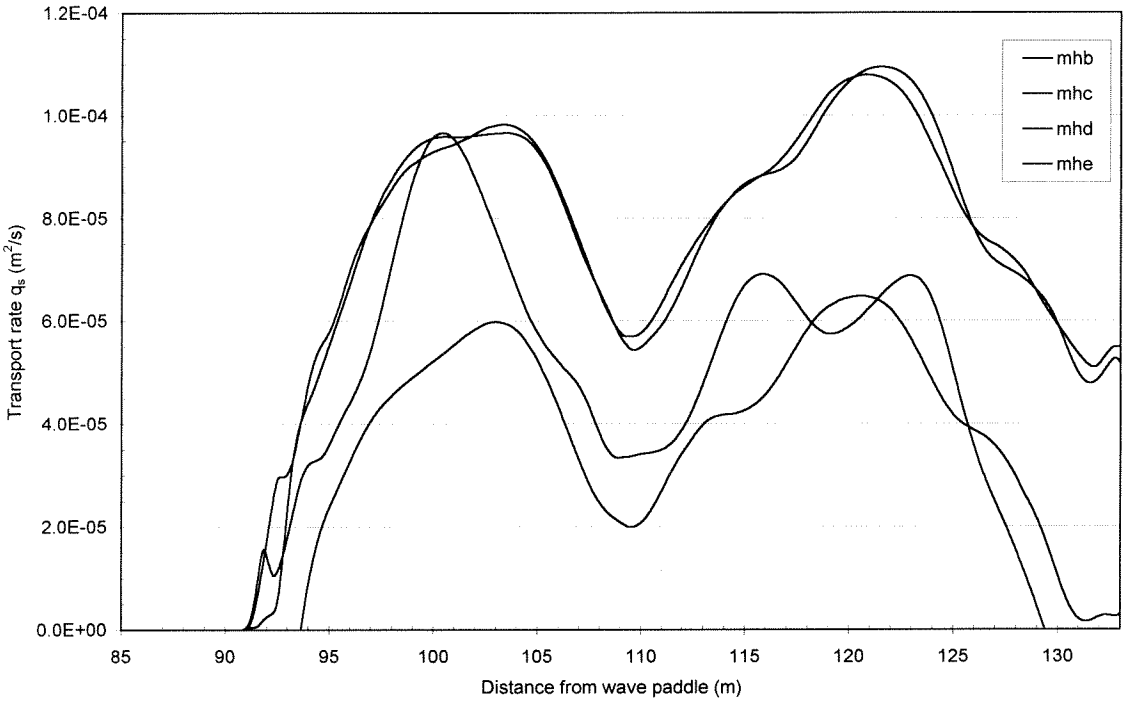

Figure 4.25: Measured net transport rates along the test section for condition mh.

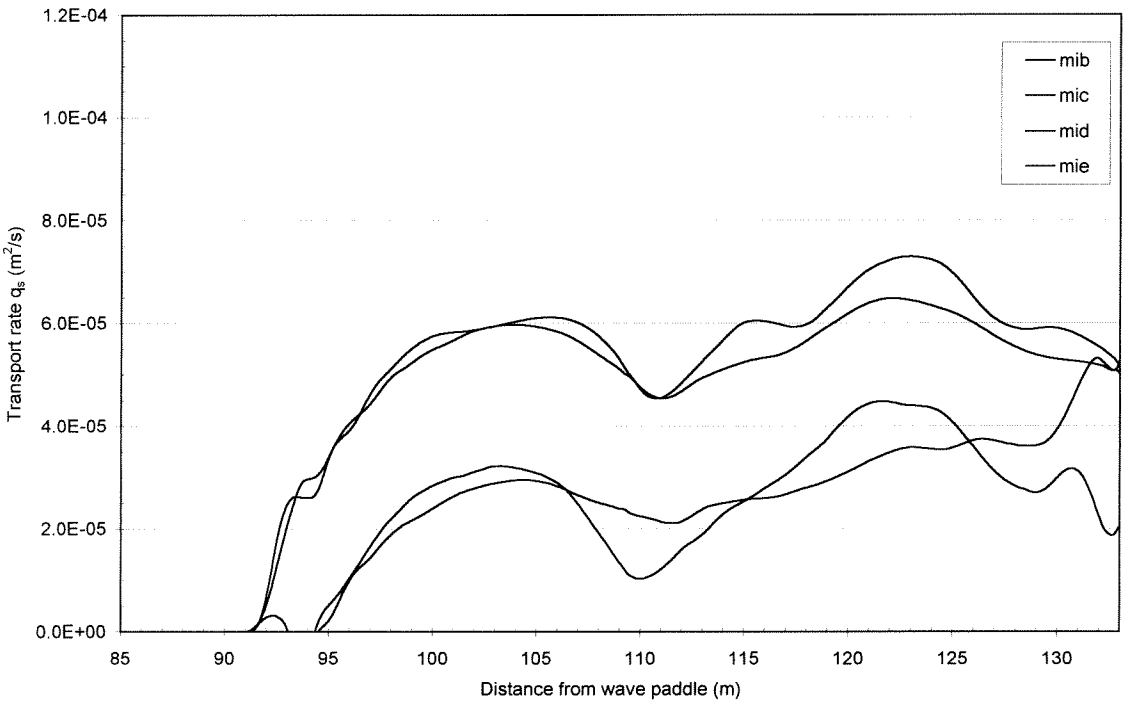

Figure 4.26: Measured net transport rates along the test section for condition mi.

From Figure 4.23-4.26 it can be seen that the net transport rates of the tests with the same condition do not have a time-depended influence between the tests. The transport rates of the tests with the same condition do not appear to have a particular following order.

Each test gave a (positive) time-averaged sand transport rate in the direction of wave propagation. As a result of the 'onshore' directed sediment transport, an erosion hole

developed at the beginning of the test section and sand accumulated in front of the downstream sand trap.
From the plotted net transport rate distributions and the bed profiles (see Figure 4.16-4.20), it can be seen that these boundary effects are local, with an influence of several meters. They do probably not disturb the conditions in the central part of the test section. It is more likely that the differences in transport rates along the central part of the test section are caused by the bottom topography. This is mainly the result of the fact that the bed was not flattened before each test.

The instrument frames and the movable pole can be expected to have some influence on the net transport rate at the measuring location (x=109.2 m). This can be seen for all conditions, especially for condition mh and mi where the net transport rate decreases around the measuring location. For condition mf the opposite occurs, the transport rate increases around the measuring position.

Figure 4.25 and 4.26 show large differences between the transport rate distributions of the different tests with the same condition. This is probably caused by the inaccuracy of the applied bed profile adjustments (see Section 4.7).

In the Figure 4.27 the net transport rate distributions, averaged for all conditions are plotted.

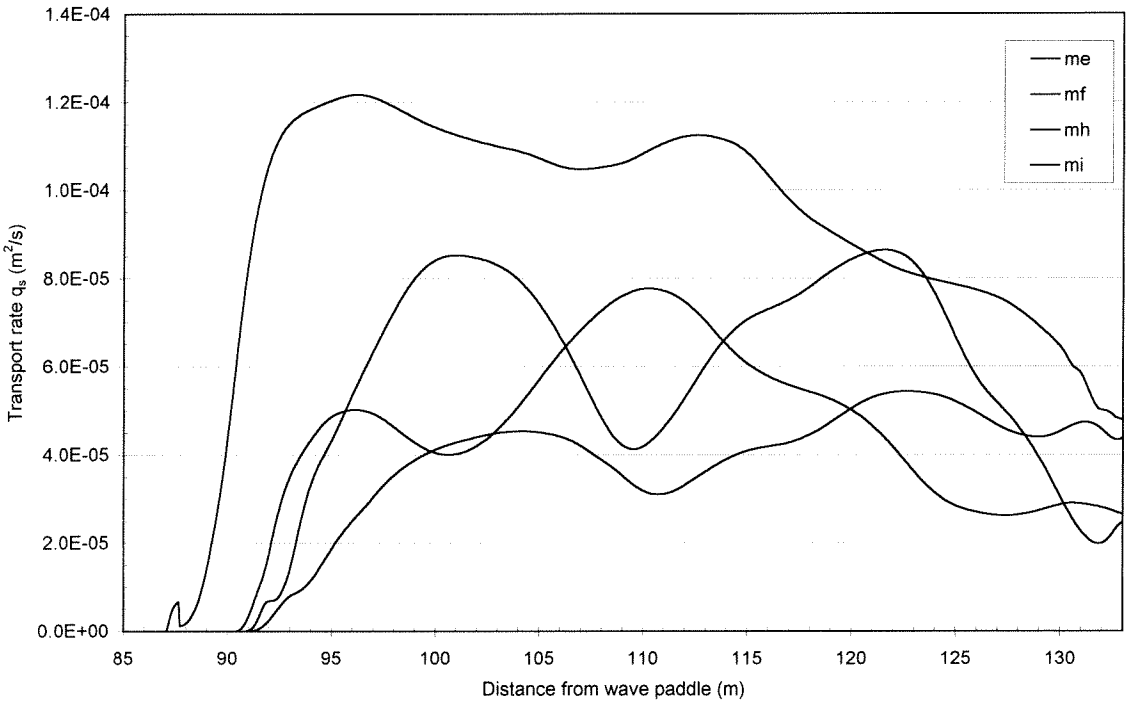

Figure 4.27: Measured net transport rates, averaged for condition me, mf, mh and mi.

4.5 Net transport rates

Time-averaged transport rates near the measuring position of the ADV are derived from the calculated transport rate distributions. For each test condition a mean value of the net transport rate is determined by averaging 4-6 tests. For all conditions the first tests (resp. mea, mfa, mha and mia) are left out. The first 6 tests were held under 6 different wave conditions. It is expected that it takes a while for the bedforms to adapt to the changed wave conditions. During the adaptation of the bed to a new wave condition it is expected that the bedforms have too much influence on the transport rates.
The following tables also include data on the flow characteristics, measured by the ADV at approximately 0.1 m above the bed, see also Section 4.2. The following parameters are presented:

T	=	average wave period over a run, determined from the wave height meters
U_{rms}	=	the root mean square value of the near-bed velocity
$<q_s>$	=	time-averaged net transport per unit width, derived at x=109.2m
σ	=	standard deviation of the time-averaged net transport rate
r	=	relative error
r_{avg}	=	relative error of averaged transport rate

Definitions:

Standard deviation: $$\sigma = \sqrt{\frac{1}{N}\sum_{i=1}^{N}(< q_s >_i - < q_s >_{avg})^2} \qquad (4.5)$$

In which:

$<q_s>_i$	=	measured transport rate for the individual test
$<q_s>_{avg}$	=	average value of the transport rate for all tests with one condition
N	=	total number of tests for one condition

Relative error: $$r = \frac{\sigma}{< q_s >} \times 100\% \qquad (4.6)$$

Relative error averaged over N tests: $$r_{avg} = \frac{r}{\sqrt{N}} \times 100\% \qquad (4.7)$$

condition	test	T (s)	U_{rms} (m/s)	$<q_s>$ (10^{-6} m^2/s)	σ (10^{-6} m^2/s)	r (%)	r_{avg} (%)
me	b,c,d,e,f,g	9.10	0.68	106.7	20.8	19.5	8.0
mf	b,c,d,e,f,g	9.10	0.66	76.7	6.92	9.0	3.7
mh	b,c,d,e	6.50	0.62	41.5	17.8	42.8	21.4
mi	b,c,d,e	6.50	0.59	34.2	19.5	57.0	28.5

Table 4.6: Net transport rates measured at x = 109.2 m.

From Table 4.6 it can be seen that the variation of the average value of the measured transport rate is relatively large for condition mh and mi. The relative error r and the relative error of averaged transport rate r_{avg} are large for condition mh and mi. This can be partly explained by the number of tests: 6 for condition me and mf, 4 for condition mh and mi.

From Figures 4.23-4.26 it can be seen that the transport rate distributions are not constant around the measuring location of the ADV (x=109.2 m). To get an idea of the magnitude of the fluctuation of the net transport rates near the measuring location, four other transport rates are defined. These net transport rates are averaged over distances of 2.5, 5, 10 and 15 m in longitudinal direction of the flume, centred around x = 109.2 m. Tables with the results for each distance and each test can be found in the Appendix H. In Table 4.7 the net transport rates, averaged over the different intervals and the standard deviation are presented.

$<q_{s,j}>$ = time-averaged transport rate, averaged over interval j = 2.5 m, 5 m, 10 m and 15 m, centred around 109.2 m
$<q_s>_i$ = time-averaged transport rate as function of the distance from the wave paddle
σ_j = standard deviation of the transport rate along the test section
M_j = total number of data points per interval j

Standard deviation:
$$\sigma_j = \sqrt{\frac{1}{M_j}\sum_{i=1}^{M_j}(< q_s >_i - < q_{s,j} >)^2} \qquad (4.8)$$

condition	$<q_{s,2.5}>$ (10^{-6} m^2/s)	$\sigma_{2.5}$ (10^{-6} m^2/s)	$<q_{s,5}>$ (10^{-6} m^2/s)	σ_5 (10^{-6} m^2/s)	$<q_{s,10}>$ (10^{-6} m^2/s)	σ_{10} (10^{-6} m^2/s)	$<q_{s,15}>$ (10^{-6} m^2/s)	σ_{15} (10^{-6} m^2/s)
me	107.1	2.1	107.6	4.0	108.3	6.5	108.1	7.9
mf	76.3	1.5	74.8	3.1	69.9	7.2	64.3	10.90
mh	43.1	1.9	47.1	5.4	56.1	11.3	63.1	14.1
mi	34.4	2.5	35.3	4.0	37.9	5.0	39.6	5.0

Table 4.7: Standard deviation of the transport rates for different intervals, along the test section.

Figure 4.28 shows the net transport rates averaged over different intervals as function of U_{rms}. From Table 4.7 and Figure 4.28 it can be seen that averaging over different intervals has the largest influence on condition mh and mf. The transport rate for condition mh increases, while the transport rate for condition mf decreases for increasing length of the interval.

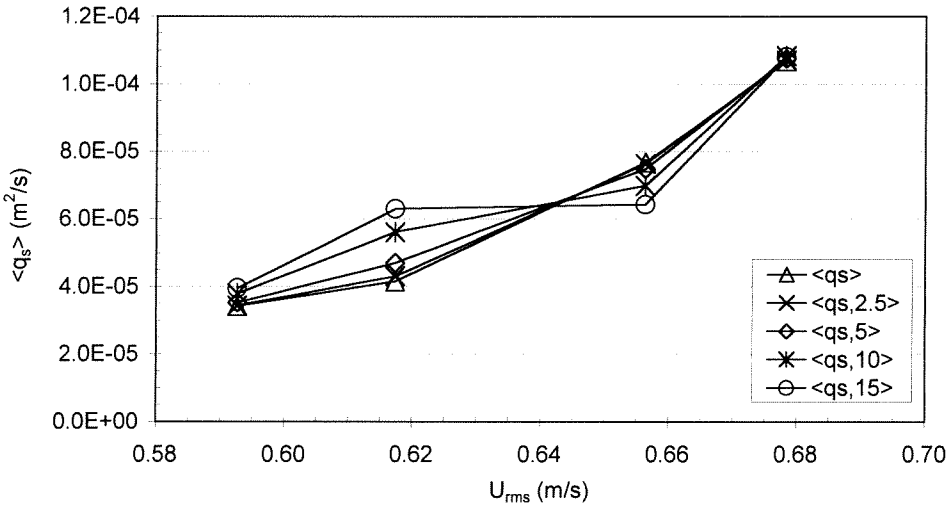

Figure 4.28: Net transport rates, averaged over different intervals as function of U_{rms}, for all conditions.

The measured transport rates, averaged over the different intervals are compared with the transport rate at x=109.2 m. This is done by calculating the relative difference between $<q_s>$ and $<q_{s,j}>$.

$<q_s>$ = time-averaged transport per unit width, measured at x=109.2m
$<q_{s,j}>$ = time-averaged transport per unit width, averaged over interval j = 2.5 m, 5 m, 10 m and 15 m centred around x=109.2 m
r_j = relative error of time-averaged transport rate, averaged over interval j and the time-averaged transport rate at x=109.2, expressed in percents
$r_{j,avg}$ = averaged relative error
$\sigma_{r,j}$ = standard deviation of r_j
N = total number of tests for one condition

$$r_j = \frac{\left(\langle q_{s,j}\rangle - \langle q_s\rangle\right)}{\langle q_s\rangle} * 100\% \tag{4.9}$$

$$\sigma_{r,j} = \sqrt{\frac{1}{N}\sum_{i=1}^{N}(r_j - r_{j,avg})^2} \tag{4.10}$$

condition	$r_{2.5}$ (%)	$\sigma_{r,2.5}$ (%)	r_5 (%)	$\sigma_{r,5}$ (%)	r_{10} (%)	$\sigma_{r,10}$ (%)	r_{15} (%)	$\sigma_{r,15}$ (%)
me	0.52	1.06	1.26	2.85	2.71	7.52	2.99	11.17
mf	-0.59	0.33	-2.50	0.64	-9.02	1.74	-16.40	3.26
mh	4.13	2.01	15.06	7.33	40.57	19.69	60.17	27.11
mi	1.93	5.03	7.69	14.74	20.82	31.41	29.57	42.68

Table 4.8: Relative error between $<q_s>$ and $<q_{s,j}>$ and the standard deviation of the relative error, expressed in percentages.

From Table 4.8 it can be seen that the relative error increases for increasing length of the interval, for all conditions, but most for condition mh.

It is concluded that averaging over 2.5 m, 5 m, 10 m, and 15 m affects the transport rate, showing that the transport rates fluctuate around the measuring position. It is difficult to determine which interval reproduces the most realistic net transport rate. A choice is made here in order to simplify the further analysis of the net transport rate.

It seems logical to average the transport rate over a certain interval instead of considering the transport rate at a single point (the measuring location of the ADV, at x=109.2 m). On the other hand the interval can not be taken too long because the velocities are only measured in one point and may deviate too much over the length of the interval. Based on these considerations the length of the interval is chosen similar to the horizontal length of the orbital motion. The horizontal length of the orbital motion can be estimated with 2* the semi-excursion length of a water particle (a). From Table 4.3 it can be seen that the horizontal length of the orbital motion varies between 2.0 and 2.7 m. Further analysis is done with the net transport rate, averaged over 2.5 m $<q_{s,2.5}>$. It must be noted that based on Figure 4.27 a different representative transport rate (averaged over a longer interval) may be chosen for condition mf and mh.

The following parameters for $<q_{s,2.5}>$ are presented in Table 4.9:

- average wave period (T), determined from the wave height meters
- the root mean square value of the near-bed velocity (U_{rms})
- time-averaged net transport rate per unit width ($<q_{s,2.5}>$)
- standard deviation (σ) of the time-averaged net transport rate
- relative error (r)
- relative error of averaged transport rate (r_{avg})

condition	T (s)	U_{rms} (m/s)	σ_{rms} (m/s)	$<q_{s,2.5}>$ (10^{-6} m^2/s)	σ (10^{-6} m^2/s)	r (%)	r_{avg} (%)
me	9.10	0.68	0.022	107.1	20.1	18.7	7.7
mf	9.10	0.66	0.017	76.3	7.03	9.2	3.8
mh	6.50	0.62	0.007	43.1	18.3	42.4	21.2
mi	6.50	0.59	0.016	34.4	19.1	55.5	27.7

Table 4.9: Net transport rates averaged over 2.5 m, centred around x = 109.2 m.

Table 4.9 shows large relative errors for condition mh and mi compared with condition me and mf. This can be caused by the lower degree of wave asymmetry for condition mh and mi. It is expected that the transport rates in positive and negative direction during the positive and the negative half wave cycles are still large, but due to the relative low degree of wave asymmetry, they are of similar magnitude. Therefore relatively small variations in the half cycle transport may lead to relatively large variations in the net transport rate. Figure 4.29 shows the net transport rate $<q_{s,2.5}>$, as function of U_{rms}, for all conditions, with their standard deviations.

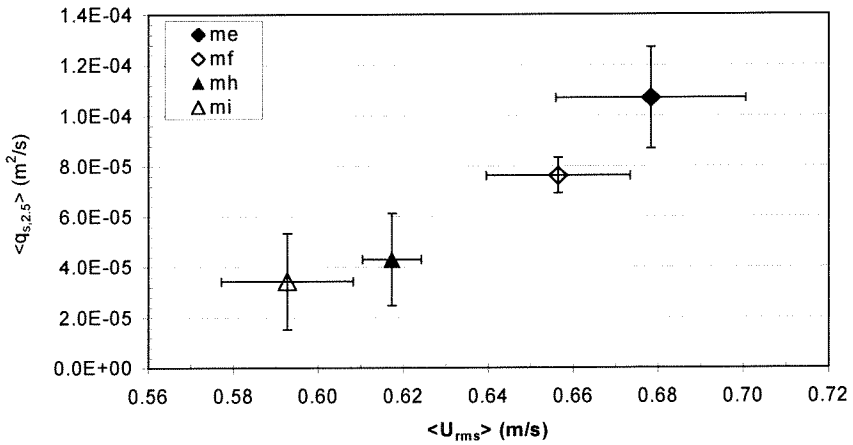

Figure 4.29: Net transport rate $<q_{s,2.5}>$, as function of U_{rms}, for all conditions, with their the standard deviations.

4.6 Analysis of the net transport rates

4.6.1 Flow velocity influence

Figure 4.30 shows the net transport rates, with their standard deviations, averaged over a distance of 2.5 m, as a function of $<U^3>$, $<|U^3|U>$, $<U^5>$ and $<|U^5|U>$, plotted on double logarithmic scale.
Added to the figure is a dashed line with a slope 1:1 which indicates a linear relation between $<q_{s,2.5}>$ and $<|U^{n-1}|U>$. The best fit line through the measurements should be parallel to the 1:1 line for a good agreement.

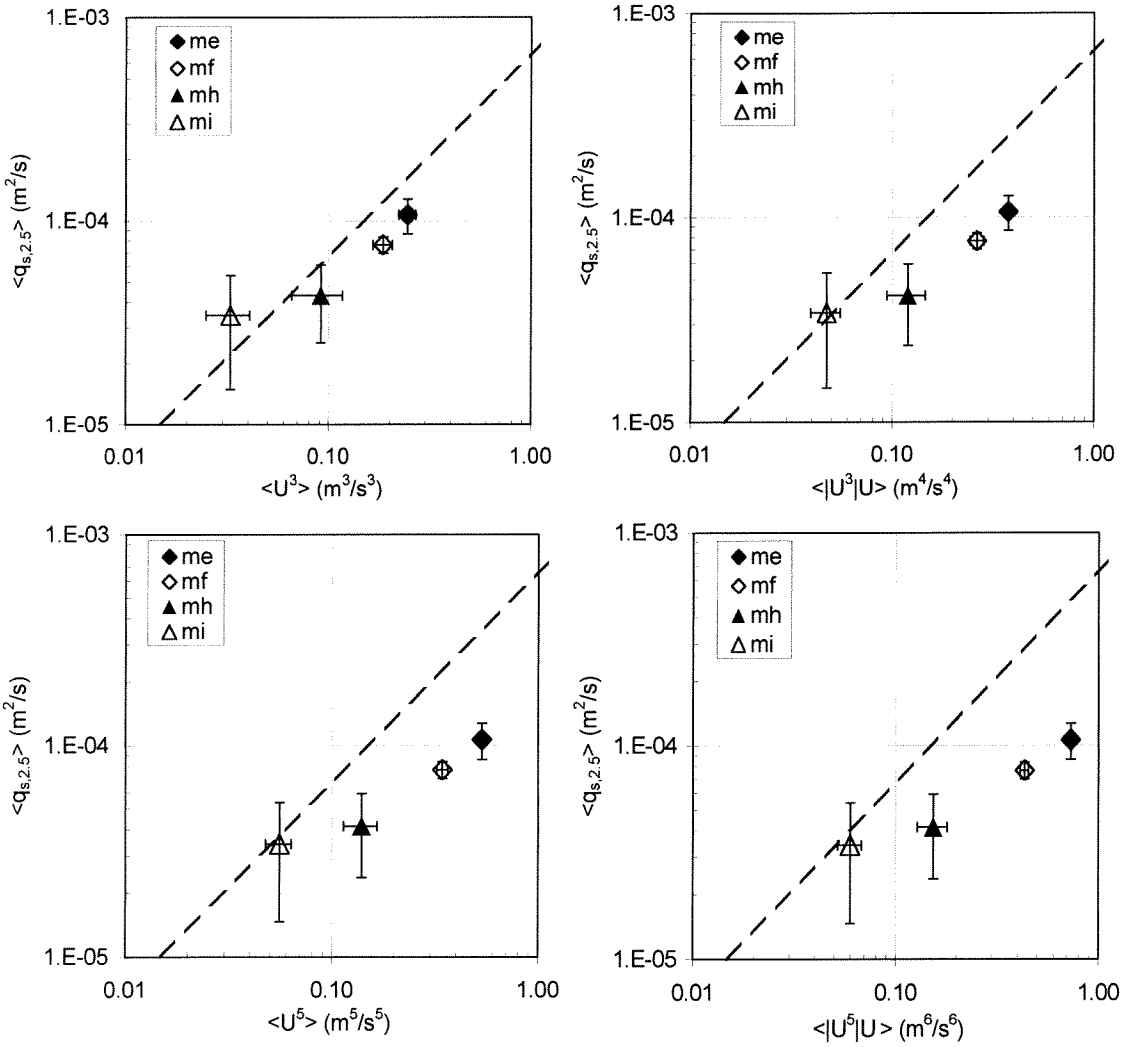

Figure 4.30: Net transport rate $<q_{s,2.5}>$ as a function of different velocity moments $<|U^{n-1}|U>$.

It can be seen from the panels of Figure 4.30 that condition me, mf and mh follow the dashed 1:1 line in the upper left panel reasonably well. This indicates that a power law relation (see Eq. 2.12) with power n=3 can be used to predict the net sand transport rate. For the larger powers the net transport rates deviates increasingly from dashed 1:1 line. This indicates that the powers n=4, n=5 and n=6 are probably too large.

From Figure 4.30 it can also be seen that condition mi deviates from the relation between the other conditions. The linear relation between condition me, mf and mh crosses the standard deviation of condition mi. The deviation of the net transport rate of condition mi could therefore also be explained by the inaccuracy of the net transport rate measurement.
In the following sections different influences on the net transport rate will be reviewed and a possible cause of this deviation will be investigated.

4.6.2 Wave period influence

Figure 4.31 shows the net transport rate $<q_{s,2.5}>$ as function of $<U^3>$. In the figure a linear trendline is added, showing a linear relation between condition me, mf and mh. The net transport rate for condition mi, with a wave period of 6.5 s, seems larger than would be expected from the relation between condition me, mf and mh. From Figure 4.31 no clear wave period influence can be seen.

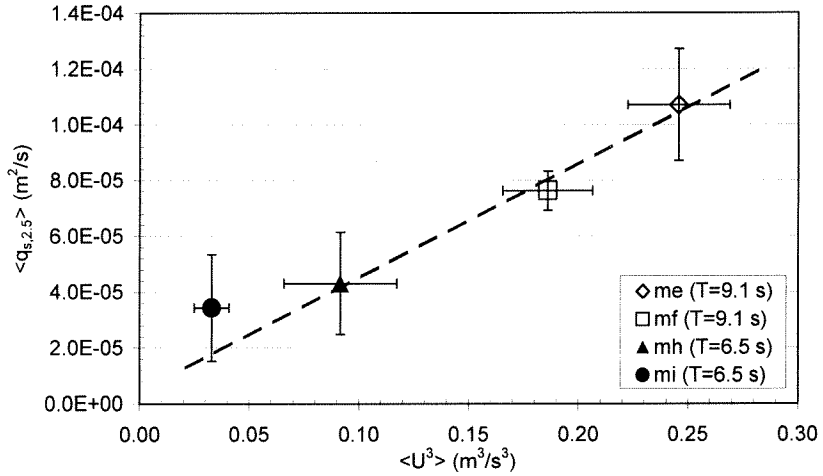

Figure 4.31: Net transport rate $<q_{s,2.5}>$ as function of $<U^3>$.

4.6.3 Wave asymmetry influence

The increasing degree in wave asymmetry for condition me towards condition mi causes a increase in the third order velocity moment $<U^3>$. This can be seen from Figure 4.32 (left-hand panel). From the right-hand panel of Figure 4.32 it can be seen that for an increasing degree of wave asymmetry, the net transport rates also increases. However, condition mi clearly deviates from the other conditions, the net transport rate is larger than would be expected from the left-hand panel.

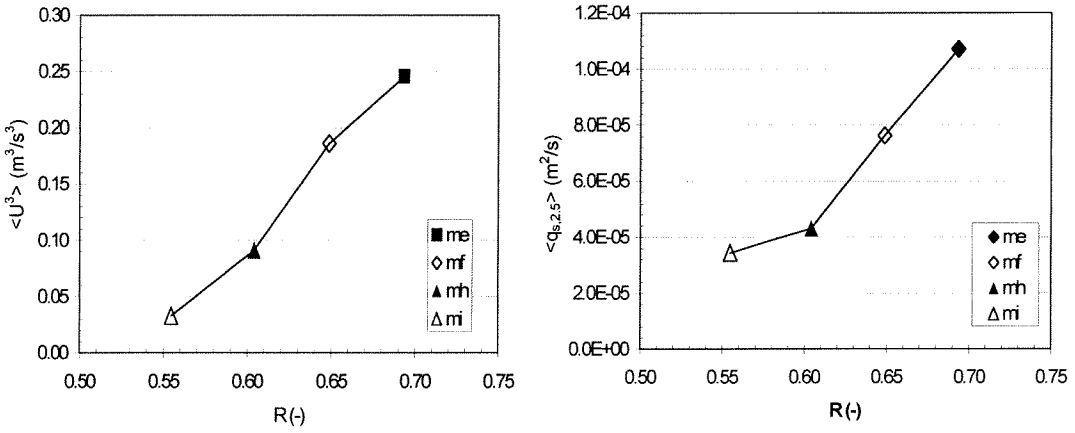

Figure 4.32: Third order velocity moment $<U^3>$ (left-hand panel) and the net transport rate $<q_{s,2.5}>$ (right-hand panel) as function of the degree of wave asymmetry R.

4.6.4 Other influences

From Figure 4.30 it can be seen that a linear relation may exist between transport rate and the third order velocity moment, for condition me, mf and mh. The net transport rate for condition mi is larger than would be expected from the linear relation between condition me, mf and mh. This may be explained by the fact that the inaccuracy of a measurement, influences low values of the net transport rate more than large values. Another reason could be the occurrence of different transport mechanisms, for example, flow separation and vortex shedding. Whether this is the case can be checked by reviewing some of the following parameters. The following parameters can be found in Table 4.10:

- degree of wave asymmetry (R), defined as $[U_{cr}/(U_{cr}+|U_{tr}|)]$
- wave friction factor (f_w), with $k_s=D_{50}$
- orbital velocity amplitude (U_a), defined as $U_a=½(U_{cr}+U_{tr})$
- mobility number Ψ ($=½(\Psi_{cr}+\Psi_{tr})$)
- maximum Shields parameter θ_w ($= ½(\theta_{cr}+\theta_{tr})$)
- phase lag parameter (p), based on calculated sheet flow layer thickness (Eqs.2.7;2.7)
- net transport rate $<q_{s,2.5}>$

condition	R (-)	f_w (10^{-3})	U_a (m/s)	Ψ (-)	θ_w (-)	p (-)	$<q_{s,2.5}>$ (10^{-6} m^2/s)
me	0.69	6.64	1.05	319	1.06	0.067	107.1
mf	0.65	6.68	1.01	279	0.93	0.059	76.3
mh	0.60	6.90	0.96	253	0.87	0.064	43.1
mi	0.55	7.04	0.93	232	0.81	0.064	34.4

Table 4.10: Wave friction factor, maximum Shields parameter and phase lag parameter, averaged for each condition.

In Section 4.3.4 it was already concluded that sharp crested vortex ripples do not appear during the present tests. It was seen that the values of the maximum Shields parameter $\theta_{w,cr}$ and the mobility numberΨ_{cr} (both based on U_{cr}), exceeded the limit values on which the transition to sheet flow over flat beds occurs. However, it can also be seen that the values of $\theta_{w,cr}$ and Ψ_{cr} decrease for condition mf, mh and mi. Condition mi has the lowest values of $\theta_{w,cr}$ and Ψ_{cr} and also the steepest bedforms. Therefore, the relatively large net transport rate may

be explained by the fact that for this condition other transport mechanisms occurred, which had a positive effect on the net transport rate.

From Table 4.10 it can be seen that the value of the phase lag parameter is about the same for all conditions. Therefore no differences in phase lag effects between the different conditions are expected. For values of the phase lag parameter smaller than 0.5 no phase lag effects are expected to occur. This was found by Dohmen-Janssen (1999) in an oscillatory water motion, superimposed on a steady current and a D_{50} of 0.21 mm.

It can be concluded, based on these results, that with a value of the phase lag parameter $p<0.07$, sediment transport reducing phase lag effects do not play a role during the tests.

In Chapter 5 the measured transport rates will be compared to the predicted transport rates of three quasi-steady models and one semi-unsteady model. From the comparison it should be clear if phase lag effects had a significant influence on the measured net transport rates.

4.7 Accuracy of the results

The accuracy of the results is determined by the accuracy of the MTA and parameters concerning the calculation technique. This technique is described in Chapter (3.4.2). Inaccuracy in these parameters will lead to an error in the determined net transport $<q_s>$. These parameters are:

parameter	indicating
ε_0	Porosity of the sand [-]
Δt	Duration of a test [s]
Δx	Place step [m]
Δz	Change in bottom level between two tests [m]

The accuracy and used values of the parameters concerning the calculation technique will be discussed in the following section:

Porosity (ε_0)
The porosity (ε_0) of the sand is not measured during the experiment. The value of the porosity is determined from values used in other experiments in which sand was used with comparable characteristics (Al-Salem, 1993; Ramadan, 1994; Katopodi et al., 1994; Janssen & Van der Hout, 1997). The porosity is taken constant: ε_0=0.38. It is assumed that the variation of the porosity during the experiment is not very large. It is not known if this is the case for the present experiment.

Duration (Δt)
Duration of a test (Δt) is determined accurately by the data acquisition systems and the steering signal of the wave paddle. Because the duration is accurately determined it will not contribute much to the inaccuracy of the results. For all tests a duration of 1800 s is used. Except for test mea, which had a total duration of 1920 s.

Place step (Δx)
The distance between the data points (Δx) is determined by the pulse rate of the MTA and the velocity of the carriage. Because the pulse rate is very accurate, the accuracy of Δx is determined by the velocity of the carriage. It was seen that the velocity of the carriage was not constant during a test. This leads to different values of Δx. In the net transport rate calculations, Δx is assumed constant because it was found that the variation in Δx is small and does not have a large influence on the accuracy of the results.

Bed level difference (Δz)
The accuracy of the change in bottom level between two tests (Δz) is influenced by the placement of the transducers, the accuracy of the MTA and the horizontal and vertical position of the profiles.

The placement of the transducers in cross direction of the flume has an influence on the measured bed profiles. The bedforms may vary in cross direction of the flume. Therefore the bed profiles measured with each transducer may also differ. By averaging over all 32 transducers specific information about the difference between the bed height in cross direction is lost. It was seen after the experiment had ended and the flume was drained, that the bedforms that developed during the tests, were stretched out over the complete width of

the flume. It is therefore expected that averaging in cross direction does not influence the net transport rates.

The MTA records the bed level with an accuracy of 2-3 mm in vertical direction. It is not likely that this inaccuracy will cause a systematic offset in vertical direction of a bed profile. However, the influence of the vertical accuracy of the MTA on the measured bed profiles is not clear. This influence can be estimated by measuring the same profile twice and compare the measured profiles in order to get an indication of the accuracy. During the present tests not one profile is measured twice. Therefore no indication of the accuracy of the MTA can be given.

The vertical offset (the bed level height relative to the flume bottom) of all bed profiles does not have a large influence on the transport rate. The accuracy is well below 1 cm and is negligible compared to the following corrections.

It was found that the most important influence on the accuracy of the calculated transport rates comes from corrections made for the erosion hole and from the difference between the bed profiles in vertical and horizontal direction. The influence on the accuracy from corrections made for the sand deposition is not taken into account because they have no effect on the accuracy of the transport rates at the measuring location.

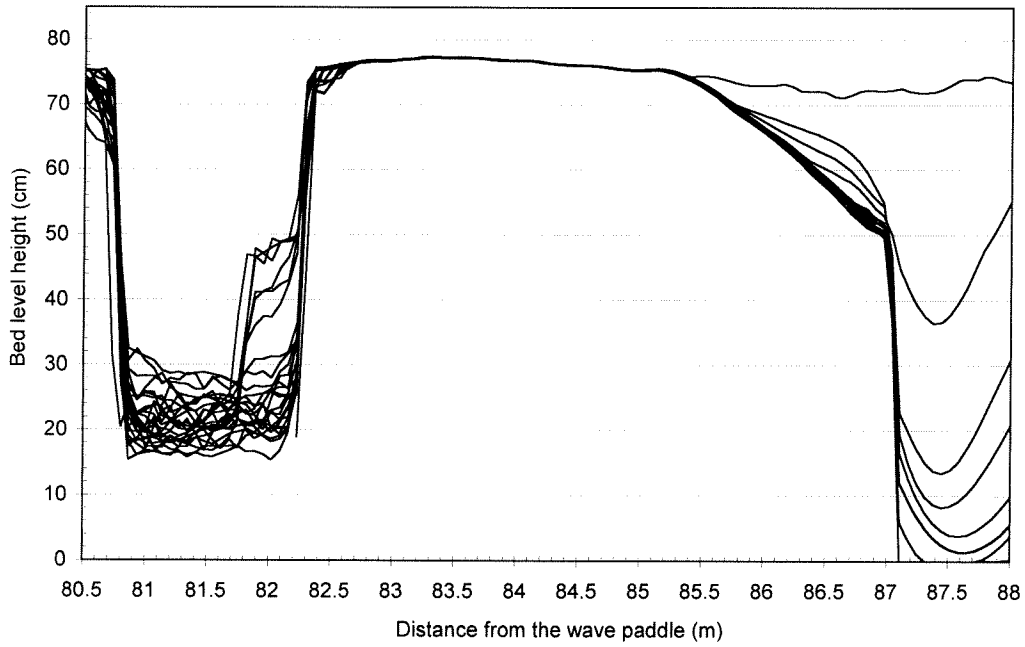

Figure 4.33: Upstream sand trap and asphalt layer

The difference between the bed profiles in vertical and horizontal direction is estimated by considering a few reference locations. Figure 4.33 shows the upstream sand trap and the asphalt layer. In Figure 4.34 the downstream sand trap and the asphalt layer with the cement block are shown for all bed profiles. The asphalt layers shown in Figure 4.33, between x=82.6 m and x=85.3 m, except for the cement block and Figure 4.34, between x=134.8 m and x=136.8 m, can be used to estimate the difference in vertical direction between the bed profiles. By calculating the standard deviation σ between these intervals the accuracy in vertical direction can be estimated. An indication of the accuracy is given by calculating the sand transport rate, using the value of $2*<\sigma_{mean}> = 0.13$ cm as an offset in z-direction between

two bed profiles. The standard deviation $<\sigma_{mean}>$ is the average standard deviation of the asphalt layers with a value of $<\sigma_{mean}>=\frac{1}{2}(0.066+0.059)$ (see Table 4.11). This transport rate can be compared with the normal transport rate.

standard deviation $<\sigma>$ in vertical direction (cm)	standard deviation $<\sigma>$ in horizontal direction (cm)	averaged over interval (m)
0.066	-	x=134.8 and x=136.8
0.059	-	x=82.6 and x=85.3
-	1.21	x=85.5 and x=87.0

Table 4.11: Standard deviation between bed profiles.

The same can be done for the difference between the bed profiles in horizontal direction. This is done by calculating the horizontal difference between the bed profiles for the asphalt layer located between x=85.5 m and x= 87 m (see Figure 4.33). It was found that the difference in horizontal direction has a mean value of 1.57 cm with a standard deviation $<\sigma>$ of 1.21 cm. Again an indication of the accuracy can be given by applying a value of $2*<\sigma> = 2.42$ cm as an offset in x-direction in the calculation of the sand transport rate and compare it with the normal transport rate.

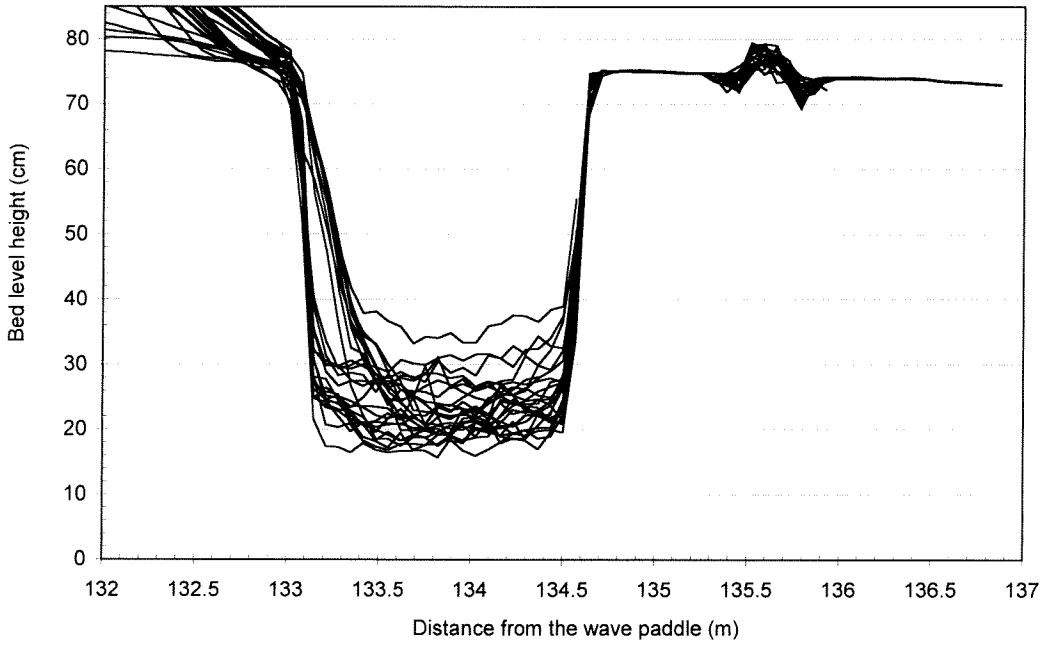

Figure 4.34: Downstream sandtrap and asphalt layer with cement block.

The accuracy of the correction, made for the erosion hole is estimated by considering different bed level extrapolations. From the values of height ec (Appendix D, Tables D.1-D.3) it can be seen that below a level of about 20 cm above the flume bottom, the bed level is not known. A lower boundary is found by a linear extrapolation of the known bed level to the level of the flume bottom (see Figure 4.35). From Figure (4.36) it can be seen that the linear extrapolation gives a higher sand transport rate compared to the normal transport rate. An upper boundary is found by extrapolating the known bed level by using an order 3 polynomial relation (see Figure 4.35). It is seen in Figure (4.36) that the polynomial extrapolation gives a

lower sand transport rate. These upper and lower boundary estimates are determined for all conditions.

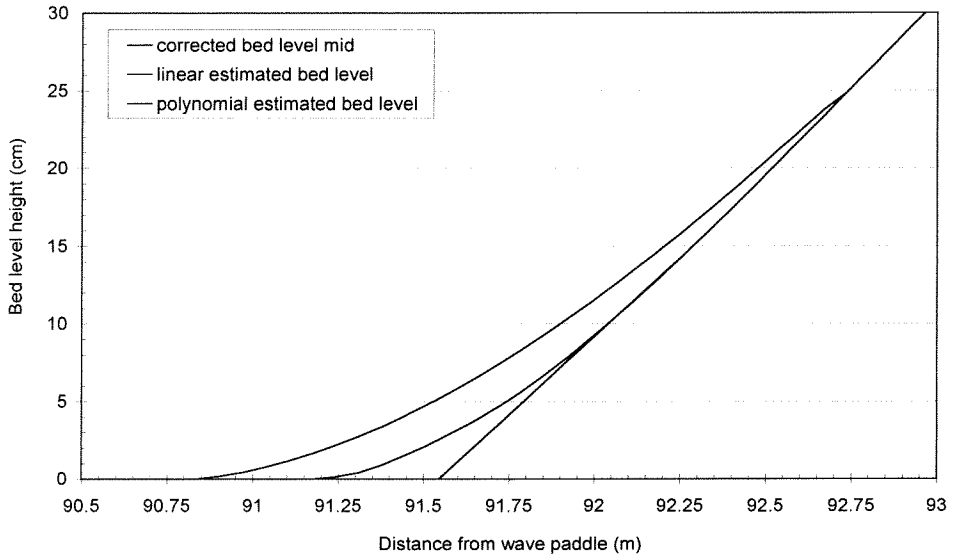

Figure 4.35: Linear and polynomial estimates for the corrected bed level height.

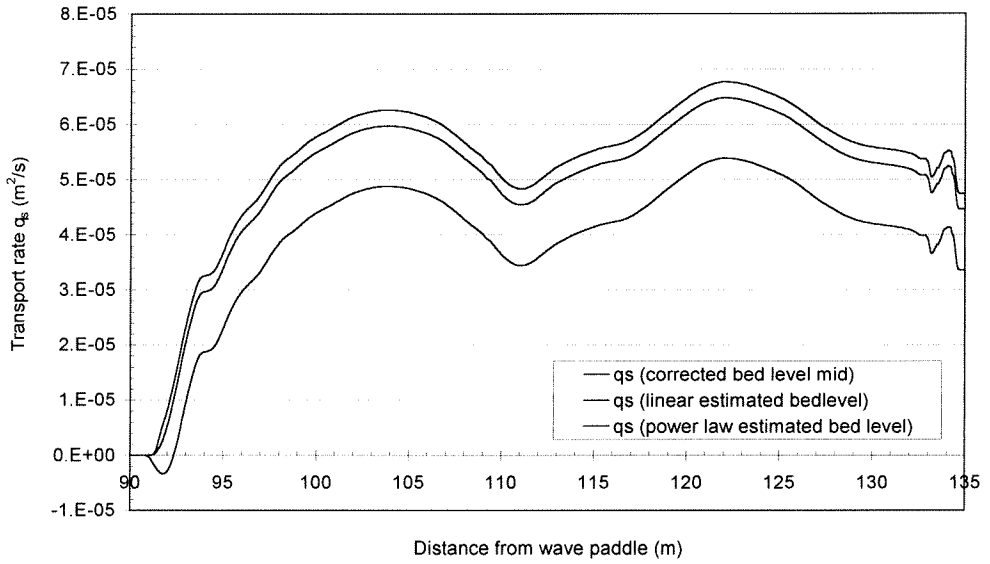

Figure 4.36: Net transport rates for linear and polynomial estimated bed levels.

In the following table the differences, expressed as percentages, between the normal sand transport rates $<q_{s,2.5}>$ and the deviating transport rates $<q_{s,j}>$ are shown. The parameters r_{lin} and r_{pol} represent the percentages of resp. the linear and the polynomial estimates for the bed level. The parameters r_{ver} and r_{hor} represent the percentages of resp. the vertical and horizontal difference between the bed profiles. The transport rates are averaged over a distance of 2.5 m, centred around the measuring location at x = 109.2m. The relative errors r_j expressed in percentages are derived with the following relation:

$$r_j = \frac{\left(\langle q_{s,j} \rangle - \langle q_{s,2.5} \rangle\right)}{\langle q_{s,2.5} \rangle} * 100\% \qquad (4.11)$$

condition	r_{lin} (%)	σ_{lin}	r_{pol} (%)	σ_{pol}	r_{ver} (%)	σ_{ver}	r_{hor} (%)	σ_{hor}
me	6.0	5.2	-7.1	1.5	9.4	2.5	4.5	2.3
mf	3.8	2.5	-9.0	2.9	12.5	1.1	7.8	0.7
mh	4.6	2.9	-13.8	11.0	26.0	13.1	16.2	8.2
mi	8.0	4.7	-26.4	17.6	37.6	25.4	24.2	16.0

Table 4.12: Accuracy of the results, determined with relative errors.

From the table it can be seen that the largest influence on the accuracy can be expected from the correction of the erosion hole (especially r_{pol}) and the difference between the level of the bed profiles in vertical direction (r_{ver}) and the difference between the bed profiles in horizontal direction (r_{hor}). The relative error for each test can be found in Appendix I.

4.8 Summary of the main results

The main results of the present experiments with respect to the measured net transport rates are summarised as follows;

- For all tests the measured net sediment transport rates were, in the direction of wave propagation.
- The measured net transport rates showed a linear relation with the third order velocity moment $<U^3>$ for condition me, mf and mh. Condition mi seems to deviate from this relation. This may be explained by inaccuracy in the sediment transport measurement. The linear relation between $<q_{s,2.5}>$ and $<U^3>$ indicates that the assumption of a direct relation between the instantaneous sediment transport and the instantaneous horizontal free-stream velocity is justified.
- Based on the value of phase lag parameter p, which was smaller than 0.07 for the present tests, it is expected that sand transport reducing phase lags between sediment concentration and the near-bed velocity were not present. Phase lag effects may become important for $p>0.5$.
- No clear influence between the different wave periods and the net transport rates were found.

The net sediment transport rate distribution was not constant along the test section. The instrument frames and the movable pole probably influenced the net transport rate distribution. A representative transport rate was found by averaging over a distance of 2.5 m in longitudinal direction of the flume, centred around 109.2 m. This length is about 2 times the semi-excursion amplitude of the water particles.

The bedforms, which developed during the experiments are not expected causing vortex shedding or flow separation, although the steepness of the bed (dz/dx) increased towards the end of the experiment from 0.02 to 0.085. As an indication for the occurrence of flow separation, the ratio semi-excursion length and bedform wavelength (a/λ) is determined. For values of a/λ_r larger than 0.5, ripples first introduce random instability, including flow separation above the lee slopes. For the present tests it was found that $a/\lambda \leq 0.14$.
The maximum Shields parameter $\theta_{w,cr}$ (based on U_{cr}) had a value larger than 1 for all tests. A plane bed is expected for values of the maximum Shields parameter larger than about 0.8-1. The value of the mobility number Ψ_{cr} (based on U_{cr}) was larger than 330. The inception of sheet flow over flat beds is found for values of $\Psi>100$ to 200.

The phase lag parameter p (see Eq.2.6) depending on the sheet flow layer thickness (see Eq.2.7) indicates that phase lag effects were not present during the experiments. This is also confirmed by the fact that no sand was found, upstream of the test section. If phase lag effects did occur, it is expected that sand is transported in the opposite direction of wave propagation. This has to be confirmed by comparing the measured transport rates with the predictions of the transport models (see Chapter 5).

It is concluded that measuring sand transport rates in wave flumes is more difficult, compared to water tunnels. The accuracy of the measured transport rates depends on many factors, for example: the assumption made for the porosity, the uncertainty of the extrapolated bed level of the erosion hole, the vertical resolution of the MTA, etc. On the other hand the accuracy can be increased by pre-processing the data. This is done by comparing all measured bed profiles and minimise differences between them in vertical and horizontal direction. It was found that the differences in level between two bed profiles had a large influence on the accuracy.

An indication of the accuracy is given by determining the relative errors for an offset in vertical and horizontal direction between two bed profiles. For the determination of the relative errors, $<q_{s,2.5}>$ is used. It was found that a systematic difference of 1.3 mm in vertical direction between two bed profiles, results in a relative error (r_{ver}) of 9% for condition me, up to 38% for condition mi (see Table 4.12). Also the correction of the erosion hole has a large influence on the accuracy, especially the polynomial estimation of the bed level, with a relative error (r_{pol}) for condition me of 7%, up to 26% for condition mi. A horizontal offset between two profiles also causes inaccuracies. It was found that r_{hor} was 5% for condition me and increasing to a value of 24% for condition mi.
It was found that all relative errors increased from condition me to mi. The large relative errors for condition mi (also for mh) may be an explanation for the inaccuracy between the different tests for that condition.

It is not easy to determine an overall accuracy for the measured transport rate. For example, the average of all relative errors for a condition, presented in Table 4.12 does not represent the total relative error for a condition. The relative errors only give an indication of the influence of a single deviation on the accuracy. The best way to get an indication of the accuracy of a measured bed profile, is to measure the same bed profile more than once and compute the differences between them. This could not be done for the present experiments because non of the bed profiles is measured twice. To give an indication for the maximum value of the accuracy of the measured transport rates it is recommended to review the highest value of the different relative errors. This means that for the conditions me, mf, mh and mi, the relative errors are resp. 10%, 13%, 26% and 38% (see Table 4.12).

Chapter 5 Comparison of experimental results

5.1 Introduction

The time-averaged sediment transport rates, as presented in Chapter 4, are compared with experimental data from an oscillating water tunnel and predictions of a number of cross-shore transport models (see Chapter 2). The aim of this comparison is to determine whether;

- net transport rates measured in a wave flume can be compared to net transport rates measured in a water tunnel,
- the transport models can predict the measured experimental data,
- phase lag effects were present.

A comparison between other experimental data-sets is presented in Section 5.2. A comparison of the present results with predictions of quasi-steady transport models of Bailard (1981), Al-Salem (1993) and Ribberink (1998) is made in section 5.3.1. The comparison of the present results with the predictions of the semi-unsteady model of Dibajnia & Watanabe (1992) is made in Section 5.3.2.

5.2 Comparison of experimental results with other data-sets

The present results will be compared with transport rates measured in the LOWT of Delft Hydraulics (see Section 2.5), i.e. the measurements of Al-Salem (1993), Katopodi et al. (1994) and Janssen and V.d. Hout (1997).

In Figure 5.1 the net transport rates for the present experiments and the different experimental data-sets as function of the third order velocity moment are displayed.

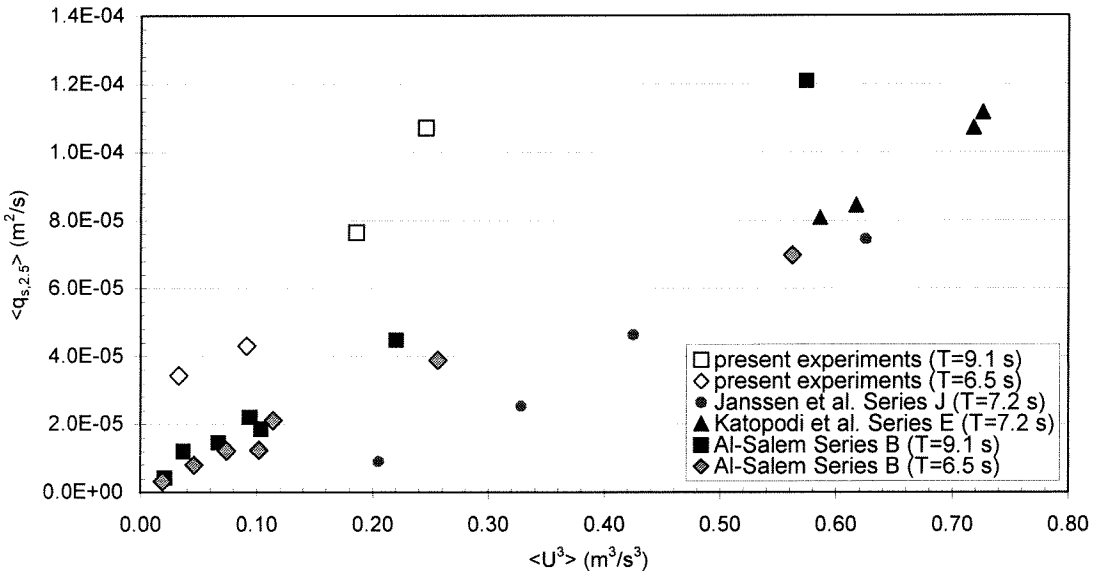

Figure 5.1: The net transport rates for the present experiments and the different experimental data-sets as function of $<U^3>$

From Figure 5.1 it can be seen that the net transport rates for the present experiments are larger than all the net transport rates of other data-sets. In order to determine the differences in

transport rate (quantitatively) between the present experiments and different data-sets, a comparison can be made

Al-Salem (1993)

Figure 5.2 shows the present experimental results and the measurements of Al-Salem (Series B, 1993) as function of $<U^3>$. In this figure a linear trendline, based on the measurements of Al-Salem and another linear trendline, based on the present experiments can be seen. From this figure it can be seen that the net transport rates of the present experiments are a factor 2.5 larger than the net transport rates of series B. The net transport rate of condition mi is a factor 5 larger, compared to the net transport rates of series B.

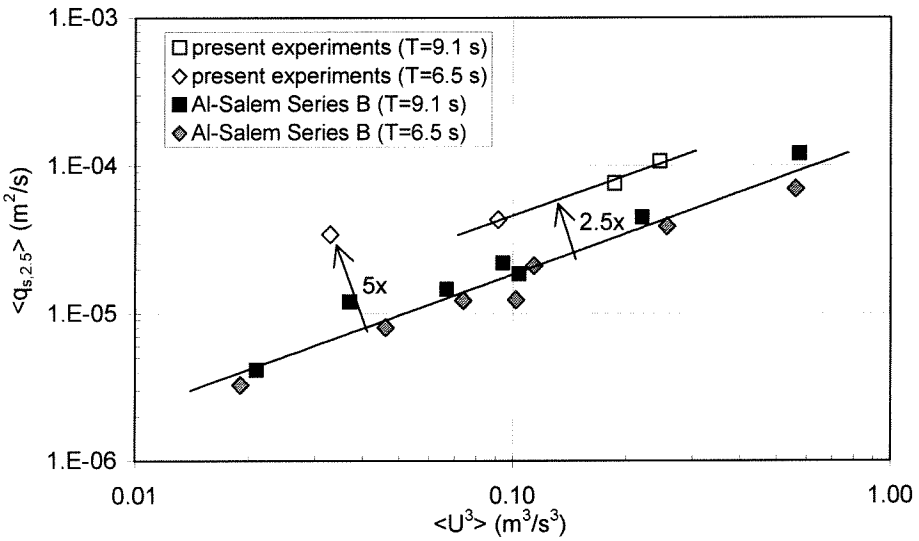

Figure 5.2: Comparison between present experimental results and the measurements of Al-Salem (1993).

From this figure it can be seen that the measured transport rates of series B, are a factor 2-3 lower than the net transport rates, measured during the present experiment. A systematic influence of the wave period on the net transport rate was present for series B. Figure 5.2 shows that test conditions with a period of 9.1 s gave larger net transport rates than test conditions with a period of 6.5 s. Such an influence can not be seen for the present tests. Periods and near-bed velocities are in the same range for both experiments, only the median grain diameter of the experimental sand is somewhat different: 0.21 mm for series B and 0.24 mm for the present tests. The influence of this difference in median grain diameter is very small. The accuracy of the sediment transport measurements in the wave flume is too low to be able to measure the difference between these two median grain sizes.

Katopodi et al. (1994) and Janssen & V.d. Hout(1997)

Figure 5.3 shows a comparison between the present experimental results and the measurements of Katopodi et al. (Series E, 1994) and those of Janssen & V.d. Hout (Series J, 1997). In this figure a linear trendline, based on the measurements of series E and J can be seen. Because this trendline is not parallel to the trendline based on the present results, the powerlaw formulation (Eq.5.1) can not be used in this case.
In this figure it can be seen that the net transport rates of condition me, mf and mh are resp. a factor 7.5, 9.5 and 21 larger than the net transport rates of series E and J.

The third order velocity of condition mi is not in the same range as the third order velocities of series E and J. Therefore condition mi is not comparable with the measurements of series E and J. However, when the transport rate of mi is compared to the linear trendline (based on the measurements of series E and J), it is found that the transport rate of condition mi is a factor 123 larger. As said before, this is not a realistic value.

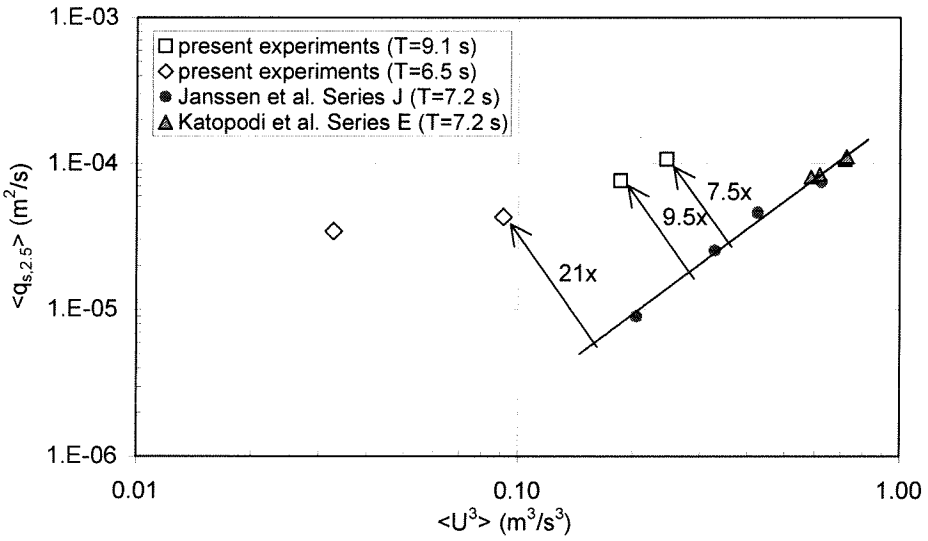

Figure 5.3: Comparison between present experimental results and the measurements of Katopodi et al. (1994) and those of Janssen & V.d. Hout (1997).

It must be said that series E and J were carried out under an oscillatory water motion, superimposed on a steady current. The median grain diameter of the experimental sand is different: 0.21 mm for series E and J and 0.24 mm for the present tests. Also here it can be said that the difference between the median grain sizes is too small to measure a difference in the sediment transport rates.

5.3 Comparison with models

5.3.1 Verification of quasi-steady models

Bailard (1981)

In the present study the total net transport rates were measured. The formula of Bailard predicts the bed-load and suspended load transport with Eq. 2.14 and 2.15. In the formula the following parameters were used: the angle of internal friction $\varphi=27°$, the bed load efficiency factor $\varepsilon_b=0.1$, the suspended load efficiency factor $\varepsilon_s=0.02$. Bailard does not specify a formulation for the friction factor f_w nor for the roughness height k_s. For the wave friction factor the expression of Swart (1974) is applied (see Eq.2.4). Based on earlier experiences the Nikuradse roughness height of $k_s=D_{50}$ (=0.24 mm) is applied. The semi-excursion length of the water particles (a) due to the horizontal oscillatory flow is based on $½(a_{cr}+a_{tr})$. For the present experiment a relative density of s=1.65 and a sediment fall velocity of $W_s=0.035$ m/s are applied.

The verification of the Bailard (1981) model with the experimental results is shown in Figure 5.4. The solid lines in the figures represent perfect agreement between the predicted and measured transport rates. The two dashed lines indicate a factor 2 difference.
From Figure 5.4 it can be seen that the measured transport rates are predicted with a difference of a factor two or more. All conditions are underpredicted, especially condition mi.

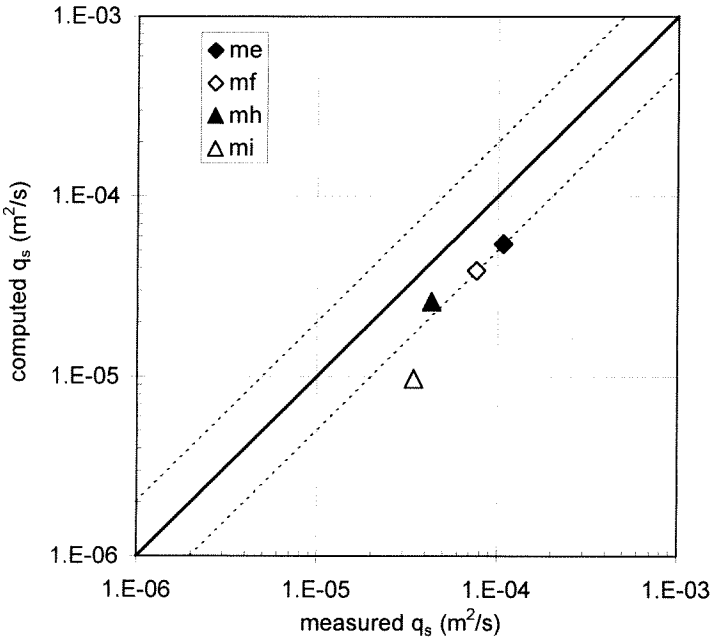

Figure 5.4: Measured and calculated sediment transport rates (Bailard, 1981).

Al-Salem (1993)

The verification of the model of Al-Salem (1993), see Eq. 2.16, with the present experimental results is shown in Figure 5.5. The left panel of Figure 5.5 shows the results of Eq.2.16 with a value for constant A of 5, derived by Al-Salem (1993). The right panel shows the results of Eq.2.16 with a value for constant A of 4. This value was derived by Ribberink and Al-Salem (1994) after curve fitting with more other experimental data-sets.
Again, the expression of the wave friction factor f_w formulated by Swart (1974) is applied (see Eq.2.4). The value of the roughness height is set on $k_s=D_{50}$. From Figure 5.5 it can be seen that Eq. 2.16 with different values for the constant factor A underpredicts the measured net transport rates with about a factor 2 for condition me, mf and mh. The measured net transport rate is slightly better predicted by applying a value for the constant factor A of 5 (Al-Salem, 1993).

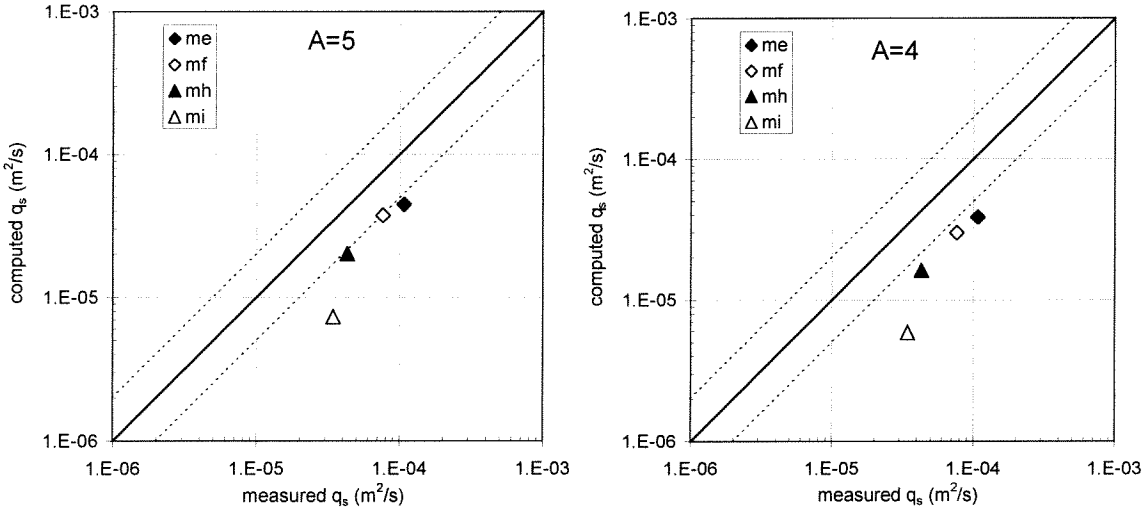

Figure 5.5: Measured and computed sediment transport rates for the models of Al-Salem (1993, left-hand panel) and Ribberink & Al-Salem (1994, right-hand panel).

Ribberink (1998)

Ribberink (1998) included the critical Shields parameter θ_{cr} in his formulation for the net transport rate. The critical Shields parameter is determined by the value of the non-dimensional grain size D_* (see Eq.2.18). A value of the critical Shields parameter of θ_{cr}= 0.044 is applied for all conditions.
Ribberink (1998) derived an expression for the roughness height in sheet flow conditions, see Eq.2.19. This expression is used to compute the wave friction factor of Swart (1974), see Eq.2.4. The wave friction factor is used to calculate the time-dependent Shields parameter, see Eq.2.3. The following values for coefficient m and exponent n were applied: m=11 and n=1.65.
Figure 5.6 shows the comparison between the measured and the computed transport rates. It can be seen that the formula of Ribberink (1998) underpredicts the measured transport rates with about a factor 3 or more.

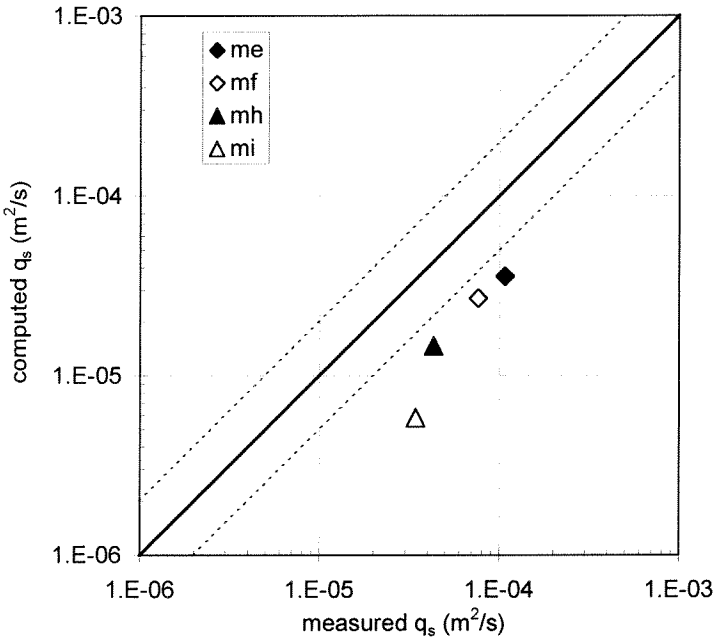

Figure 5.6: Measured and computed sediment transport rates (Ribberink, 1998).

5.3.2 Verification of semi-unsteady model

Dibajnia & Watanabe (1992)

The semi-unsteady model of Dibajnia & Watanabe (1992) includes a phase lag effect to take into account the effect of unsteadiness, see Section 2.9.2. The model describes the total (bed-load and suspended-load) net transport rate (see Eq. 2.20). Figure 5.7 shows the comparison between the measured and the computed net transport rates. It can be seen the measured net transport rates are reasonably well predicted by the model of Dibajnia & Watanabe (1992). All conditions are predicted within a factor 2 difference.

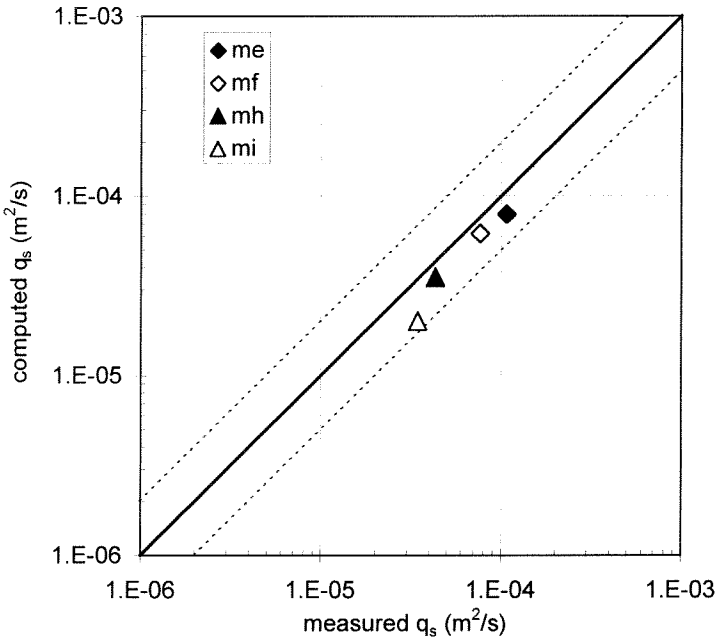

Figure 5.7: Measured and computed sediment transport rates (Dibajnia & Watanabe, 1992).

The parameters ω_c and ω_t (Eq. 2.23 and 2.24) determine if phase lag effects might occur. If the values of ω_c and ω_t are smaller than 1, no phase lag effects are taken into account (see Eq.2.25). It was found that the values of the parameters ω_c and ω_t were smaller than 1 for all tests, see Table 5.1.

condition	ω_c (-)	ω_t (-)
me	0.49	0.08
mf	0.39	0.08
mh	0.37	0.13
mi	0.28	0.14

Table 5.1: Values of the parameters ω_c and ω_t, averaged for all conditions.

5.4 Conclusion comparison with models

All models underpredict the measured net transport rates. Figure 5.8 shows the computed and measured net transport rates as function of U^3 for all conditions. From Figure 5.8 it can be seen that the total-load model of Dibajnia & Watanabe gives the best results. From the straight course of the computed transport rates, plotted in Figure 5.8, it can be concluded that phase lag effects did not occur during the present tests.

The models of Bailard (1981) and Al-Salem (1993), with a value for constant A of 5, give comparable results. The model of Al-Salem (1993), with a value for constant A of 4 (Ribberink & Al-Salem, 1994) and Ribberink (1998) also perform similar.
It must be said that Ribberink considers all transport in the sheet flow layer as bed-load transport. It was found (Dohmen-Janssen, 1999) that in sheet flow conditions the suspended-load transport is only a small part (maximum 10-20%) of the total load transport.

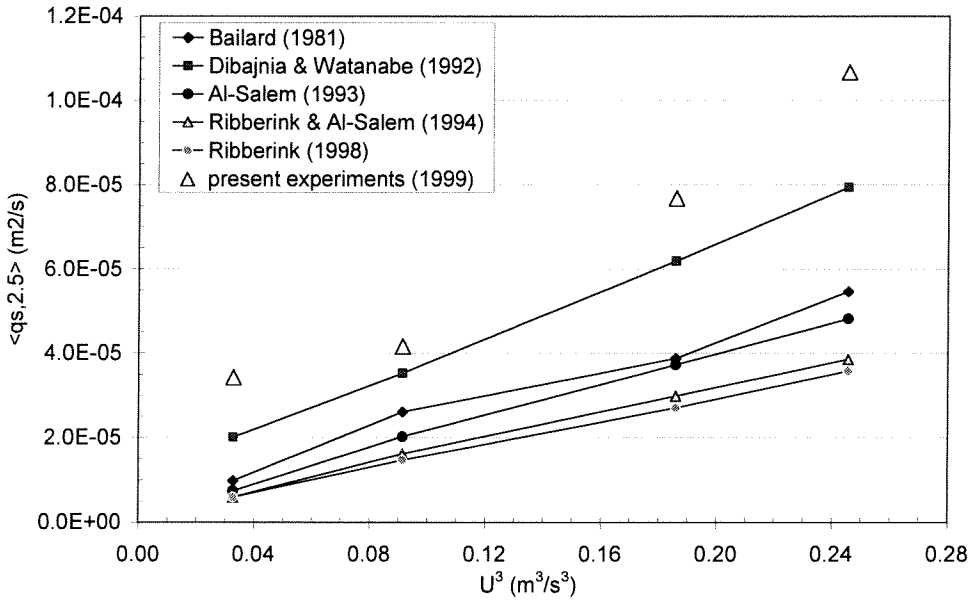

Figure 5.8: Computed and measured net transport rates as function of U^3, for all conditions.

By applying a different formulation for the roughness height the agreement between computed and measured transport rate will improve, because other formulations predict larger values for the roughness height. By applying such a formulation the measured transport for condition me mf and mh will be better predicted. Figure 5.9 shows the computed and measured net transport rates as function of U^3 for all conditions with an increased roughness height k_s of $10*D_{50}$ ($\approx$ 2.4 mm).

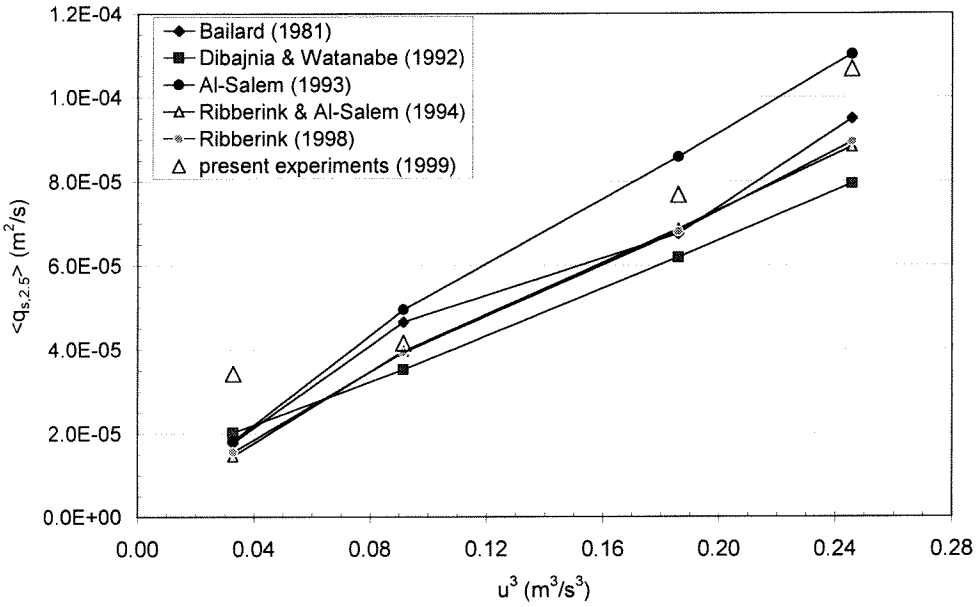

Figure 5.9: Computed and measured net transport rates as function of U^3, for all conditions.

For each model, a mean relative error r_m and the standard deviation of the mean relative error σ_r are calculated, as follows:

$$r_m = \frac{1}{N}\sum_{i=1}^{N}\left[\frac{\langle q_{sci}\rangle - \langle q_{smi}\rangle}{\langle q_{smi}\rangle}\right] \tag{5.2}$$

$$\sigma_r = \sqrt{\frac{1}{N}\sum_{i=1}^{N}(r_i - r_m)^2} \tag{5.3}$$

Here $\langle q_{sci}\rangle$ is the calculated net transport rate for condition i, $\langle q_{smi}\rangle$ is the measured net transport rate for condition i and N is the number of conditions, the results are presented in Table 5.2. Again, it can be seen from Table 5.2 that all models underpredict the measured net transport rate.

transport model	r_m (-)	σ_r (-)
Bailard (1981)	-0.52	0.14
Dibajnia & Watanabe (1992)	-0.26	0.11
Al-Salem (1993)	-0.60	0.13
Ribberink & Al-Salem (1994)	-0.68	0.10
Ribberink (1998)	-0.70	0.09

Table 5.2: Relative error and standard deviation between measured net transport rates and predicted net transport rate.

Chapter 6 Conclusions and recommendations

6.1 General

The main objectives of this study were:

a) To obtain a detailed data set on time-averaged sediment transport rates, measured under progressive waves in sheet flow conditions.
b) To compare the measured time-averaged sediment transport rate with different sediment transport models and other experimental data sets in order to verify if there are differences between net transport rates, measured in a purely horizontal oscillatory water motion (water tunnel) or measured under progressive waves.

To accomplish these objectives, experiments were carried out in a large wave flume. Four different test conditions with monochromatic asymmetrical waves were studied with sand, which had a median grain diameter of 0.24 mm. By measuring the bed level height of the test section after each test, a time-averaged total (bed-load and suspended-load) net sand transport rate (without pores and per unit width) could be determined. This transport rate was determined by averaging the net transport rate distribution along the test section, over a distance of 2.5 m, centred around the location were the velocities are measured. The velocities were measured, just outside the wave boundary layer, in order to obtain information about the instantaneous free-stream velocity.

An important aspect of this study consisted of the development of software, which was used for pre-processing data. The bed profile data, recorded with the MTA, needed different adjustments in order to calculate the difference between two bed profiles. Net sand transport rates could eventually be calculated from the bed profile differences.

The instantaneous free-stream velocity is used to predict the net transport rate. This was done with four different transport models, three quasi-steady models and one semi-unsteady model. Quasi-steady transport models are based on the assumption of a direct relation between instantaneous sediment transport and the instantaneous horizontal free-stream velocity during the wave-cycle. Semi-unsteady models also use this free-stream velocity but a phase lag effect is included.
Furthermore, the present data-set is compared with two other experimental data-sets, obtained from measurements in a water tunnel.

6.2 Conclusions

- All studied test conditions with monochromatic asymmetrical waves showed a net time-averaged transport rate in the direction of wave propagation, despite the fact that the average velocity, just outside the wave boundary layer, had an opposite direction. The phase lag parameter p for each test was smaller than 0.07. It was found earlier (M. Dohmen-Janssen, 1999) that for values of p lower than 0.5, phase lag effects are not expected to occur. Therefore it would be expected that phase lag effects did not occur for the studied test conditions. This was confirmed by comparing the results with predictions of the net transport rates with different quasi-steady transport models and a semi-unsteady model. The semi-unsteady model did not show any phase lag effects.

- A linear relation between the net transport rate and the third order velocity moment was found for the present experiment. However, one condition (mi) deviated, the net transport rate was larger than would be expected from the third order velocity moment. The accuracy of the net sediment transport measurement could be the cause of the deviation of condition mi.

- The measured net transport rates are underpredicted by all transport models. The quasi-steady model of Bailard (1981) underpredicts the measured net transport rates with about a factor 2. The measured transport rates are underpredicted by the quasi-steady model of Al-Salem (1993). When coefficient A=5 (1993) is applied, the measured transport rate is underpredicted with about a factor 3 and applying coefficient A=4 (1994) leads to an underprediction with about a factor 3-4. The quasi-steady model of Ribberink (1998) underpredicts the measured net transport rate with about a factor 4. The semi-unsteady model of Dibajnia & Watanabe performs best. The transport rates are underpredicted with about a factor 1-2.

- A comparison with the experimental data-set of Al-Salem (1993) shows that the present results are about a factor 2-3 larger than results under comparable conditions (with a smaller median grain diameter of 0.21 mm, opposed to 0.24 mm of the present experimental sand). The present results are larger than series E, conducted by Katopodi (1994) and series J, conducted by Janssen & V.d. Hout (1997), with a factor of about 7-8 and larger. The test conditions of series E and J consisted of an oscillatory water flow, superimposed on a steady current.

- This study shows that net transport rates, measured in a large-scale wave flume, are larger than the net transport rates, measured (under the same test conditions) in a large oscillating water tunnel. An explanation could be the presence of the Longuet-Higgins streaming, a small net current close to the bed, in the direction of wave propagation. This Longuet-Higgins streaming occurs only under propagating waves and is absent in a water tunnel, where the flow is purely horizontal.

- This study also shows that carrying out measurements in a wave flume is more difficult than measurements in a water tunnel. The deviation of the net transport rate measurements for the conditions me, mf, mh and mi, are expected to be at least resp. 10%, 13%, 26% and 38%. Combined with the fact that the instrument set-up in the flume had some influence on the net transport rate and that not the complete width of the flume is profiled, one has to be careful when comparing the present results to water tunnel measurements.

6.3 Recommendations

With the data of this study, a start is made to investigate differences between net transport rates under progressive surface waves and in horizontal oscillatory flow (wave flumes and water tunnels). More experiments under progressive waves in the sheet flow regime have to be performed in order to determine the differences between net transport rates, measured in water tunnels and net transport rates, measured in large wave flumes. Other wave heights and periods have to be applied in order to obtain more information about the influence of the near-bed velocity and the wave period on the net transport rates. Extra attention has to be paid on the development of bedforms.

The net transport rate of one condition (mi) deviates from the other conditions. This is could be caused by the influence of the bedforms. It is difficult to maintain a flat bed when experimenting in a large wave flume. More knowledge about sheet flow processes in case of rippled beds is needed.

The results of this experiment and other experimental results, obtained from large wave flumes, should be used to improve existing transport models or to develop a new model. Better results with the existing models can be obtained by applying larger values for the roughness height k_s. Different expressions for k_s are known in literature, a study has to be made to determine which expression could be used best.

A limit value for the phase lag parameter p has to be determined in case of sheet flow in a wave flume. Therefore more experimental research in large wave flumes should be carried out with sand sizes and wave conditions where phase lag effects are expected to influence the net transport rate.

Low values of the net transport rate are influenced more by the inaccuracy than large values of the transport rate. This points out that under medium wave conditions the duration of the tests have to be chosen long enough to make sure that a measurable amount of sand is transported. Also for medium wave conditions more tests can be performed in order to increase the statistical accuracy of the measured net transport rate. It is suggested that in order to increase the accuracy of the transport rates measured in medium wave conditions more tests should be performed with longer durations.

A Multiple Transducer Array is used to profile the bed. The accuracy of the MTA in vertical direction is 2-3 mm and gives therefore enough resolution for an accurate measurement of the bed level height. It is advisable to profile the bed more than once, after a test is carried out. This manner, a good insight of the accuracy of the measuring instrument can be obtained.
It is suggested that instead of rotating the MTA (in a horizontal plane), more MTA's should be used to profile the bed. It is useful to measure the bed level height in cross-direction of the flume, a more realistic net transport rate can be obtained in this manner. Rotating the MTA in a horizontal plane, decreases the resolution in x-direction of the measurement. By using, for instance, 3 MTA's positioned parallel with the flume walls, divided over the width of the flume, information in cross-direction is obtained with a high resolution in x-direction. With a velocity of the measuring carriage of 0.11 m/s a resolution of 0.3 cm in x-direction is possible. This way small bedforms (>0.3 cm) can be detected, which can be important to determine if other transport mechanisms were present besides sheet flow processes.
During the present experiment some difficulty is experienced with the measuring range of the MTA. A developed scourhole, upstream of the test section could not be profiled completely. It is useful to make sure that the measuring range of the instrument is large enough to be able to profile all possible scourholes.

The construction of sand traps has to be investigated more. The sandtrap used in the present experiment did not function well. More attention must be paid to the construction of the sand trap. Flow disturbance should be minimised and a reliable weighing system should be applied to the design of the trap.
When a sandtrap performs correctly, a sand balance can be made from both sides of the test section, starting upstream and downstream of the test section. This will also give an indication of the accuracy of the sand transport measurement. Another option is to profile the whole length of the wave flume. Depending on the length of the flume, this can be a time consuming task.

References

ABOU-SEIDA, M.M. (1965). *Bed-load fuction due to wave action.* Hydraulic Eng. Lab Report 2-11, University of California, Berkeley.

AL-SALEM, A.A. (1993). *Sediment transport in oscillatory boundary layers under sheet flow conditions.* Ph.D. Thesis, Delft University of technology.

BAILARD, J.A. (1981)., *An energetics total load sediment transport model for a plane sloping beach.* J.Geophysic Res.,Vol.86, No.C11,pp.10,938-10,954.

BAGNOLD, R.A. (1963). *Mechanics of marine sedimentation.* In: The Sea, Vol. 3, ed. M.N. Hill, Interscience, New York.

BATTJES, J.A. AND M.J.F. STIVE (1985). *Calibration and varification of a dissipation model for random braeking waves.* Journal of Geophysical Research, Vol. 90 No.C5, pp.9159-9167.

DIBAJNIA, M. & WATANABE, W. (1992). *Sheet flow under non-linear waves and currents.* Proc. Of the 23rd Int. Conf. On coastal Eng., Venice, pp. 2015-2028.

DINGLER, J.R. AND D.L. INMAN (1976). *Wave formed ripples in nearshore sands.* Proc. 15th Coastal Eng. Conf., pp. 2109-21.

DOHMEN-JANSSEN, C.M. (1999). *Grain size influence on sediment transport in oscillatory sheet flow; phase lags and mobile-bed effects.* Ph.D. Thesis, Comm. On Hydr. and Geotechn. Eng., Delft University of Technology, The Netherlands, Report No. 99-4.

DOHMEN-JANSSEN, C.M. (2000). *Sheet flow under monochromatic waves and wave groups; CCM measurements in the Large Wave Flume, Hannover.* Report No. 20000R-003/MICS-012, Civ. Eng. & Man., University of Twente, The Netherlands.

FOSTER, D.L.,R.A. HOLMAN AND R.A. BEACH (1994). *Sediment suspension events and shear instabilities in the bottom boundary layer.* Proc. Coastal Dynamics '94, ASCE, Barcelona, Spain, Feb.1994, pp. 712-726.

GUY, H.P., D.B. SIMONS AND E.V. RICHARDSON (1966). *Summary of alluvial channal data from flume experiments.* 1956-1961. US Geological Survey, Prof. Paper 462-I, Washington D.C.

HORIKAWA, K., A. WATANABE AND S. KATORI (1982). *A laboratory study on suspended sediment due to wave action.* Proc. 18th Int. Conf. On Coastal Engineering, ASCE, Cape Town.

JANSSEN, C.M. (1995). *Sand transport in oscillatory sheet flow; a literature review.* Comm. On Hydr. and Geotechn. Eng., Delft University of Technology, The Netherlands.

JANSSEN, C.M., W.N. HASSAN, R. V.D. WAL, J.S. RIBBERINK (1996). *Net sand transport rates and transport mechanisms of fine sand in combined wave-current sheet flow conditions.* Data report H2462, Part IV, Delft Hydraulics, The Netherlands.

JANSSEN, C.M.& G. VAN DER HOUT, (1997). *Sediment transport for two sands with different grain diameters under combined wave-current sheet flow conditions.* Data report Z2137, Part I, April 1997, Delft Hydraulics, The Netherlands.

JONSSON, I.G. (1966). *Wave boundary layers and friction factors.* Proc. 10th Int. Conf. On Coast. Eng., pp. 127-148.

KALKANIS, G. (1964). *Transport of bed material due to wave action.* Coastal Engineering Research Center, Report TM-2, US Army Corps of Engineers.

KATOPODI, I., J.S. RIBBERINK, P. RUOL, H. KOELEWIJN, C. LODAHL, S. LONGO, A. CROSATO AND H. WALLACE (1994). *Intra-wave sediment transport in an oscillatory flow superimposed on a mean current.* Data report H1684, Part III, Delft hydraulics, The Netherlands.

KAWATA, Y., T. SHIRAI, Y. TSUCHIYA (1992). *Field observation on sand ripples under rough sea state.* Proc. 23rd Coastal Eng. Conf. pp.2164-75.

KING, D.B. (1991). *Studies in oscillatory flow bedload sediment transport.* Ph. D thesis, Univ. of California, San Diego.

LONGUET-HIGGINS, M.S. (1956). *The mechanics of the boundary layer near the bottom in a progressive wave.* Proc. 6th Int. Conf. On Coast. Eng., Miami, pp.184-193.

MANOHAR, M. (1955). *Mechanics of bottom sediment movement due to wave action.* Technical Memorandum 75, Beach Erosion Board, US Army Corps of Engineers.

NNADI, F.N. AND K.C. WILSON (1992). *Motion of contact-load particles at high shear stress.* J. Hydr. Eng., Vol. 118, No.12, pp.1-15.

NIELSEN, P. (1979). *Some basic concepts of wave sediment transport.* Inst. of Hydrodyn. and Hydr. Eng., Tech. Univ. Of Denmark, series paper no. 20.

OSBORNE, P.D. AND C.E. VINCENT (1993). *Dynamics of large and small scale bedforms on a microtidal shoreface under shoaling and breaking waves.* Marine Geol. 115, pp. 207-26

RAMADAN, K.A.H. (1994). *Time-averaged sediment transport phenomena in combined wave-current flows.* Report H1889.11, Part I, Jan. 1994, Delft Hydraulics, The Netherlands.

RIBBERINK, J.S. AND A.A. AL-SALEM (1990). *Bedforms, sediment concentrations and sediment transport in simulated wave conditions.* Proc. 22nd Int. Conf. On Coastal Eng., ASCE, Delft.

RIBBERINK, J.S. AND CHEN, Z. (1993). *Sediment transport of fine sand under asymmetric oscillatory flow.* Report H840, Part VII, January 1993, Delft Hydraulics, The Netherlands.

RIBBERINK, J.S. AND AL-SALEM, A.A. (1994). *Sediment transport in oscillatory boundary layers in cases of rippled bed and sheet flow.* Journal of Geoph. Res., Vol.99, No. C6, pp.12707-12727.

RIBBERINK, J.S., I. KATOPODI, K.A.H. RAMADAN, R. KOELEWIJN AND S. LONGO (1994). *Sediment transport under (non)linear waves and currents.* Proc. 24th Int. Conf. on Coast. Eng., Kobe, Japan, pp. 2527-2541.

RIBBERINK, J.S. (1998). *Bed-load transport for steady flows and unsteady oscillatory flows.* Coast. Eng., Vol 34, pp. 59-82.

RIENECKER, M.M. AND J.D. FENTON (1981). *A Fourier approximation method for steady water waves.* Journal of Fluid Mechanics, Vol. 104, pp. 119-137.

ROELVINK, J.A. (1988). *Large scale cross-shore transport tests.* Delft Hydraulics, Report H596, Feb.

SAVIOLI, J. AND P. JUSTESEN (1997). *Sediment in oscillatory flows over a plane bed.* J. of Hydr. Res., Vol. 3, No. 2, pp. 177-190.

SAWAMOTO, M. AND T. YAMASHITA (1986). *Sediment transport rate due to wave action.* Journal of Hydrosc. aNd hydr. Eng., Vol.4, No.1.

SLEATH, J.F.A. (1975). *Transition in oscillatory flow over rippled beds.* Proc. Inst. Civ. Eng. 59, pp.309-22.

SLEATH, J.F.A. (1978). *Measurements of bed load in oscillatory flow.* J. Waterway, Port, Coastal and Ocean Eng., ASCE, Vol. 104, No. WW4, pp. 291-307.

SLEATH, J.F.A. (1987). *Turbulent oscillatory flow over rough beds.* J. Fluid Mech., Vol. 182, pp. 369-409.

SWART, D.H. (1974). *Offshore sediment transport and equilibrium beach profiles.* Delft. Hydr. Lab. Pub., No. 131, Delft Hydraulics, The Netherlands.

VAN DEN BERG, J.H. (1986). *Aspects of sediment- and morphodynamics of subtidal deposits of the Oosterschelde.* The Netherlands, Rijkswaterstaat, Communications No.43.

VAN RIJN, L.C. (1993). *Principles of sediment transport in rivers, estuaries and coastal seas.* Amsterdam Aqua Publications – I11, issn 90-800356-2-9 bound, NUGI 186/831.

Appendix

A Instruments

The frame of UF contains:

- MTA (Multiple Transducer Array). Located about 45 cm above the sand bed for measuring time dependent bedforms with length scales ranging from 6 cm to 2 meters.
- ADV (Acoustic Doppler Velocimeter). Measurements of time dependent 3-D velocities with the measure volumes located between 2 and 10 cm above the sand bed.
- ABS (Acoustic Backscatter Sensor). Measurements of time dependent concentrations profiles (from transducer to the bed, about 61 cm).
- OBS (Optical Backscatter Sensor). Measurements of time dependent concentrations at a fixed location about 54 cm above the bed.
- Pressure sensor. Measurements of time dependent pressure at a fixed location about 45 cm above the sand bed.

Also used by UF but not mounted on the frame:

- RSS (Rotating Scanning Sonar). Acoustic generated images of the seabed within a radius of 5 to 10 meters that are recorded on videotape. In this experiment the transducer head was located about 45 cm above the sand bed, attached to the sidewall.
- MTA. Mounted on the bed-profiling frame of the carriage. Array of 32 transducers each separated by 2 cm, each of which measures the distance to the seabed approximately every 0.6 seconds. By moving the carriage along the flume, this provides a survey of the seabed elevation along the approximate centreline of the flume over the test section.

The frame of UEA contains:

- ABS's. Measurements of suspended sediment concentration and size using three transducers at frequencies of 1.96MHz, 4.07MHz, and 5.57MHz. The ABS also recorded the EMCM that was on the UEA frame. The EMCM measures vertical and horizontal velocity at a fixed point.
- Tridisma :
  ABS's. Time series of suspended sediment concentration were measured using a 1MHz, 2MHz, and a 4MHz transducer.
  CC (Cross-Correlation). Uses two transducers at 2MHz with identical narrow beam patterns. Potentially should be able to give a vertical profile from the transducer to the bed at 1cm intervals of horizontal velocity at a frequency of 470Hz.
  ADCP (Acoustic Doppler Current Profiler). Time series of vertical velocity at 1cm intervals from the transducer to the bed at a frequency of 4.7Hz.

The University of Twente (UT) used the following instruments mounted on the movable pole of the carriage:

- TSS (Transverse Suction System). Time-averaged concentration profiles (averaged over 6 or 12 minutes) are measured for each test at 10 elevations, logarithmically spaced. Distance between lowest suction tube (no.1) and highest suction tube (no.10) is 0.50 m. The lowest suction tube is usually positioned about 0-5 cm above the bed. The samples taken from each suction tube during a test were stored. By analysing these suction samples the median grainsize distribution (perhaps even the full grain size distribution) of the suspended sediment can be known.
- ADV (brought in by the University of California (UCSB)). Measurements of time dependent 3-D velocities with the measure volumes located between 2 and 10 cm above the sand bed.

Another instrument was placed on the bottom, in the middle of the flume.

- CCM (Conductivity Concentration Meter). Two time-series of sediment concentrations in the sheet flow layer (1 from each probe) at different elevations, varying from a few mm below the initial bed level (pick-up layer) to several mm above the initial bed level (upper sheet flow layer). Note: concentrations at different elevations measured after each other, not simultaneously. A cross-correlation technique can be applied to measure time-dependent velocities in the sheet flow layer at the same elevations as the concentrations.

The GWK

- Wave height meters. Time-series of water surface elevation at each wave gauge, i.e. at 22 points along the flume.
- ADV's and EMF's (Electromagnetic Flow meter). Time-series of flow velocities (3D for ADV's; 2D for EMF's) at 7 fixed points (ADV's: 0.1 m; 0.38 m; 0.67 m; EMF's: 1.22 m; 1.79 m; 2.39 m and 3.04 above the initial sand bed level (which is located 0.75 m above the concrete flume bottom).

B Near-bed velocities for the individual tests

In this section the near-bed velocities for all tests will be presented. Table B1 includes the following parameters, apart from the parameters that are already discussed:

h_{ADV} = level of the sampling volume of the ADV in mm, relative to the top of the sand bed, before and after the run.

σ_T = standard deviation of the wave period during a run in s, determined from the wave height meter.

run #	h_{ADV} (mm)		T (s)	σ_T (s)	<U> (m/s)	U_{rms} (m/s)	U_c (m/s)	U_t (m/s)	R (-)
	before	after							
meb	192	-	9.11	0.67	-0.054	0.67	1.44	-0.63	0.70
mec	52	-	9.10	0.67	-0.056	0.67	1.44	-0.64	0.69
med	68	-	9.10	0.64	-0.056	0.64	1.40	-0.62	0.69
mee	70	118	9.10	0.69	-0.050	0.69	1.49	-0.64	0.70
mef	70	135	9.11	0.71	-0.050	0.71	1.51	-0.67	0.69
meg	60	123	9.11	0.68	-0.048	0.68	1.44	-0.64	0.69
mfb	61	114	9.11	0.65	-0.037	0.65	1.28	-0.67	0.66
mfc	60	114	9.10	0.67	-0.044	0.67	1.32	-0.71	0.65
mfd	61	121	9.11	0.66	-0.045	0.66	1.32	-0.73	0.65
mfe	123	124	9.11	0.67	-0.036	0.67	1.35	-0.71	0.65
mff	99	105	9.06	0.62	-0.028	0.62	1.25	-0.67	0.65
mfg	97	107	9.10	0.67	-0.029	0.67	1.35	-0.72	0.65
mhb	113	116	6.50	0.61	-0.018	0.61	1.13	-0.64	0.64
mhc	116	113	6.50	0.62	-0.041	0.62	1.09	-0.73	0.60
mhd	100	110	6.50	0.62	-0.049	0.62	1.07	-0.76	0.59
mhe	101	100	6.50	0.61	-0.036	0.61	1.08	-0.73	0.60
mib	113	100	6.50	0.57	-0.041	0.57	0.94	-0.76	0.55
mic	102	87	6.50	0.59	-0.040	0.59	0.99	-0.78	0.56
mid	97	88	6.50	0.61	-0.041	0.61	1.01	-0.81	0.56
mie	117	119	6.50	0.60	-0.058	0.60	0.98	-0.80	0.55

Table B.1: Height of the sample volume above the bed and the near-bed velocities for each test

C Table vertical shift

test #	z(ADV,a)-z(ADV,b) (cm)	z(ADV) (cm)	z(MTA) (cm)	z(ADV)-z(MTA) (cm)
mee	-0.3	71.7	70.7	1.0
mef	-0.3	72.1	70.7	1.4
meg	-0.1	72.4	71.3	1.1
mfb	-0.5	72.0	70.5	1.5
mfc	-0.4	71.0	70.0	1.0
mfd	-0.6	70.8	69.4	1.4
mfe	0.6	70.8	68.8	2.0
mff	0.2	70.0	68.7	1.3
mfg	0.0	69.1	67.7	1.4
mhb	-0.4	69.3	68.9	0.4
mhc	-0.9	70.3	68.8	1.5
mhd	0.2	70.2	68.9	1.3
mhe	0.3	70.2	69.2	0.9
mib	-0.1	71.4	70.8	0.6
mic	-0.2	73.3	72.0	1.3
mid	0.5	74.3	73.2	1.0
mie	-0.9	74.6	73.5	1.1
average	-0.2	-	-	1.2

Table C.1: Bed level heights, measured with ADV and MTA, for all tests.

D Bed profile adjustments and corrections

A summary is given below of all adjustments done on the bed profiles

MTA file:	filename, used by the UF for the MTA files, meaning mm-dd-yy_testnumber
test #:	name of a test (a,b,c,..,etc) with a certain condition (me,mf,mg,..,etc)
Scale factor:	scales the profiles to the same length, using the first profile as a reference.
Vertical shift:	corrects the difference in level of the profiles, using the first profile as a reference

erosion hole correction:

length ec:	length of the correction (m)
length eh:	length of the undetectable scour hole (m)
height ec:	height of the correction (cm)

deposition correction:

length dc:	length of the correction (m)
height dc:	height of the correction (cm)
height d:	height of the deposition (cm)

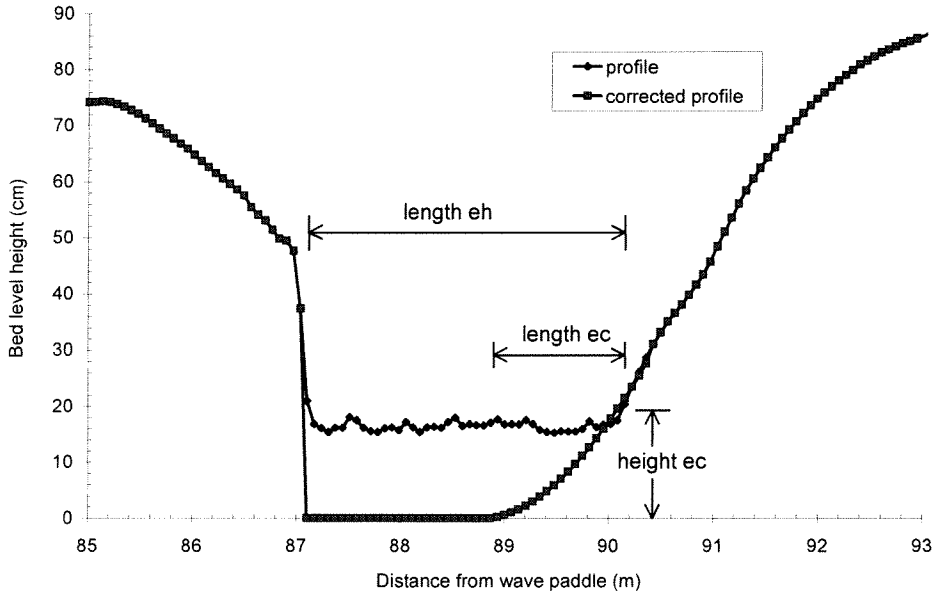

Figure D.1: Erosion correction parameters.

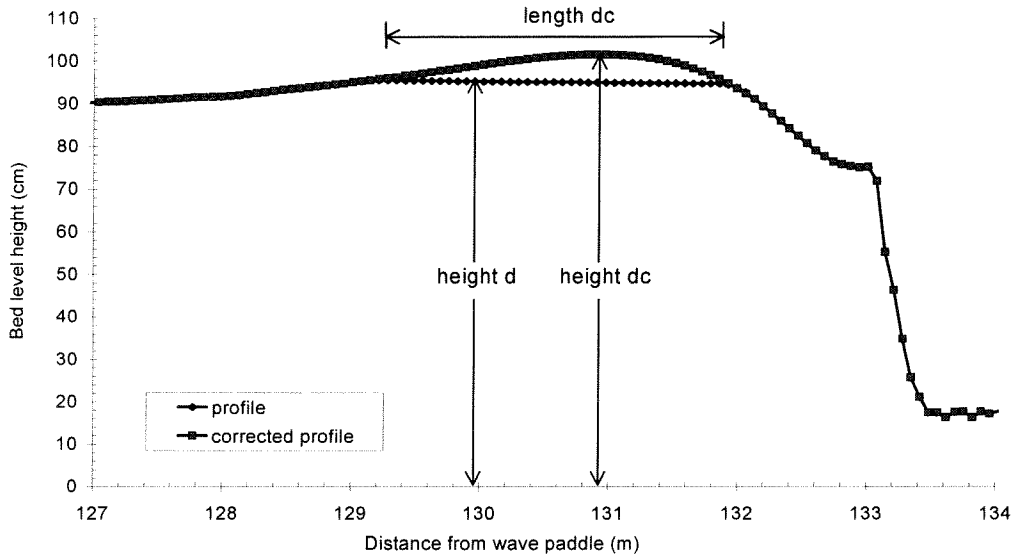

Figure D.2: Deposition correction parameters

test		scale factor (-)	vertical shift (cm)	erosion hole correction			deposition correction		
MTA File	test #			length ec (m)	length eh (m)	height ec (cm)	length dc (m)	height d (cm)	height dc (cm)
082399_2a		reference	-	-	-	-	-	-	-
082399_3a	mea	0.0004	-	-	-	-	-	-	-
082399_4a	mfa	0.0000	-	1.02	1.02	19.6	-	-	-
082499_1a	mga	0.0033	-	1.43	1.43	30.5	-	-	-
082499_2a	mha	0.0026	-	1.43	1.43	25.5	-	-	-
082499_3a	mia	0.0007	-	1.43	1.43	27.5	-	-	-
082499_4a	mja	-0.0014	-	1.90	1.90	34.5	-	-	-

Table D.1: Correction factors mea t/m mja.

test		Scale factor (-)	Vertica l shift (cm)	Scour hole correction			Deposition correction		
MTA File	test #			length ec (m)	length eh (m)	height ec (cm)	length dc (m)	height d (cm)	height dc (cm)
082499_5a	meb	-0.0022	-	0.88	1.56	20.0	-	-	-
082599_1a	mec	0.0030	-	2.18	2.79	23.0	-	-	-
082599_2a	med	-0.0010	0.40	1.29	3.06	19.6	-	-	-
082599_3a	mee	-0.0010	-	0.95	3.47	21.4	-	-	-
082599_4a	mef	-0.0021	-	0.54	3.6	18.8	-	-	-
082699_1a	meg	0.0033	-	0.75	4.08	23.0	1.1	95.7	96.4
082699_2a	mfb	0.0034	-	0.75	4.15	18.3	1.77	95.5	97.4
082699_3a	mfc	0.0023	-	0.95	4.42	18.8	1.56	95.5	97.0
082699_4a	mfd	0.0021	0.52	1.02	4.62	27.5	1.50	95.6	97.4
082699_5a	mfe	0.0007	0.15	0.95	4.69	26.2	1.50	95.3	97.1
082799_1a	mff	0.0033	-	1.16	4.96	30.7	1.29	95.3	96.9
0827992a	mfg	0.0035	-1.00	0.68	4.49	16.9	1.43	95.4	97.2

Table D.2: Correction factors for condition me and mf.

test		Scale factor (-)	Vertical shift (cm)	Scour hole correction			Deposition correction		
MTA File	test #			length ec (m)	length eh (m)	height ec (cm)	length dc (m)	height d (cm)	height dc (cm)
082799_3a	mhb	0.0024	-1.00	0.75	4.62	13.1	2.45	95.0	99.8
083099_1a	mhc	0.0033	0.50	0.95	4.90	19.7	2.79	94.8	101.6
083099_2a	mhd	0.0017	-	0.88	5.1	17.4	2.65	97.5	103.4
083099_3a	mhe	0.0003	0.15	1.22	5.24	24.3	3.26	97.4	105.4
083099_4a	mib	-0.0001	0.70	1.22	5.37	27.1	2.92	98.3	105.3
083099_5a	mic	-0.0005	0.80	1.50	5.58	25.4	2.79	98.9	105.8
083099_6a	mid	0.0000	-	1.50	5.64	22.1	2.92	99.1	105.8
083199_1a	mie	0.0039	0.50	1.36	5.58	23.4	2.92	99.6	103.1

Table D.3: Correction factors for condition mh and mi.

E Table bed steepness

test #	bed steepness		
	dz (cm)	dx (cm)	steepness dz/dx (-)
mea	1.75	115.27	0.015
mfa	0.96	40.68	0.024
mga	4.22	142.39	0.030
mha	2.42	155.95	0.016
mia	0.79	33.90	0.023
mja	1.47	67.81	0.022
meb	1.64	67.81	0.024
mec	8.93	386.49	0.023
med	9.37	311.90	0.030
mee	11.17	454.29	0.025
mef	2.01	81.37	0.025
meg	3.23	142.39	0.023
mfb	4.53	223.76	0.020
mfc	5.74	237.32	0.024
mfd	7.64	250.88	0.030
mfe	9.17	257.66	0.036
mff	10.61	250.88	0.042
mfg	12.94	271.22	0.048
mhb	6.03	122.05	0.049
mhc	3.00	81.37	0.037
mhd	5.51	94.93	0.058
mhe	8.04	135.61	0.059
mib	8.30	122.05	0.068
mic	6.48	81.37	0.080
mid	5.50	67.81	0.081
mie	4.29	47.46	0.090

Table E.1: bed steepness for all tests

test #	$\theta_{w,cr}$ (-)	$\theta_{w,tr}$ (-)	Ψ_{cr} (-)	Ψ_{tr} (-)
meb	1.74	0.33	524	100
mec	1.75	0.35	524	104
med	1.66	0.33	496	97
mee	1.85	0.34	558	104
mef	1.90	0.37	578	114
meg	1.73	0.34	523	104
mfb	1.39	0.38	414	114
mfc	1.46	0.43	439	128
mfd	1.46	0.44	440	133
mfe	1.53	0.43	459	128
mff	1.33	0.38	394	112
mfg	1.52	0.43	457	129
mhb	1.16	0.37	322	104
mhc	1.07	0.49	299	136
mhd	1.04	0.53	291	146
mhe	1.06	0.49	294	135
mib	0.82	0.54	225	146
mic	0.89	0.55	246	153
mid	0.94	0.60	259	165
mie	0.87	0.58	241	161

Table E.2: Maximum Shields parameter and mobility number, based on U_{cr} and U_{tr}.

F Sand loss

As discussed before it was observed that large amounts of sand passed the downstream sand trap and was deposited at the end of the test section (around x=150 m). As a result the volume of sand in the test section decreased, which can be calculated from the bed profiles. The volume change ΔV m^3 (without pores) is calculated from the difference between two profiles (Δz), the place step (Δx), the porosity (ε_0) and the width of the flume (W), expressed in the following equation:

$$\Delta V = \Delta x \cdot \Delta z \cdot W \cdot (1 - \varepsilon_0) \qquad \text{(F.1)}$$

The following values were used: $\Delta x = 0.068$ m, W = 5.0 m and $\varepsilon_0 = 0.38$.
The sand loss from the test section is presented for all tests in the following table. The first two columns represent the volume decrease of the test section over the complete width of the flume. The third column represents the volume change per unit width.

test #	volume test section (m^3)	volume change test section (m^3)	volume change (m^3/m)
start volume	98.42	-	-
mea	97.22	1.204	0.2408
mfa	96.90	0.314	0.0629
mga	96.75	0.154	0.0308
mha	96.74	0.006	0.0012
mia	96.60	0.142	0.0284
mja	96.43	0.169	0.0337
meb	96.35	0.084	0.0167
mec	95.70	0.646	0.1292
med	95.37	0.338	0.0676
mee	94.94	0.425	0.0850
mef	94.30	0.642	0.1284
meg	93.77	0.533	0.1065
mfb	93.56	0.208	0.0416
mfc	93.35	0.209	0.0418
mfd	93.12	0.232	0.0464
mfe	92.95	0.169	0.0337
mff	92.50	0.451	0.0902
mfg	92.33	0.171	0.0341
mhb	92.42	-0.090	-0.0180
mhc	91.98	0.435	0.0871
mhd	91.47	0.508	0.1016
mhe	91.44	0.040	0.0080
mib	91.27	0.166	0.0332
mic	90.77	0.497	0.0993
mid	90.33	0.443	0.0887
mie	89.84	0.484	0.0969

Table F.1: Sandloss from the testsection for all tests.

The values of the averaged volume change <ΔV> per unit width and the standard deviation σ for each condition are displayed in the following table:

condition	test	<ΔV> (m^3/m)	σ (m^3/m)
me	b,c,d,e,f,g	0.089	0.043
mf	b,c,d,e,f,g	0.048	0.021
mh	b,c,d,e	0.045	0.059
mi	b,c,d,e	0.080	0.031

Table F.2: Averaged sand loss for each condition.

The total volume change ΔV and the averaged volume change <ΔV> per unit width and the standard deviation σ

test #	ΔV (m^3/m)	<ΔV> (m^3/m)	σ (m^3/m)
mea-mie	1.716	0.066	0.053
mfa-mie	1.475	0.059	0.040

Table F.3: Sandloss from the test section, averaged for all tests.

G Transport distributions

Figure G.1 shows the transport rate distributions of the first 6 tests. These tests were carried out to check whether sheet flow occurred during the conditions and to let the sand bed settle.

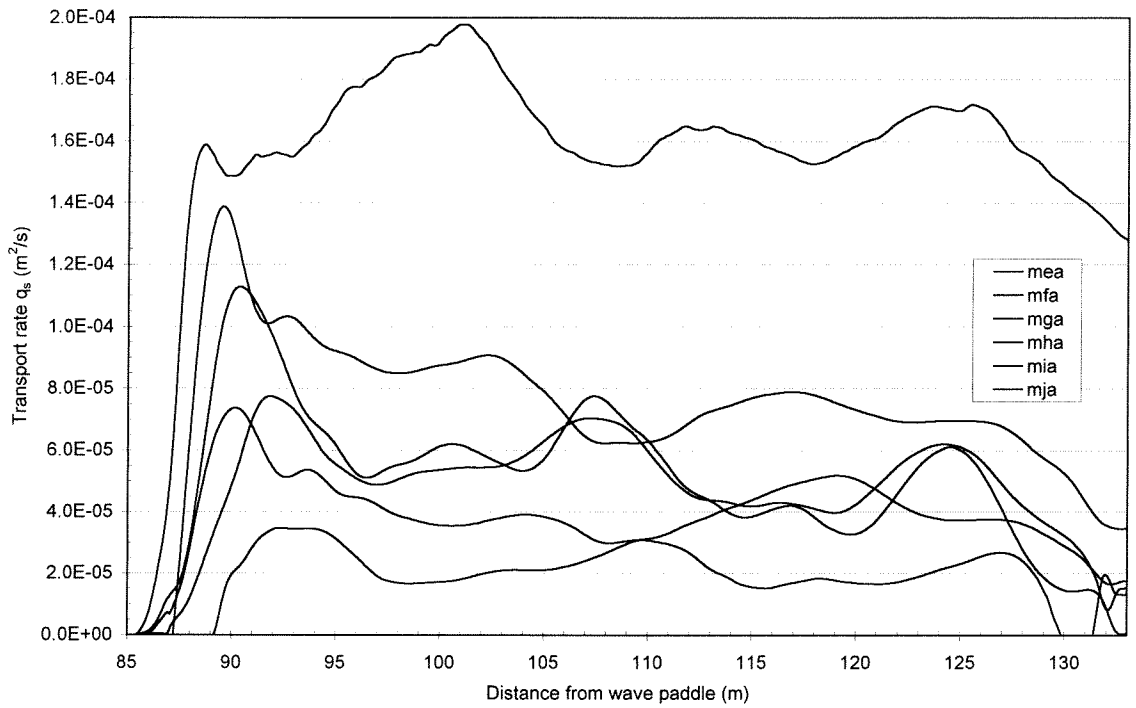

Figure G.1: Measured net transport rates along the test section for the first 6 tests of the experiment.

H Transport rates

$\langle q_s \rangle$ = time-averaged net transport per unit width, measured at x=109.2m
$\langle q_{s,2.5} \rangle$ = time-averaged net transport per unit width, averaged over 2.5 m, centred around x=109.2 m.
$\langle q_{s,5} \rangle$ = time-averaged net transport per unit width, averaged over 5 m, centred around x=109.2 m.
$\langle q_{s,10} \rangle$ = time-averaged net transport per unit width, averaged over 10 m, centred around x=109.2 m.
$\langle q_{s,15} \rangle$ = time-averaged net transport per unit width, averaged over 15 m, centred around x=109.2 m.
σ = standard deviation of the time-averaged net transport rate
r = relative error
r_{avg} = relative error of averaged transport rate

condition	test	T (s)	U_{RMS} (m/s)	$\langle q_{s,5} \rangle$ (m^2/s)	σ (m^2/s)	r (%)	r_{avg} (%)
me	b,c,d,e,f,g	9.10	0.68	1.08E-04	1.85E-05	17.2	7.0
mf	b,c,d,e,f,g	9.10	0.66	7.48E-05	6.99E-06	9.3	3.8
mh	b,c,d,e	6.50	0.62	4.71E-05	1.89E-05	40.1	20.0
mi	b,c,d,e	6.50	0.59	3.53E-05	1.85E-05	52.4	26.2

Table H.1: Net transport rates averaged over 5 m, centred around x = 109.2 m.

condition	test	T (s)	U_{RMS} (m/s)	$\langle q_{s,10} \rangle$ (m^2/s)	σ (m^2/s)	r (%)	r_{avg} (%)
me	b,c,d,e,f,g	9.10	0.68	1.08E-04	1.47E-05	13.6	5.5
mf	b,c,d,e,f,g	9.10	0.66	6.99E-05	7.10E-06	10.2	4.1
mh	b,c,d,e	6.50	0.62	5.61E-05	1.97E-05	35.1	17.5
mi	b,c,d,e	6.50	0.59	3.79E-05	1.79E-05	47.3	23.7

Table H.2: Net transport rates averaged over 10 m, centred around x = 109.2 m.

condition	test	T (s)	U_{RMS} (m/s)	$\langle q_{s,15} \rangle$ (m^2/s)	σ (m^2/s)	r (%)	r_{avg} (%)
me	b,c,d,e,f,g	9.10	0.68	1.08E-04	1.22E-05	11.3	4.6
mf	b,c,d,e,f,g	9.10	0.66	6.43E-05	7.43E-06	11.6	4.7
mh	b,c,d,e	6.50	0.62	6.31E-05	1.95E-05	30.9	15.4
mi	b,c,d,e	6.50	0.59	3.96E-05	1.76E-05	44.5	22.3

Table H.3: Net transport rates averaged over 15 m, centred around x = 109.2 m.

test #	$\langle q_s \rangle$ (m^2/s)	$\langle q_{s,2.5} \rangle$ (m^2/s)	$\langle q_{s,5} \rangle$ (m^2/s)	$\langle q_{s,10} \rangle$ (m^2/s)	$\langle q_{s,15} \rangle$ (m^2/s)
meb	7.44E-05	7.62E-05	7.84E-05	8.28E-05	8.53E-05
mec	1.07E-04	1.07E-04	1.08E-04	1.11E-04	1.12E-04
med	9.33E-05	9.38E-05	9.59E-05	1.01E-04	1.05E-04
mee	1.20E-04	1.20E-04	1.19E-04	1.17E-04	1.15E-04
mef	1.29E-04	1.28E-04	1.28E-04	1.25E-04	1.21E-04
meg	1.20E-04	1.19E-04	1.18E-04	1.14E-04	1.08E-04
mfb	8.04E-05	8.03E-05	7.92E-05	7.57E-05	7.20E-05
mfc	7.24E-05	7.19E-05	7.05E-05	6.52E-05	5.94E-05
mfd	8.06E-05	8.03E-05	7.86E-05	7.31E-05	6.70E-05
mfe	6.87E-05	6.81E-05	6.66E-05	6.14E-05	5.52E-05
mff	8.74E-05	8.70E-05	8.52E-05	7.97E-05	7.34E-05
mfg	7.32E-05	7.24E-05	7.06E-05	6.54E-05	5.96E-05
mhb	3.37E-05	3.41E-05	3.67E-05	4.46E-05	5.34E-05
mhc	5.46E-05	5.70E-05	6.15E-05	7.17E-05	7.84E-05
mhd	5.70E-05	5.88E-05	6.36E-05	7.34E-05	7.99E-05
mhe	1.99E-05	2.17E-05	2.54E-05	3.40E-05	4.00E-05
mib	1.10E-05	1.25E-05	1.51E-05	1.99E-05	2.31E-05
mic	4.99E-05	5.02E-05	5.14E-05	5.44E-05	5.62E-05
mid	4.96E-05	4.93E-05	4.99E-05	5.20E-05	5.34E-05
mie	2.32E-05	2.33E-05	2.34E-05	2.48E-05	2.57E-05

Table H.4: Net transport rates for each test, averaged over different intervals.

I accuracy for each test

test	r_{lin} (%)	r_{pol} (%)	r_{ver} (%)	r_{hor} (%)
meb	2.0	-9.6	13.9	0.0
mec	15.1	-6.3	8.9	5.6
med	9.4	-7.7	10.2	6.4
mee	3.5	-7.8	8.0	5.0
mef	2.6	-5.8	7.5	4.7
meg	3.4	-5.6	8.0	5.1
mfb	4.2	-8.9	11.9	7.5
mfc	2.7	-12.0	13.3	8.3
mfd	4.3	-9.3	11.9	7.4
mfe	8.2	-11.4	14.1	8.6
mff	0.8	-8.4	11.0	6.7
mfg	2.5	-3.9	13.2	8.1
mhb	5.1	-14.3	28.1	17.2
mhc	3.1	-6.6	16.8	10.3
mhd	1.9	-5.1	16.3	10.0
mhe	8.5	-29.2	44.2	27.1
mib	15.0	-51.8	76.5	47.5
mic	6.0	-20.3	19.1	12.0
mid	5.8	-22.3	19.4	12.4
mie	5.3	-11.3	41.1	26.4

Table I.1: Relative error for transport rate $<q_{s,2.5}>$ expressed in percentages.